THEORETICAL INVESTIGATION OF ENERGY TRANSFER OF OZONE IN ARGON AND XENON MATRICES

By

MEENAKSHISUNDARAM PADMASANI SUDHAKARAN

Bachelor of Science
University of Madras
Madras, India
1979

Master of Science
University of Madras
Madras, India
1981

Submitted to the Faculty of the Graduate College
of the Oklahoma State University
in partial fulfillment of the requirements
for the Degree of
DOCTOR OF PHILOSOPHY
May, 1988

THEORETICAL INVESTIGATION OF ENERGY TRANSFER OF OZONE IN ARGON AND XENON MATRICES

Thesis Approved:

Leonel M. Raff
Thesis Advisor

J Paul Devlin

J P Chandler

Donald L. Thompson

Norman N. Durham
Dean of the Graduate College

ACKNOWLEDGEMENTS

It is with a profound sense of indebtedness that I wish to place on record my sincere thanks to Dr.L.M.Raff for having suggested the problem and for his constant guidance, advice, suggestions and encouragement during the course of the work and during the preparation of this thesis.

I gratefully acknowledge Dr.D.L.Thompson, Dr.J.P.Devlin and Dr.J.P.Chandler for their help and advice as members of my advisory committee.

I would also like to thank the Chairman of the Dept. of Chemistry for providing me with continuous financial support. It is also my great pleasure to thank Dr.I.NoorBatcha and Dr.P.M.Agrawal for their help and discussions at various stages of this research. Also, I would like to express my very sincere thanks to Mr.R.Mohan who taught me a lot about the tricks of FORTRAN programming and about the VAX system.

Writing a thesis like this is never a private project. Hence, acknowledgement is also made of the helpful discussions with fellow graduate students of this group and of the Department of Chemistry of OSU.

Finally, I would also like to thank all my friends and well wishers both in USA and in India for all their

encouragement and moral support. In addition, I thank all the memebers of my family and my wife Shashikala for their unbound love and affection without which I could not have completed this work.

TABLE OF CONTENTS

LIST OF TABLES

LIST OF FIGURES

CHAPTER I

INTRODUCTION

Over the years, the subject of energy transfer has been the important point of many experimental and theoretical studies. There are several papers seen in the literature which discuss the collisional, vibrational-vibrational and vibrational-rotational energy transfer in the gas phase. In this thesis, we present energy transfer and other calculations of ozone isolated in rare gas matrices at low temperature known as 'Matrix Isolated' conditions. Matrix isolation is a technique for trapping species as isolated entities in an inert solid or matrix. Rare gases and nitrogen are some of the materials that are commonly used as the matrix element. Under matrix isolated conditions, the properties of the trapped species are investigated by spectroscopic methods. In fact, the discovery that low-temperature solids can be used to isolate and study free radicals and other molecules spectroscopically occured independently and almost simultaneously in the laboratories of Porter and Pimentel. Porter (1, 2) observed the optical spectra of several free radicals in organic solvents and Pimentel's group pioneered the infrared studies of substances under matrix isolated

conditions (3, 4, 5). The advantage of this technique is that under matrix isolated conditions, the lifetime of a trapped species is considerably increased. Also, since the matrix is maintained at a low temperature, possible side reactions are effectively prevented. Furthermore, if we consider reactions taking place in a cryogenic environment, the following three points can be noted:

1. reaction occurs between reactants held at a fixed distance and in a particular orientation,
2. selective excitation provides the effect of very high temperature on one vibrational degree of freedom at a time and in the complete absence of translational and rotational excitation, and
3. since we use an infrared photon whose energy is a few kilocalories per mole, this method is very usefeul for reactions with low activation energies.

For a detailed account of matrix isolation techniques and other related review articles, references (6-9) can be consulted.

Reactions carried out under matrix conditions at cryogenic temperatures are found to exhibit several interesting effects not seen for the corresponding gas-phase or solution reactions. For example, Turner and coworkers (10-12) investigated the infrared laser-induced intramolecular ligand exchange between isotopically labeled CO and $Fe(CO)_4$ when isolated in a nitrogen matrix. These reactions were observed to exhibit both orientational and

matrix-site selectivity (12). The observation of orientational selectivity demonstrates that free rotation of the reactants does not occur in the matrix environment. Apart from this example, sometimes the reaction products obtained under matrix isolation conditions are different from those obtained in the gas-phase or solutions reactions and frequently, the activation energies are significantly different. In some cases, gas-phase reaction rates and mechanisms are altered significantly under matrix-isolated conditions.

In addition to finding differences in reaction mechanisms and other factors, it has been found that vibrational frequencies in matrices are usually lower than those observed in the gas phase. For example, a detailed comparison of gas phase and matrix spectra of ClCN in argon, neon and CF_4 matrices was made by Murchison and Overend (13). These authors (14) repoted the infrared spectra of several isotopically substituted N_2O molecules isolated in a solid N_2 matrix at 15 K. They concluded that the effect of the matrix cage may be represented by a small perturbation in the intramolecular force constants determined from the isolated molecule in the gas phase.

The vibrational analysis of ozone and oxygen-18 substituted ozone molecules was done by Andrews and Spiker (15) using an argon matrix at 16 K. They obtained the values of 1105 cm^{-1}, 704.5 cm^{-1} and 1040 cm^{-1} for the

symmetric stretch, bending and asymmetric stretch modes, respectively. These values compared to the gas-phase values (42 and references therein) of 1103 cm^{-1}, 701 cm^{-1} and 1042 cm^{-1} show good agreement. Similarly, the infrared absorption spectra of isotopic ozone isolated in rare gas matrices was reported by Brewer and Wang (16 a) and these workers obtained the values 1105 cm^{-1}, 700 cm^{-1} and 1035 cm^{-1} for the symmetric stretch, bending and asymmetric stretch modes in a krypton matrix at 20 K. For a xenon matrix at 20 K, these values are 1100 cm^{-1}, 695 cm^{-1}, and 1035 cm^{-1}, respectively. For the oxygen-18 ozone molecule, the bending and asymmetric stretch values given by these investigators are 665 cm^{-1}, 982 cm^{-1} and 660 cm^{-1}, 975 cm^{-1} in krypton and xenon matrices respectively, at 20 K. Thus, it can be noted that the matrix-phase values are close to, but are less, than the corresponding gas-phase values.

The first infrared-induced photochemical process under matrix isolated cndition was observed by Baldeschwieler and Pimentel (17). They observed the cis-trans isomerization of nitrous acid in solid nitrogen matrix at 20 K. The kinetics of this system was investigated by Hall and Pimentel (18). These workers proposed an isomerization mechanism with an efficient intramolecular energy transfer between vibrational modes. The height of the potential barrier to isomerization was estimated to be 9.7 $\pm$ 0.7 kcal/mole in the matrix and

8.7 ± 1.0 kcal/mole for gaseous nitrous acid.

Davies and coworkers (10-12) used a combination of matrix isolation and IR laser induced photochemistry to identify the intramolecular ligand exchange process occurring between isotopically labelled CO and $Fe(CO)_4$. From their work, they concluded that these reactions exhibit both orientational and matrix-site selectivity.

In 1979, Hauge and coworkers (19) reported the reactions of molecular fluorine with small hydrocarbons (methane, acetylene, ethylene and allene) in fluorine and argon-fluorine matrices at 15 K. Fluorine is known to react explosively with hydrocarbons in the gas phase via a free radical mechanism. However, in the matrix, the rates and mechanisms were altered significantly. The reaction of ethylene with fluorine proceeds photochemically when exposed to light in the wavelength range 1-4 μ. The products obtained were either 1,2-gauche- and trans-difluoroethane or vinyl fluoride and hydrogen fluoride. To explain this, they postulated a concerted four-center addition of F_2 to the double bond to produce the vibrationally excited 1,2-difluoroethane products. Vinyl fluoride and hydrogen fluoride are then produced by unimolecular decomposition (of these primary products) if the internal energy is not removed through coupling to the matrix. As can be seen, this mechanism is different from the gas phase (free radical, chain) mechanism. In addition to this mechanism, these authors

had also proposed two other mechanisms one involving a rapid energy transfer to the matrix and one involving a 1:1 (F_2-C_2H_4) adduct and a 2:1 (F_2-$C_2H_4F_2$ adduct) to explain the observed products.

Using a method called single-photon-absorption reaction chemistry in the solid state (SPARCSS),which catalyses specific chemical reactions, Catalano and Barletta (20) were able to study the following sets of reactions: NO + SF_6, N_2O + SF_6, CH_4 + SF_6, CH_4 + BCl_3 and CO + SF_6. None of these sets of reactants will react at ambient temperature in the gas-phase. However, at a matrix temperature of 12 K, these reactions were studied by this SPARCSS technique. SPARCSS reactions proceed in the solid state at low temperature by selective excitation with photons of low energy and fluxes of very low power density. The photon energies are those which correspond to infrared allowed vibrational fundamental transitions from the 0 ---> 1 states. Based on the preliminary investigation, they hypothesized that the energy of activation must be lowered to such an extent that an excitation of 0 ---> 1 vibrational mode brought about the reaction.

In another investigation, Catalano and coworkers (21) studied the reaction between SiH_4 and UF_6 under thermal gas phase and photon initiated conditions in cryogenic matrices. The gas phase thermal reaction occurred at 130-140 ^{0}c producing HF, SiH_3F and a solid uranium

fluoride product. When ν_3 of UF_6 (613 cm^{-1}) was excited within the SiH_4 matrix at 12 K, the products obtained were SiH_3F, UF_5 and UF_4. These authors calculated an apparent activation energy of about 30 kcal/mole for the gas-phase reaction. However, for the matrix isolated reaction, they concluded that the activation energy must be about 1.8 kcal/mole, which is considerably lower than the corresponding gas-phase value. This could probably be due to a favourable spatial orientation of the reactants in the matrix.

The results of Frei and Pimentel (22) are also very interesting. Their studies show significant differences in the rates of product formation upon induced irradiation of various modes. That is, they have observed mode-specific rate enhancement. The reactions of C_2H_4 with F_2 to form either 1,2-difluoroethane or HF + CH_2=CHF are found to increase two and five orders of magnitude as the photon wave number increases from 953 to 1896 cm^{-1} and 953 to 4209 cm^{-1}, respectively. The transititon from 953 to 1896 cm^{-1} involves similar vibrational motions and therefore they postulated that any difference in quantum yields was probably associated with a barrier to reaction between these two photon energies and not due to mode specificity. They also found the IR transitions at 2989 cm^{-1}, which involves an in-plane C-H stretch gave a higher quantum yield than the transititon at 1896 cm^{-1}, which involves an out-of-plane

motion. They found it unlikely that these differences in the quantum yields directly indicate mode specificity of the motions excited. However, their observation that excitation of the ($\nu_2 + \nu_{12}$) combination band of C_2H_4 at 3076 cm^{-1} which resulted in a quantum efficiency greater than that for excitation of ν_9 at 3105 cm^{-1}, suggested the possibility of mode specificity being present.

In another paper, Knudsen and Pimentel (23) have reported similar results for the reaction of allene with F_2 in N_2, Ar, Kr and Xe matrices at 12 K. These workers have found the product ratios to depend upon the stabilization rate of the difluoro product. Therefore, a strong dependence on this ratio upon the matrix composition has been noted. Furthermore, the product ratio has been found to be independent of excitation frequency, but the relative quantum yields show a strong dependence upon this frequency. Again, there was some evidence of mode specificity in the reaction in that the selective quantum yield did not increase monotonically with the excitation frequency. This evidence suggested that excitation of the CH_2 rocking and bending overtones produced a greater propensity for reaction than excitation of the asymmetric C-C stretching mode at nearly the same frequency.

In 1981, Frei and coworkers (24) studied the vibrational excitation of ozone and molecular fluorine reaction in cryogenic matrices. They attempted to induce

reactions between ozone and C_2H_2, C_2H_4, NO_2 and NO and between F_2 and C_2H_4 by selective vibrational excitation of nearest neighbour reactant pairs. The samples were trapped in an inert gas or nitrogen matrix at 12 K and irradiated with a laser to induce reaction. The authors concluded that a molecular four-center reaction mechanism must be involved rather than the free-radical mechanism seen in the gas-phase reaction.

The dynamics of O_3 + NO has been studied experimentally and theoretically by different groups. In 1963, Clyne, Thrush and Wayne (25) examined the kinetics of the O_3 + NO reaction by monitoring the chemiluminescence of NO_2 formed in the reaction. That is, the following reactions took place:

1. $O_3 + NO \longrightarrow O_2 + NO_2 \quad (^2A_1)$
2. $O_3 + NO \longrightarrow O_2 + NO_2 \quad (^2B_1)$

It was concluded that reaction 1 and 2 occur on different adiabatic potential surfaces with rate coefficients

$$k_1 = (5.7\ E{+}11)\ \exp(-2460/RT)$$
$$k_2 = (5.7\ E{+}11)\ \exp(-4200/RT) \quad cm^3/(mol.s)$$

for reactions 1 and 2, respectively. Later measurements by Clough and Thrush (26 a,b) gave values of

$$k_1 = (4.3\ E{+}11)\ \exp(-2330/RT)$$
$$k_2 = (7.6\ E{+}11)\ \exp(-4180/RT) \quad cm^3/(mol.s)$$

for the reactions mentioned above.

Kurylo, Braun, Kaldor and coworkers (27-29) studied the dynamics of reactions

3. $O_3^{\dagger} + NO \longrightarrow O_2 + NO_2 \quad (^2A_1)$

4. $O_3^{\dagger} + NO \longrightarrow O_2 + NO_2 \quad (^2B_1)$

using a CO_2 laser to vibrationally excite the asymmetric stretching mode of O_3 to the (0,0,1) state followed by detection of the NO_2 chemiluminescence. The results indicated the intramode V-V coupling process to be very fast and they measured a rate coefficient (1.2 E+13). exp(-3030/RT) $cm^3/(mol.s)$ as a weighted average of reactions out of a coupled set of vibrational levels. That is, no mode-specific vibrational enhancement of rate was observed in reactions 3 and 4.

Similar results were obtained by Hui and Cool (30-31) and by Gorden and coworkers (32,33). They observed that, when the stretching modes ($\nu_1 + \nu_3$) of ozone were excited, the activation energies for reactions 3 and 4 were decreased by about 50 %. Enhancement of the same order was observed even when the bending mode of ozone was excited. Mode-selective enhancement was not observed. In addition to the above mentioned papers, there are also two other reports in the literature (34-35).

In 1979, Lucas and Pimentel (36 a) studied the reaction between NO and O_3 in a solid nitrogen matrix at 12 K. In 1981, a heavy-atom tunneling mechanism was proposed by Frei and Pimentel (36 b) when they reexamined this system in solid argon and krypton matrices at 6-20 K. When the NO in $NO.O_3$ nearest-neighbour pairs was vibrationally excited with a CO laser, the rate constant

inreased linearly with laser power. Also, the dark reaction in a krypton matrix was found to be three-fold faster than in a nitrogen matrix. Furthermore, an upper limit of 5.35 kcal/mole was assigned for the activation energy for $NO-O_3$ reaction in nitrogen matrix. This activation energy can be compared with the 2.4 kcal/mole value reported for the gas-phase reaction (25). Lucas and Pimentel (36 a) have suggested that the orientational effects of the matrix cage can be primarily responsible for the differences observed between matrix and gas phase reactions.

The technique of classical trajecory methods are in between theory and experiment, having properties in common with and capable of useful interactions with both. These methods can be used to test theories of molecular behaviour using interatomic forces. They can relate laboratory results to each other and to other experiments that need to be performed. Furthermore, this method cannot be generalised since it depends on the problem to be solved and also on the available information. Excellent reviews of this topic can be found in references (37-39). A review of quasiclassical trajectory studies of state-to-state collisional energy transfer in polyatomic molecules has been given by Schatz (40).

Two calculations have been reported on the $O_3.NO$ system by Chapman (41) and Viswanathan and Raff (42).

Chapman (41) considered the dynamics of this reaction on a series of model surfaces that represented various exoergicities and transititon states. For collisions involving multiple quanta excitation of ν_1, ν_2 or ν_3 of ozone, Chapman found a small vibrational enhancement of the reaction cross sections with no mode-specific behaviour being observed. The absence of mode-specific enhancement was not a result of the formation of a long-lived O_3.NO complex since all reactions were found to be direct. The calculation by Viswanathan and Raff (42) showed the intramolecular V-V transfer to be faster than the reaction rate on their five different potential surfaces. Consequently, no mode-specific vibrational enhancement was observed. Also, the reaction mechanism was found to be direct with no long-lived complex being formed.

As a first approach to the computational study of matrix-isolation chemistry, Arnold and coworkers (43) have reported the results of quasiclassical trajectory studies of vibrationally assisted reaction of the O_3.NO van der Waals complex. Such complex may be regared as being a system intermediate between a bimolelcular gas-phase system and one tht is isolated in a matrix. These workers found mode specific rate enhancement for reaction to form O_3 + NO products, for vibrational predissociation (VP) and for intramode energy transfer. Excitation of the hindered internal rotation of NO about the O_3 symmetry axis was found to significantly influence

the dynamics of this system. Similar quasiclassical trajectory calculations of the vibrational predissociation of the $C_2H_4 \cdot F_2$ van der Waals complex have been reported by Graham and Raff (44) on the surface constructed by Raff (45). In this study (44), the nonplanar rock excitation of C_2H_4 exhibited a rate four times greater than that of zero point energy and approximately three times greater for both the torsional motion and symmetric stretch. Therefore they concluded that mode specificity and rate enhancement must be due to the van der Waals molecule's inefficiency in diffusing energy intramolecularly in the given time period.

The above mentioned experiments and calculations indicate that several factors are of importance in determining the dynamics of a chemical reaction under matrix isolation conditions. The reactant-matrix structure and interaction will certainly be of crucial importance. To some extent, these interactions are measured by the observed IR frequency shifts upon matrix isolation. The rate of energy transfer between reactants and matrix has likewise been demonstrated to play an important plart in the reaction. This is particularly true in the case of very exothermic reactions. Orientation of the reactants in the matrix cage may also affect the dynamics. In this work, we undertake an examination of reactant-matrix structure, frequency shifts and the energy transfer rates as a function of

matrix material, temperature, matrix size and the particular vibrational mode excited.

We first consider ozone inside a rare gas matrix. Our understanding of this system will help us explore the O_3 + NO system, again to be considered in a rare gas matrix. The choice of rare gas matrices is made because of the availability of potential energy parameters (48 a,b,c,d) and its simplicity. For the ozone molelcule, a good potential energy surface has been developed by Murrell and Farantos (46). As various calculations on the (NO + O_3) gas phase and van der Waals NO.O_3 structure have already been done, our results give additional input to the already existing data. We therefore present our method of calculation, results and conclusions in the following chapters.

CHAPTER II

COMPUTATIONAL METHODS

A. Matrix Simulation

One of the important things to be decided in simulating a matrix is the number of atoms or molecules that must be used to describe the lattice. We need to use a sufficient number of matrix atoms (or molecules) such that they are neither too low (so that we don't observe any matrix effect) nor too large (so that calculations are not excessively expensive in terms of computer time). Also, it may happen that beyond a particular number of matrix elements, the calculated matrix effects observed may become insensitive to the inclusion of additional matrix atoms.

In 1972, for example, Bunker and Jacobson (47) used a cubical box with a 14 A edge, containing 26 CCl_4 molecules to study the cage efficiency associated with photolysis of a diatom (I_2) in a solvent of spherically symmetric molecules.

In the present calculation, 64 rare gas atoms along with ozone molecule are considered "movable". That is, these 64 rare gas atoms are considered in the Hamiltonian equations of motion. The interaction between the rare

gas atoms are assumed to be given by Lennard-Jones (12-6) potentials and the potential energy parameters used (48a-d) correspond to the gas phase values. Starting from this point, we first determine the equilibrium geometry of the matrix and the rest of the calculation begins from this equilibrium configuration of the matrix. The procedure involved in determining this equilibrium configuration of the matrix is described below:

The geometry of the matrix employed in this calculation is a cube which consists of six rows, six columns and six planes. The intersection of a row, column and a plane defines the position of a rare gas atom. Thus $Rg_{(i,j,k)}$ defines the position of a rare gas atoms which is at the intersection of the ith row, jth column and kth plane. Initially ozone is placed inside the innermost cube on the xz or xy or yz plane.

In the present study, all atomic motions are assumed to obey classical mechanics. Furthermore, we consider ozone and $Rg_{(i,j,k)}$ [(i,j,k) = 2,3,4,5] to be movable atoms. There are, therefore, 67 movable atoms in the primary zone. The rest of the rare gas atoms serve as the boundary or Q-zone. The 402 Hamiltonian equations of motion are

$$(dH/dP_{\alpha_i}) = P_{\alpha_i} / M_i = \dot{\alpha}_i \qquad (1)$$

$$(dV/d\alpha_i) = -P_{\alpha_i} \qquad (2)$$

where $\alpha = x,y,z$ and $i = 1,2,....,67$

In these equations, H = T+V where T is kinetic energy and

V is potential energy of the system. P_{α} is momentum along the α axis.

B. Selection of box size

The selection of box size of the model depends upon the density of the rare gas under consideration. To understand this, let us consider a cross section of the model shown in Figure 1.

ABCD corresponds to the innermost cube, EFGH to the cube of the movable atoms and IJKL to that of the fixed boundary of Q-zone (O is the origin). At this point, the assumption is made that atoms on FG, for example, do not move more that half the distance between Q & R. With this assumption, we can now calculate the box size of the model that correspond to the density as shown below:

Let X be the distance between AB. Then, the maximum distance to which an atom on FG can move is 2X. Thus, considering both sides, we get a maximum length of 4X. Therefore, the effective volume V_{eff} is 64 X^3. The total mass M_T of the rare gas atoms is considered to be

$$M_T = \sum_{i=1}^{64} m_{Rg_i} \qquad (3)$$

where m_{Rg_i} is the mass of the rare gas atom. Thus, the density D at temperature T is,

$$D = M_T / V_{eff} \qquad (4)$$

using a value of 1.65 g/cm^3 (56) for the density of argon, we get the length of innermost cube as 3.45 A and the box

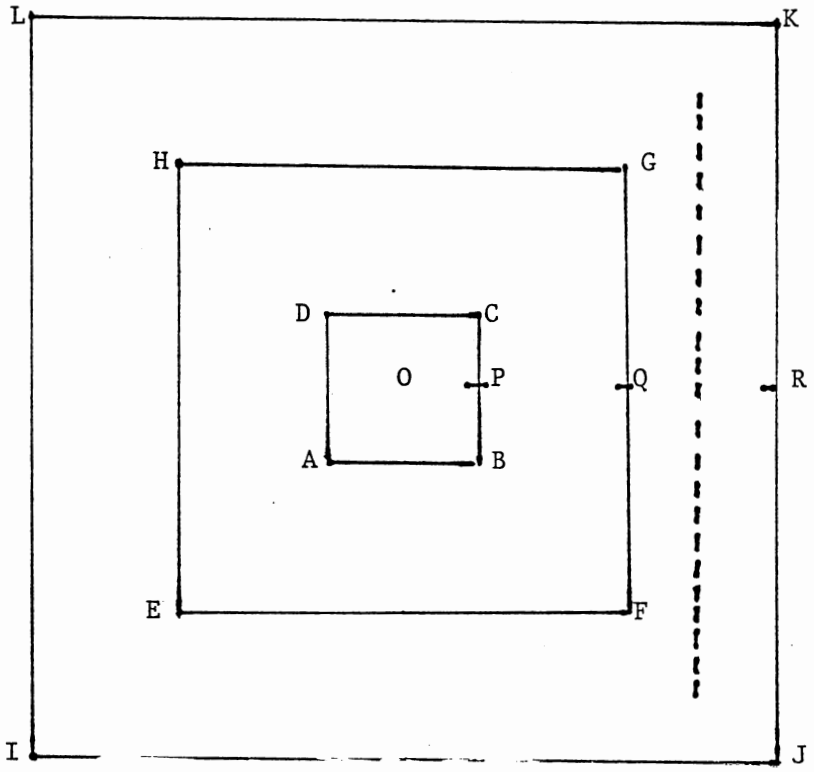

Figure 1. Cross section of the model

size as 17.25A. For xenon matrix with 2.7 g/cm^3 density(56) the corresponding values are 4.33A and 21.65A, respectively.

C. Potential energy of the system

Having decided on the size of the box, we now write the total potential energy of the system in a simple form as

$$V_{Total} = V_{Rg-Rg} + V_{Rg-O} + V_{oz} \qquad (5)$$

where

V_{Rg-Rg} = rare-gas-rare-gas interaction potential,

V_{Rg-O} = rare gas-oxygen interaction potential, and

V_{Oz} = ozone potential.

For V_{Rg-Rg} and V_{Rg-O} we assume a pairwise sum of Lennard-Jones (12-6) potentials. The ozone potential is that given by Murrel and Farantos (46).

In order to simplify the calculation, we further assume that

1. each oxygen atom (inside the innermost cube) interacts with eight other rare-gas atoms of the innermost cube. Thus, there are 24 rare gas-oxygen interactions.
2. each argon atom interacts with its nearest neighbors only.

This gives a total of 80 rare gas-rare gas interactions. With these two assumptions, Equation (5) above becomes

$$V_{Total} = \sum_{i=1}^{80} V^i_{Rg-Rg} + \sum_{j=1}^{24} V^j_{Rg-O} + V_{Oz} \qquad (6)$$

The values of the Lennard-Jones potential parameters (48a-d)

used are given in Table I.

The equilibrium geometry of the ground state of ozone has C_{2v} symmetry, with a bond angle of 116.57°. By symmetry, there must be three such minima on the surface, all equivalent, because any one of the oxygen atoms can be the central atom. It is therefore clear that symmetry must be imposed on the potential function in order to obtain the correct topography of the surface. This has actually been done in the ozone potential given by Murrel and Farantos (46).

V_{oz}, the potential for the ozone molecule, is given as a sum of three two-body terms and a three-body term, V_{O_3}.

$$V_{Oz}(R1,R2,R3)=V1(R1)+V2(R2)+V3(R3)+V_{O_3}(R1,R2,R3) \quad (7)$$

The two-body term is written as (46)

$$Vi(Ri)/eV = -5.21296(1+3.75374r/A)\,Exp(-3.75374r/A) \quad (8)$$

where r = Ri - 1.2074 A

The V_{O_3} potential is defined in terms of the symmetry coordinates Q_1, Q_2 and Q_3 which are in turn defined by the transformation

$$\begin{bmatrix} Q_1 \\ Q_2 \\ Q_3 \end{bmatrix} = \begin{bmatrix} a & a & a \\ 0 & b & -b \\ c & -d & -d \end{bmatrix} \begin{bmatrix} \delta_1 \\ \delta_2 \\ \delta_3 \end{bmatrix} \quad (9)$$

where $a = (1.0/\sqrt{3.0})$, $b = (1.0/\sqrt{2.0})$,

$c = (2.0/\sqrt{6.0})$ and $d = (1.0/\sqrt{6.0})$. (10)

$\delta_i = (Ri-R0)$, where R0 = 1.5698 A (11)

R1,R2,R3 are the distances between oxygen atoms (1 & 2), (2 & 3) and (1 & 3) respectively. The δ_i are the

TABLE I

POTENTIAL ENERGY PARAMETERS

System	(eV)	A	Reference
Ar-Ar	0.01222	3.396	48 a
Xe-Xe	0.02481	3.9	48 b
Ar-O	0.07668	3.108	48 c
Xe-O	0.0128	3.215	48 d

displacement coordinates from a D_{3h} reference structure of bond length R0.

Thus, V_{O_3} = (P+G)(1.0-tanh(2.3*Q_1)) with (12)

P = C1+C2*Q1+C3*Q1*Q1+C4*(Q2*Q2+Q3*Q3)+
C5*Q1*(Q2*Q2+Q3*Q3)+C6*Q3(Q3*Q3-3.0*Q2*Q2)+
C7*(Q2*Q2+Q3*Q3)**2 (13)

where C1 = 8.7066, C2 = 6.5822, C3 = 13.91060,
C4 = -17.1931, C5 = -3.1421, C6 = 2.6323,
C7 = 13.9659 (14)

and G = -3.0*(Exp(-7.5(Q2*Q2+Q3*Q3)))

In equations 13 & 14, Q1 = Q_1, Q2 = Q_2 and Q3 = Q_3.

It can be noted that

$$\lim_{R_i \to \infty} V_{O_3} = 0 \quad (i = 1,2,3). \tag{15}$$

This potential function for ozone reproduces the harmonic force constants, equilibrium bond lengths and dissociation energy of the molecule. The fundamental vibrational wave numbers of ozone have been calculated by Whitehead and Handy (49) and the results are compared with experiment in Table II. It can be seen that agreement between calculated and experimental values is excellent.

D. Equilibrium matrix-ozone structure

With this definition of the total potential, we can now obtain the equilibrium configuration of the system by any of the following three different methods. That is, in principle, what we need is the absolute minimum of

TABLE II

COMPUTED FUNDAMENTAL VIBRATIONAL WAVENUMBERS (cm^{-1}) FOR O_3 COMPARED WITH OBSERVED VALUES

	Symmetric Stretch	Bend	Asymmetric Stretch
Theoretical	1098	707	1043
Experimental	1103	701	1042

Reference: 42 and references therein

the potential energy function V and this can be obtained by an optimization algorithm, a Monte Carlo procedure, or by using a relaxation method.

Optimization Algorithm

The objective here is to minimize the function V which in turn is a function of 201 variable (position coordinates of the movable atoms of the lattice). We have tried subroutine LMINN developed by Dr.D.Le of the Australilan Atomic Energy Commission (courtesy of Dr.J.P.Chandler). However, as we have to start with different initial starting points and repeat the search to get absolute (global) minimum, this method was found to be very expensive in terms of computer time. Hence, this method was not pursued.

Monte Carlo Method

In this case,the coordinates of the 67 movable atoms (and thus there are 201 variables) are altered slightly and randomly using a random number generator and the potential energy of the system is computed. That configuration of the system which gives the lowest potential-energy value corresponds to the equilibrium configuration of the sytem. Once again, as there exists an infinite number of possibilities of the initial

starting point, this method has also not been pursued. We have thus used the following "Relaxation Method".

Relaxation Method

Basically there are four steps involved in this procedure:

1. specification of initial positions of atoms,
2. specification of the initial matrix temperature,
3. solving the Hamiltonian equations using a numerical integrator, and
4. converging to the absolute minimum and not to a local minimum.

The coordinate system used in this calculation is Cartesian and the origin is considered to be at the center of the innermost cube. The ozone molecule is initially placed in its equilibrium configuration on the xz, xy or yz plane inside the innermost cube such that its center of mass lies at the origin. Thus, for a given size of the matrix, the initial positions of all rare gas atoms are fixed and known.

At this point, the temperature T of the lattice is introduced in the form of kinetic energy. That is, the classical vibrational energy per atom at temperature T is kT per degree of freedom where k is the Boltzmann constant. This energy is given to the rare gas atoms in the form of corresponding momenta as shown in the following equations:

$$(P_{\alpha_i})^2 / (2.0*m) = kT \qquad (16)$$

with $$P_{\alpha_i} = \pm\sqrt{2.0*m*k*T} \qquad (17)$$

$$\alpha = x,y,z \quad \text{and } i = 1,2,..,64$$

where m = mass of rare gas atom.

The signs of individual momentum components are assigned randomly. For the ozone molecule, the procedure of assigning the initial momenta is slightly different.

Let $P_{x_{C.M.}}$ be the linear momentum of the center of mass of ozone along the x axis and M (where M = 48 amu) be the mass of ozone molecule. Then,

$$(P^2_{x_{C.M.}} / 2.0*M) = 0.5*k*T \qquad (17\ a)$$

where (0.5*k*T) is the classical translational energy of the molecule. This is now divided equally among the three oxygen atoms and assigned as the initial momentum for each oxygen atom. The same procedure is repeated for y & z respectively.

Thus, $$P^k_{\alpha} = (P_{\alpha_{C.M.}} /3.0) \qquad (18)$$

where α = x,y,z, k = 1,2,3 denote the momentum of each oxygen atom. With this initial arrangement of potitions and momenta, the 402 first-order differential equations are solved using a fourth order Runge-Kutta-Gill (RKG) algorithm.

The equations that we wish to solve have the form $y' = f(x,y)$ with starting point (x_0,y_0) and interval length h. In the Runge-Kutta procedure, we first write,

$$k_1 = hf(x_0,y_0)$$

$$k_2 = hf(x_0+mh,\ y_0+mk_1)$$

$$k_3 = hf(x_0+nh,\ y_0+rk_2 + (n-r)k_1)$$

$$k_4 = hf(x_0+ph,\ y_0+sk_2 + tk_3 + (p-s-t)k_1)$$

$$k = ak_1 + bk_2 + ck_3 + dk_4.$$

The constants should be determined in such a way that (y_0+k) becomes as good an approximation of $y(x_0+h)$ as possible. The values of these constants given by Gill (50) are,

$$m = n = 0.5,\ p = 1,,\ r = (1-(1/\sqrt{2})),\ s = -(1/\sqrt{2}),$$
$$t = (1+(1/\sqrt{2})),\ a = 1/6,\ b = (1/3)(1-(1/\sqrt{2})), \quad (19)$$
$$c = (1/3)(1+(1/\sqrt{2})),\ \text{and}\ d = 1/6.$$

Using this RKG algorithm, we now search for an absolute minimum potential energy in the following manner:

Starting from a given set of initial conditions, using the RKG integrator, we obtain the new positions of all atoms after each time step. Knowing the position of all atoms, the potential energy of the system is computed. The potential energy computed at step n is compared with that at step (n-1). If the potential energy at step n is less than the value at step (n-1), then the corresponding positions of all atoms are stored. If not, the computation of potential energy and testing is done for step (n+1). This is repeated until the potential energy attains a minimum value. Starting at this minimum potential configuration, with all momenta set to zero, the integration is continued and the configuration of the system corresponding to a new minimum potential energy is determined. This procedure is repeated until the minimum potential energy obtained

has converged to 3 or 4 significant digits. The resulting configuration will be a local or absolute minimum on the potential-energy hypersurface.

In order to obtain the configuration corresponding to the absolute minimum potential energy (and not a local minimum), the above procedure is repeated with different initial positions of the rare gas atoms until this configuration is determined. The atomic positions yielding the absolute minimum corresponds to the equilibrium position of the ozone-matrix system.

E. Specification of initial conditions

As the system is now at its minimum potential energy, any energy that we wish to add can be added in the form of kinetic energy. This is actually done in two parts: 1. using Equations (17) and (18), initial momenta corresponding to a given temperature T of the lattice are assigned to the rare gas atoms and the oxygen atoms, respectively. 2. The vibrational excitation energy of ozone is also added in the form of momenta. This is explained in detail below.

The three vibrational modes of ozone are shown in Figure 2. The magnitude of momentum to be given to each atom for each atom is given by the following equations.

$$P_1 = P_3 = \sqrt{m_O * E_1/3.0}, \tag{20}$$

$$P_2 = 2.0*P_1. \tag{21}$$

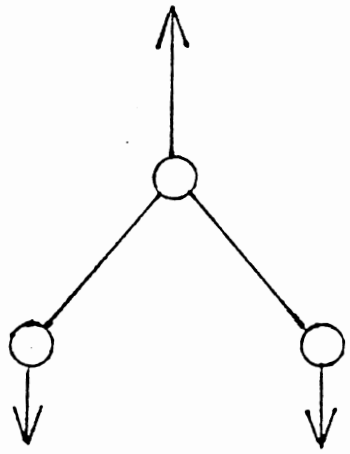

Symmetric stretch

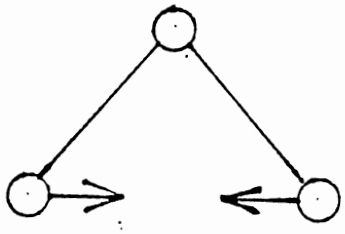

Bend

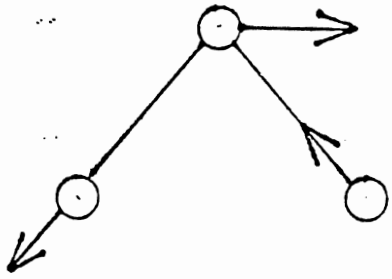

Asymmetric stretch

Figure 2. Vibrational modes of ozone

For the bending mode:

$$P_1 = P_3 = \sqrt{m_o * E_2} \quad \text{and} \quad P_2 = 0.0 \tag{22}$$

For the asymmetric stretch mode:

$$P_1 = P_3 = \sqrt{(m_o * E_3)/(1.0+(2.0*\sin^2(\theta/2.0)))} \tag{23}$$

and $$P_2 = 2.0 * P_1 * \sin(\theta/2.0). \tag{24}$$

In these equations, m_o is the mass of oxygen, P_1,P_2 & P_3 are the magnitudes of momentum of oxygen atoms 1,2,3 respectively. E_1,E_2 and E_3 are the vibrational energies of ozone corresponding to the symmetric, bending and asymmetric stretching modes. θ is the angle at the central oxygen atom.

The vibrational energy E_i, (i=1,2,3) of ozone is given by

$$E_1 = \omega_1 A + X_{11}A^2 + 0.5\ X_{13}\ AC + 0.5\ X_{12}\ AB \tag{25}$$

$$E_2 = \omega_2 B + X_{22}B^2 + 0.5\ X_{12}\ AB + 0.5\ X_{23}\ BC \tag{26}$$

$$E_3 = \omega_3 C + X_{33}C^2 + 0.5\ X_{13}\ AC + 0.5\ X_{23}\ BC \tag{27}$$

where $A = (n_1+0.5)$, $B = (n_2+0.5)$ and $C = (n_3+0.5)$.
In Equations (25-27) ω_1, ω_2 & ω_3 are harmonic frequencies and X_{ij} are anharmonic constants. Values of these constants are given in Table III.

The magnitude of momentum obtained for each atom and for each mode is then converted to the x y z components of each atom by making use of the direction cosines. For the sake of brevity, we illustrate one example here. For the s.stretch mode, let (x_2,y_2,z_2) and $(x_{C.M},y_{C.M},z_{c.m})$ be the coordinates of central oxygen atom and that of the center of mass of the ozone, respectively. Then momentum

TABLE III

ANHARMONIC CONSTANTS FOR OZONE (cm^{-1})

X_{11}= - 4.9	X_{22}= - 1.0	X_{33}= -10.6
X_{12}= - 9.1	X_{13}= -34.8	X_{23}= -17.0

Reference: 52

along the x component for the central oxygen atom is given by

$$P_{x_2} = ((x_{C.M}-x_2)*P_2)/((x_{C.M}-x_2)^2+(y_{C.M}-y_2)^2 + (z_{C.M.}-z_2)^2) \quad (28)$$

Similar arguments are used for assigning momenta to oxygen atoms for the other modes and along other components. Thus, the total momentum on each oxygen is obtained as a sum of momentum due to the temperature of the lattice and momentum due to the vibrational excitation.

F. Initial-state averaging

With this procedure, we have now excited the ozone molecule and are ready to begin our calculations. However, before beginning the integration of equations of motion, it is necessary to average properly over the initial phase space of the system. This is done by making random Monte Carlo moves using a Markov chain (57-60). The method of making these moves is outlined in the following paragraphs.

Let q_α^n (where $\alpha = x,y,z$) denote the position of a movable rare gas atom after the (nth) random Markov move. p_α^n is similarly defined for momentum component p_α. A Markov move is defined by

$$q_\alpha^{(n+1)} = q_\alpha^n \pm (0.5 - a) * \triangle q \quad \text{and} \quad (29)$$

$$p_\alpha^{(n+1)} = p_\alpha^n \pm (0.5 - b) * \triangle p. \quad (30)$$

In Equations 29 and 30, a,b are random numbers uniformly distributed on the interval (0,1). After execution of a

move, the momenta and position of a second atom are adjusted such that neither the center of mass of the lattice or the total linear momentum changes. If a move results in any of the rare gas atoms crossing the boundary defined in Figure 1, it is rejected and the procedure is repeated. If a move lowers the energy of the system, it is accepted. If the energy of the system increases, then the move is accepted with a probability of $\mathrm{Exp}(-\triangle E/kT)$ where $\triangle E$ is the change in energy caused by the move and T is the temperature of the lattice. That is, a random number c is selected and if $c < \mathrm{Exp}(-\triangle E/kT)$, the move is accepted. If not, another attempt to move from the original configuration is made. The magnitude of $\triangle p$ and $\triangle q$ are selected such that more than 50% of the moves are accepted. As calculations carried out with 500 moves produced the same results as that with 2000 moves, we have used moves (per trajectory) in all our computations.

G. Calculation of energy transfer and power spectra

After averaging over the phase space as mentioned above, we start the trajectory and all 402 equations of motion are solved. The position and momenta of each atom are thereby obtained as a function of time. We then calculate the total energy(E) of ozone for every n time steps. If E_0 is the total energy of ozone at t=0 and E

is that at t=t, then for a first-order energy transfer rate, we would expect a plot of $\ln(E/E_0)$ vs. t to give a straight line with a negative slope. From this slope, the rate coefficient at temperature T is calculated. At this point, a small note is in order. That is, for the purpose of computation the energy transfer rate, we define E to be $T_{O_3} + V_{Oz}$. The uncertainty in rate constants from the fitted first order plots are calculated using the following equations:

Let (X_i, Y_i) be the set of N points that has been measured or calculated. If we now wish to fit this to a straight line, then the equation of the line has the form $Y = A + BX$ where A is the Y-intercept and B is the slope of the fitted line. A,B and US, the uncertainty in slope B, are calculated using Equations (31-35).

$$A = \sum X_i^2 \sum Y_i - \sum (X_i Y_i) \sum X_i \quad / \text{Dr}, \tag{31}$$

$$B = N \sum X_i Y_i - \sum X_i \sum Y_i \quad / \text{Dr} \tag{32}$$

where $\text{Dr} = N \sum X_i^2 - (\sum X_i)^2$.

$$US = \left[S^2 / \left(\sum (X_i - X)^2 \right) \right]^{1/2} \tag{33}$$

$$S^2 = (1/(N-2)) * (\sum Y_i^2 - A \sum Y_i - B \sum X_i Y_i) \tag{34}$$

and $$X = \sum X_i / N \ . \tag{35}$$

In addition to computing the rate coefficients, we also compute the power spectrum of ozone by using the fast Fourier algorithm. The procedure involved is briefly outlined below.

The Fourier integral (54) is defined by the expression

$$H(f) = \int_{-\infty}^{+\infty} h(t) \text{Exp}(-i2\pi ft) dt \quad (i = \sqrt{-1}) \tag{36}$$

In this equation, h(t) is a function of variable time and H(f) is a function of variable frequency. If the integral exists for every value of the parameter f, then H(f) is the Fourier transform of h(t). In general, the Fourier transform is a complex quantity:

$$H(f) = R(f) + iI(f) = |H(f)| \mathrm{Exp}(i\theta(f)), \qquad (37)$$

where R(f) is the real part of the Fourier transform,

I(f) is the imaginary part of the transform and

$|H(f)|$ is the amplitude of Fourier spectrum of h(t) and is given by $|H(f)|^2 = [R^2(f) + I^2(f)]$. (38)

$\theta(f)$ is the phase angle of Fourier transform and is given by $\tan^{-1}$ (I(f)/R(f)).

However, it is useful to modify the Fourier transform pair (h(t),H(f)) in such a manner that the pair is amenable to digital computer computation. This modified pair, termed the discrete Fourier transform approximately as closely as possible the continous Fourier transform. By definition, Equation (39) gives the discrete Fourier transform

$$\tilde{H}(n/NT) = \sum_{k=0}^{N-1} h(kT)\mathrm{Exp}(-i2\pi nk/N) \quad n = 0,1,..(N-1) \qquad (39)$$

In Equation (39), $(h(kT),\tilde{H}(n/NT))$ is the discrete Fourier transform pair. (N is the number of samples, T is the sample width)

In practice, Equation (39) is computed using a 'Fast Fourier Transform'. That is, a particular method (algorithm) of performing a series of computations that can compute the discrete Fourier transform much more

rapidly. The algorithm is given in reference 55. The manner in which this is used to get the power spectra is explained in the following paragraph.

Let R(1) be the distance between oxygen atoms 1 & 2 and R(2) be that between 2 & 3 respectively. θ is the angle at the central oxygen atom. We store R(1), R(2) and θ as a function of time for a predetermined number of points (usually to a power of 2). These stored values are then Fourier transformed using Equation (39) with the Fast Fourier algorithm and power spectrum is computed using Equation (38).

Thus, by using the methods described above, we have calculated the energy transfer rate as a function of initial orientation of ozone in the innermost cube, matrix material, temperature of lattice, density of lattice and the excitation energy of ozone. Our results are presented in the following chapter.

H. Verification of the computer code

1. Analytical derivatives

In setting up the differential equations, we need to evaluate the derivative of the potential-energy function with respect to the coordinate of an atom i (see Eqns.1&2) This is done analytically by using the "chain rule" of calculus. However, these analytical derivatives are

verified by computing the numerical derivative at any given point selected randomly.

Let V = assumed form of potential-energy function. We are interested in determining the derivative of V at any given point 'k'. That is, what is $dV/dX\big|_{X=K}$ numerically? We first calculate the value of V at seven points X_{k-3} - X_{k+3} where the difference between any two adjacent points is h. Then the numerical derivative of V at X = k is given by

$$(dV/dX)_{X=k} = A * S1 + B * S2 + C * S3 \qquad (40)$$

where A = (3/4), B = - (3/20) and C = (3/180) and

$$S1 = (V_{k+1} - V_{k-1}) / h$$
$$S2 = (V_{k+2} - V_{k-2}) / h$$
$$S3 = (V_{k+3} - V_{k-3}) / h. \qquad (41)$$

It can easily be shown that Equation (40) is exact if V can be described over the interval h by a polynomial expansion of sixth-order or less. In our test calculations, this test has been found to give very good results, thereby confirming the fact that the analytical derivatives are correctly computed.

2.Runge-Kutta-Gill integrator

The Runge-Kutta-Gill integrator subroutine is tested by 'back integrating' the equations of motion. That is, we start the trajectory at point a noting the positions and momenta of all the movable atoms and move towards B

with the fixed step size 'dt'. At point b, the sign of dt is reversed and the trajectory is continued for the same amount of time that it has taken to reach B from A. If the positions and momenta obtained now are the same as the ones noted before, then this serves as a verification of the code. Results obtained have confirmed this to be so with four significant digits of accuracy.

3.Markov moves

The subroutine written to implement the above mentioned Markov moves is tested as follows:

Starting from a configuration of C_i, 1000 moves are made. At the end of 1000th move, using the momenta, the kinetic energy of the each of the 64 lattice atoms is computed and stored. This process is repeated for forty times. Thus, we now have 64*40 = 2560 kinetic energy values. These kinetic energy values are then histogrammed. If the histogram is Maxwillian with the peak of the histogram corresponding to 0.5*k*T, where T is the temperature of the lattice, then this verifies that the code is correct. This has been done and an example of a histogram is shown in Figure 3. Also, superimposed is the maxwillian distribution of energy at this temperature and it can be seen that the fit is very good.

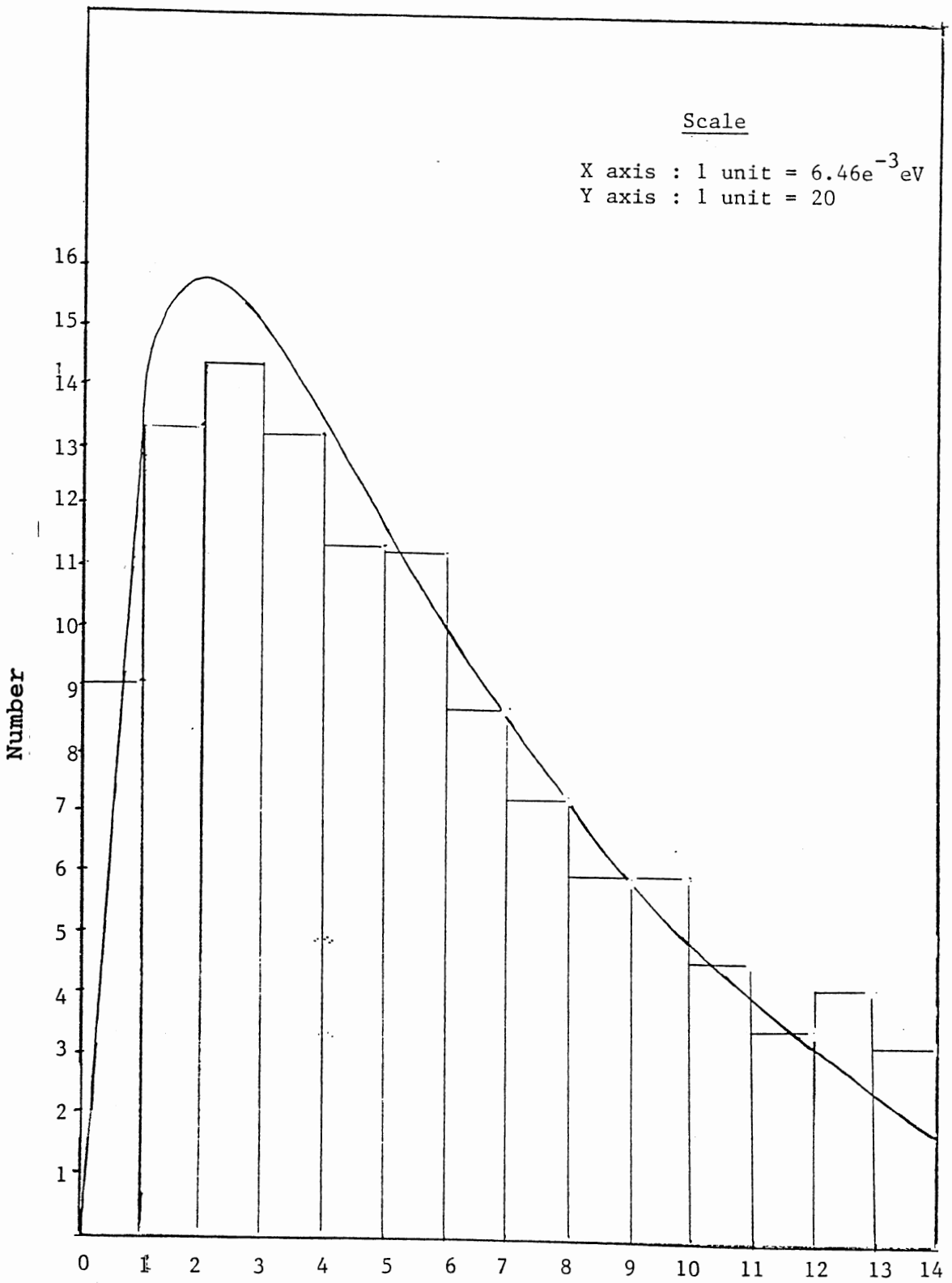

Figure 3. Distribution of kinetic energy at 300 K

CHAPTER III

RESULTS AND DISCUSSION

A. Determination of matrix configuration

Calculations performed in this study can be classified into two categories which we denote as stable-lattice-configuration and metastable-lattice-configuration calculations. When we start from a symmetric arrangement of the lattice and obtain the minimum potential energy of the system by the relaxation method described in the previous chapter, we get the stable (equilibrium) lattice configuration. On the other hand, if we start with an asymmetric arrangement of the lattice, we often obtain metastable configurations of the system corresponding to local minima on the potential-energy hypersurface. Such metastable structures could be present in matrix-isolation experiments and could account for the type of orientational effects observed by Turner and coworkers (10-12). Consequently, we have examined the structure and dynamics associated with both equilibrium and metastable O_3-matrix configurations.

Equilibrium and metastable configurations of ozone in argon and xenon matrices are given in Table IV where they

TABLE IV

CONFIGURATION OF OZONE IN ARGON, XENON MATRICES

Initial plane of ozone	R1	R2		Density (g/cm^3)	Minimum potential energy(eV)	System confgn. no.
			Gas Phase			
	1.2717	1.2717	116.57		- 6.3430	
			Argon Matrix[a]			
xz	1.270	1.269	117.00	1.036	-10.4783	I
xz	1.201	1.348	112.02	1.422	- 8.5671	II
xy	1.205	1.387	112.06	1.422	- 8.1982	III
yz	1.203	1.317	109.48	1.422	- 8.5785	IV
			Argon Matrix[b]			
xz	1.328	1.328	121.16	1.422	- 8.8978	V
			Xenon Matrix[a]			
xz	1.271	1.271	117.08	2.742	-12.3876	VI
			Xenon Matrix[b]			
xz	1.271	1.271	117.04	2.742	-12.3925	VII

Distances are in A; angle in degrees.

a : starting from an asymmetric configuration of lattice

b : starting from a symmetric configuration of lattice

are compared to the equilibrium gas-phase value. As mentioned before, R1 is the distance between oxygen atoms 1 and 2, and R2 is that between 2 and 3 of the ozone molecule. θ is the ozone apex angle. For the sake of brevity, the configurations are labeled I-VII. It can be seen that the structure of ozone in xenon matrices correspond closely to the gas-phase value. The same is true in argon matrices at low density. For argon matrices with a density of 1.422 g/cm^3, we obtain metastable ozone-matrix configurations whose energies lie about 0.3 eV or more above that for the most stable ozone-matrix configuration. These metastable structures are all characterized by having unequal O-O bond lengths, each 0.04-0.07A displaced from the equilibrium distance. The ozone apex angles are also as much as 7 less than the gas-phase value. Also, at high density, the equilibrium ozone-Ar(M) (M = matrix) configuration corresponds to a symmetric C_{2v} structure whose bond length is 1.328 A, 0.056 A greater than the gas-phase value, with a 121.16^0 apex angle.

Figure 4 shows a perspective view of metastable configuration of ozone inside an argon matrix whose density is 1.036 g/cm^3. In this plot, only corners of the innermost cube where ozone is present and the corners of the movable lattice atoms are shown for visual clarity. The distortion of the inner cube of argon atoms caused by the Ar-O interaction is obvious.

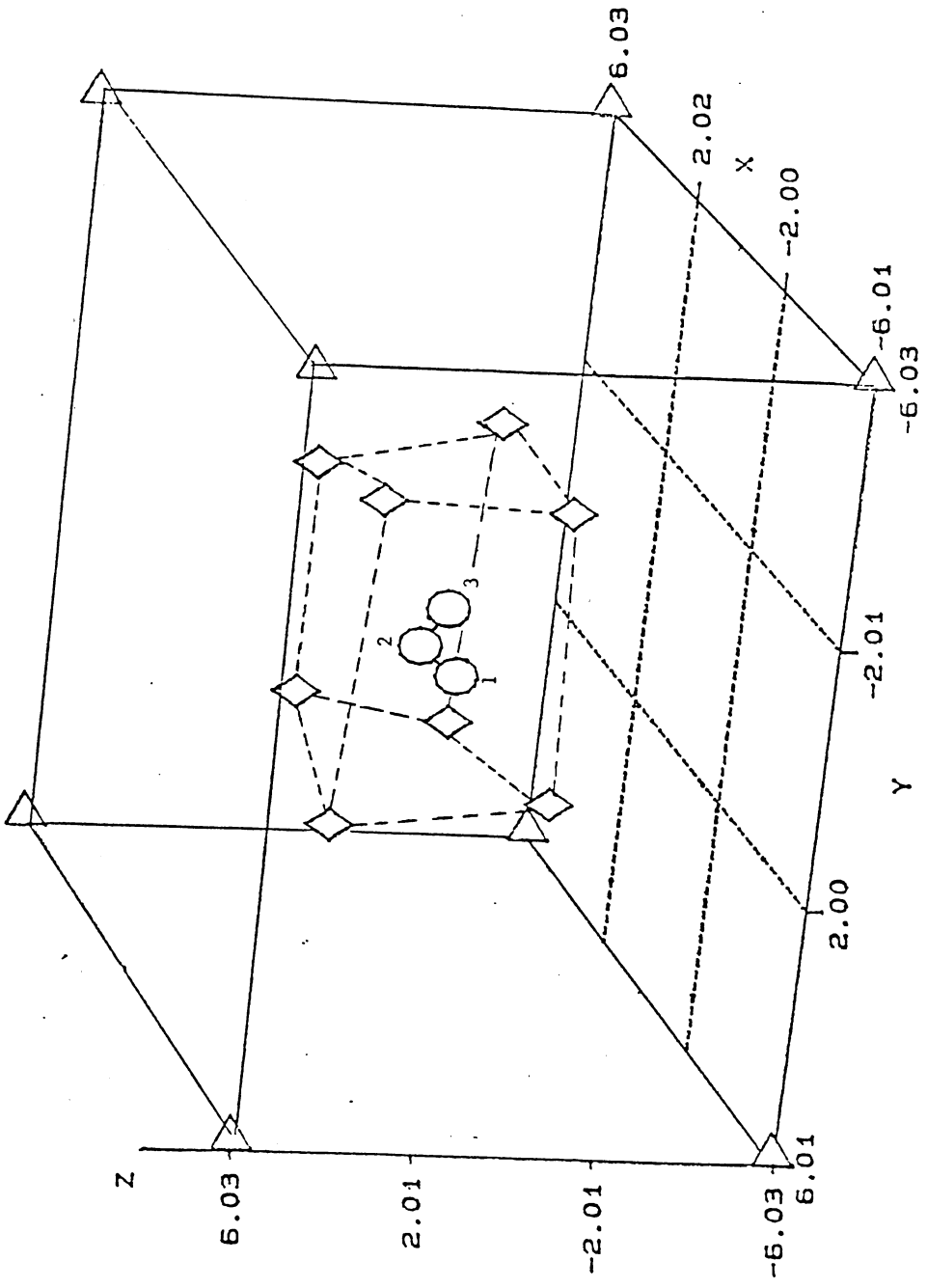

Figure 4. Ozone in Argon matrix

B. Frequency shifts

The IR frequency shifts upon matrix isolation are among the more easily measured properties of matrix-isolated molecules. Such shifts have been reported by Brewer and Wang (16 a) and Andrews and Spiker,Jr. (15) and these values are shown in Table V. In 1963, Pimentel and Charles (16 a) proposed a model which considered the encaged molecule-wall interactions. In general, frequencies observed in a matrix are less than the corresponding gas-phase values. This is because, as the lattice-atom-rare-gas interaction is increased, there is an anharmonicity introduced in the O-O bond potential and this results in a observed lower frequency. Hence the measured frequency shifts contain information related to the matrix-substrate interaction although extracting such information is difficult. Apart from this, when the initial energy in ozone is increased, once again the anharmonicity is introduced in the potential energy function and hence the frequencies are lowered. For the case of ozone, frequencies around 700 cm^{-1}, 1040 cm^{-1} and 1100 cm^{-1} are assigned to bending (ν_2), asymmetric stretch (ν_3) and symmetric stretching (ν_1) modes, respectively.

We have calculated the power spectra of ozone for various potential-energy surfaces and O_3-Matrix configurations. These are shown in Figures 5-20. In

TABLE V

COMPARISON OF IR FREQUENCIES OF O_3 (cm^{-1}) IN RARE GAS MATRICES

MODE	Gas Phase	Matrix		
		Argon[a]	Krypton[b]	Xenon[b]
Symmetric Stretch	1103	1105	1105	1100
Bending	701	704.5	700	695
Asymmetric Stretch	1042	1040.0	1035	1030

a : Temperature of matrix is 16 K

b : Temperature of matrix is 20 K

References: 15,16,42 and references therein

Table VI, major peaks identified on these spectra are presented along with initial ozone excitation energy. In all cases, the resolution is 1.99 cm^{-1}. In general, it can be seen that the power spectra of ozone obtained in gas phase and in xenon matrix are sharp. This may be a direct consequence of identical configuration of ozone in both cases (see Table IV).

Apart from this, when we consider the power spectra of ozone for configurations II,III,IV and V of the argon matrix,for approximately the same excitation energy of 0.22 kcal/mole, the average calculated bending frequency is 687.0 cm^{-1}, which is 14 cm^{-1} less than the observed value (701 cm^{-1}). Furthermore, peaks near 1070 cm-1 can be assigned to 2 ν_3 band as has been observed and assigned by Brewer and Wang (16 a) for ozone trapped in a krypton matrix at 20 K. Finally, peaks near 1100 cm^{-1} correspond to the symmetric stretch mode of ozone.

In the case of xenon matrix, when we consider the calculated frequency values, we note that the calculated frequency for the bending mode is greater than the corresponding observed value by about 20 cm^{-1}. However, for the symmetric stretch mode, the calculated peak at 1095.2 cm^{-1} is less by 7.8 cm^{-1} when compared with the observed value (1103 cm^{-1}). Again, the peak at 1077.2 cm^{-1} can be assigned to 2 as has been done by Brewer & Wang

Considering Figures 5-20, we note that different metastable configurations give rise to various

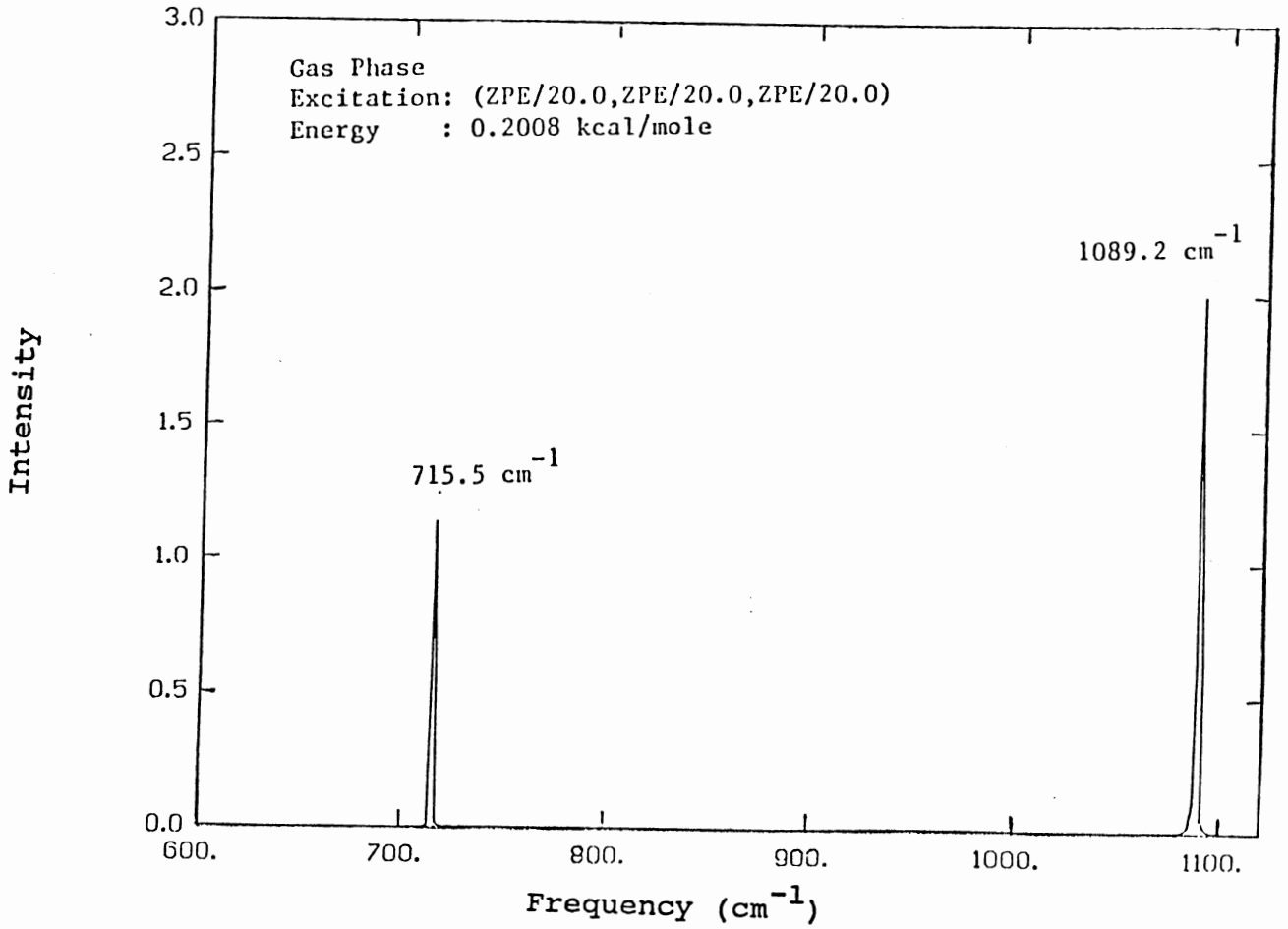

Figure 5. Power spectrum of ozone - E = 0.2008 kcal/mole

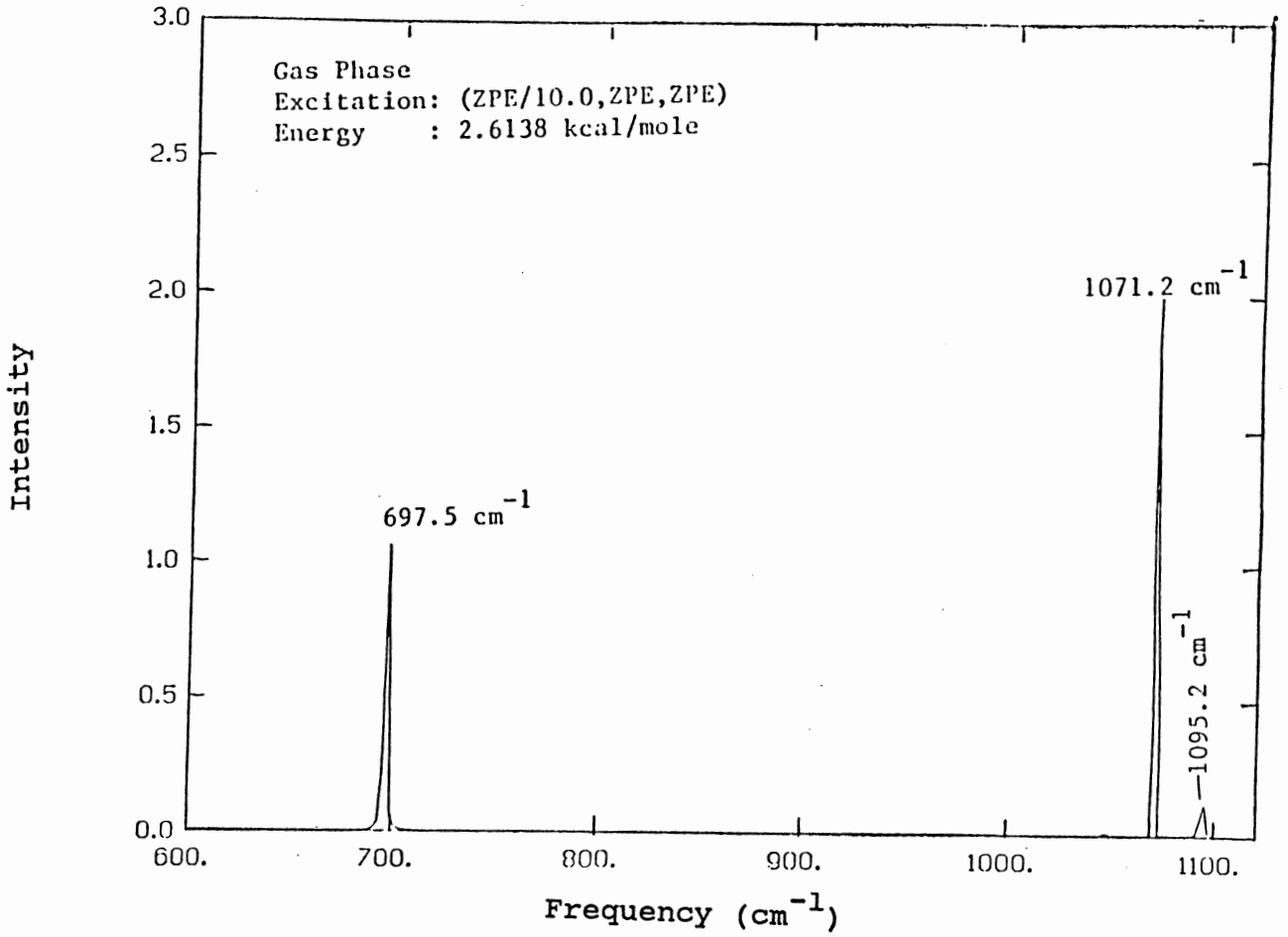

Figure 6. Power spectrum of ozone - E = 2.6138 kcal/mole

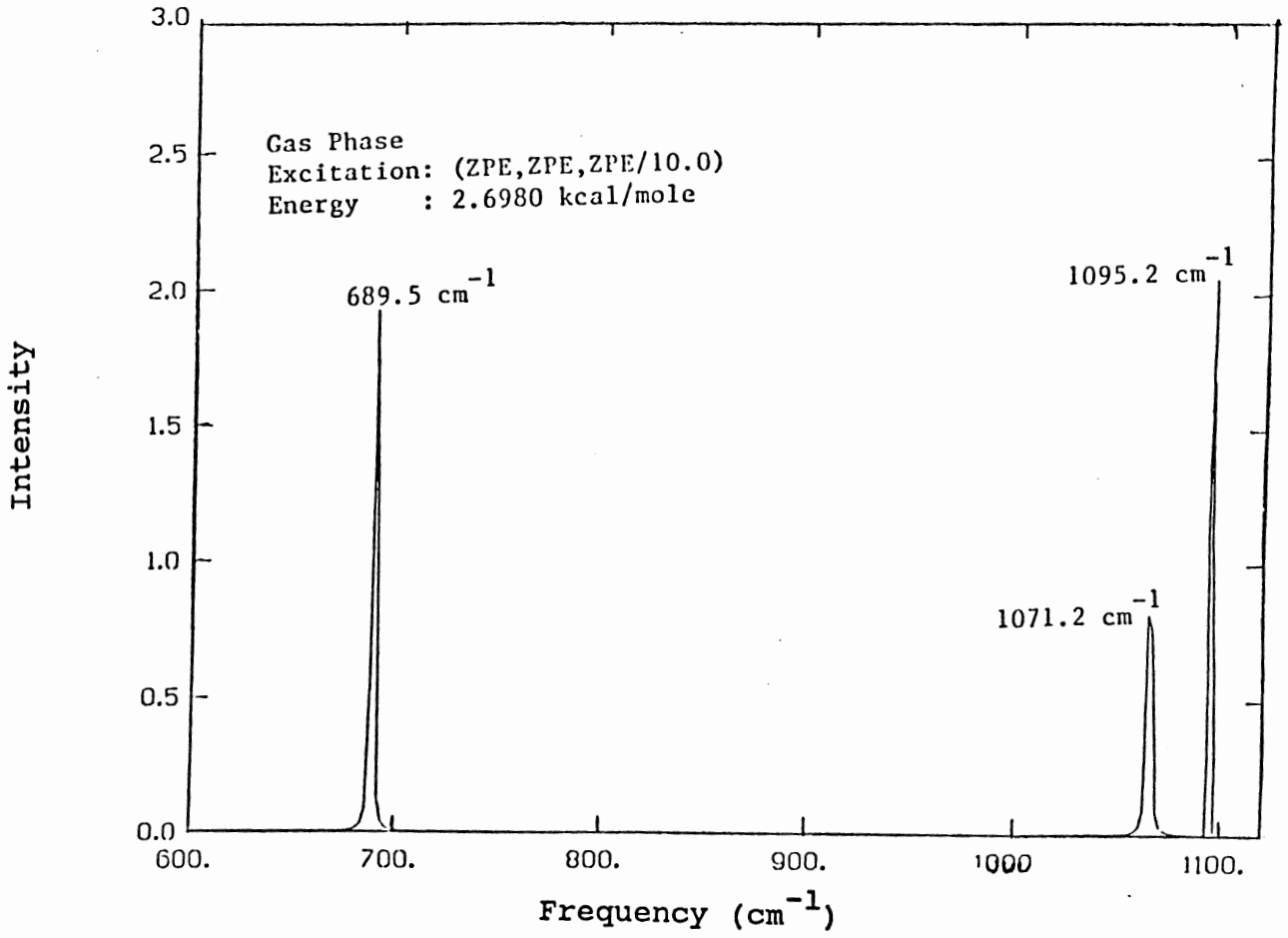

Figure 7. Power spectrum of ozone - E = 2.6980 kcal/mole

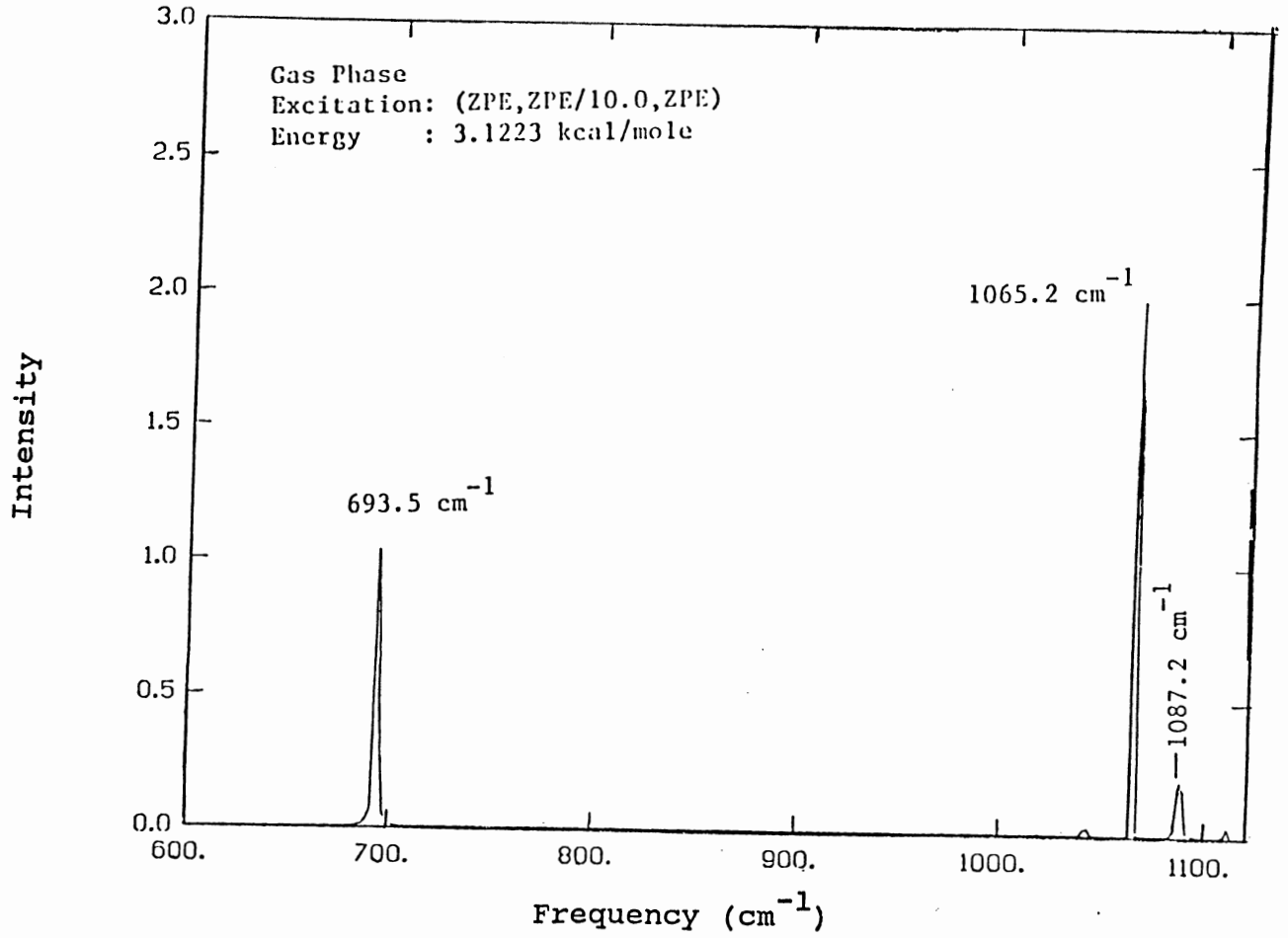

Figure 8. Power spectrum of ozone - E = 3.1223 kcal/mole

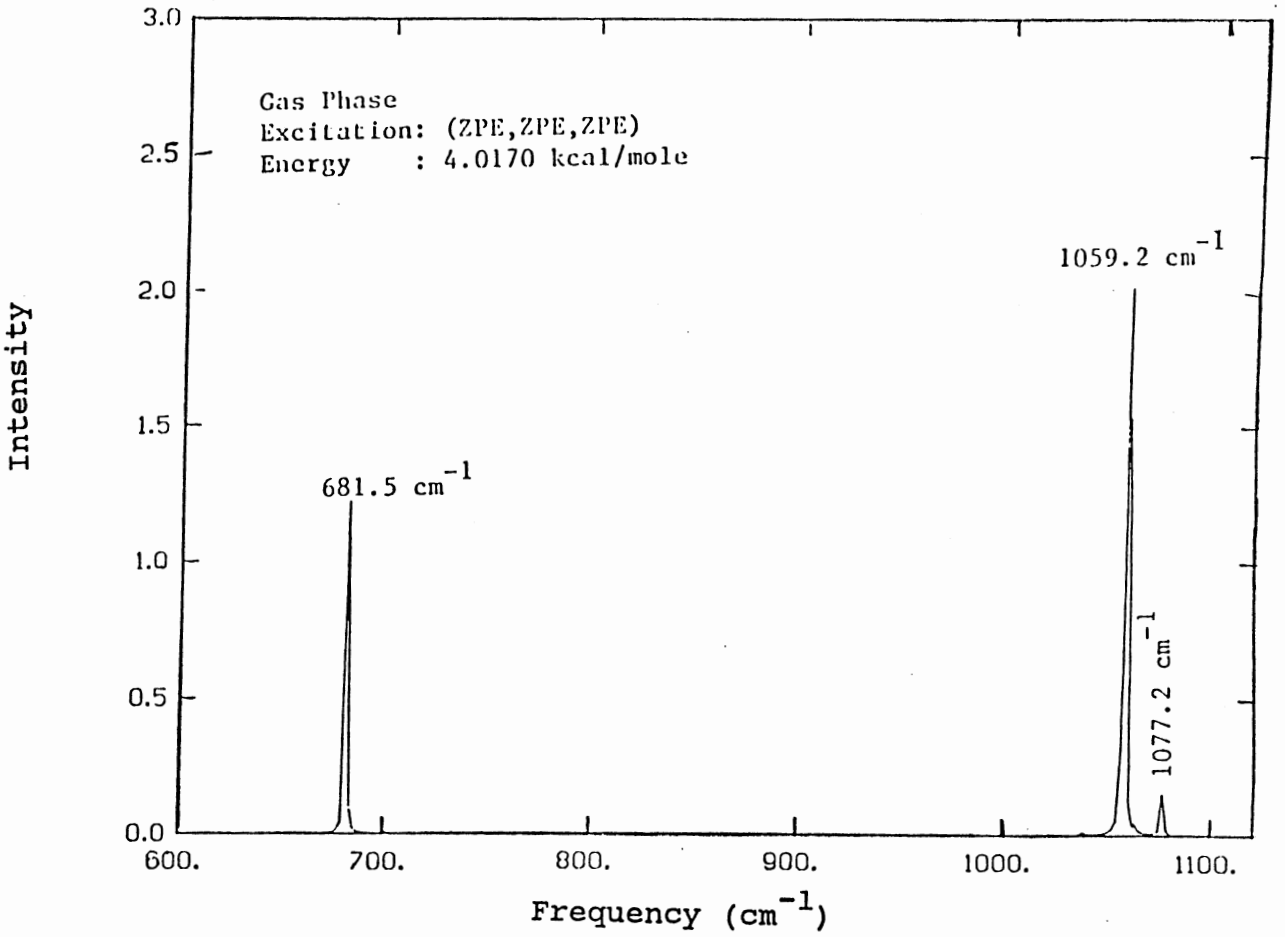

Figure 9. Power spectrum of ozone - E = 4.0170 kcal/mole

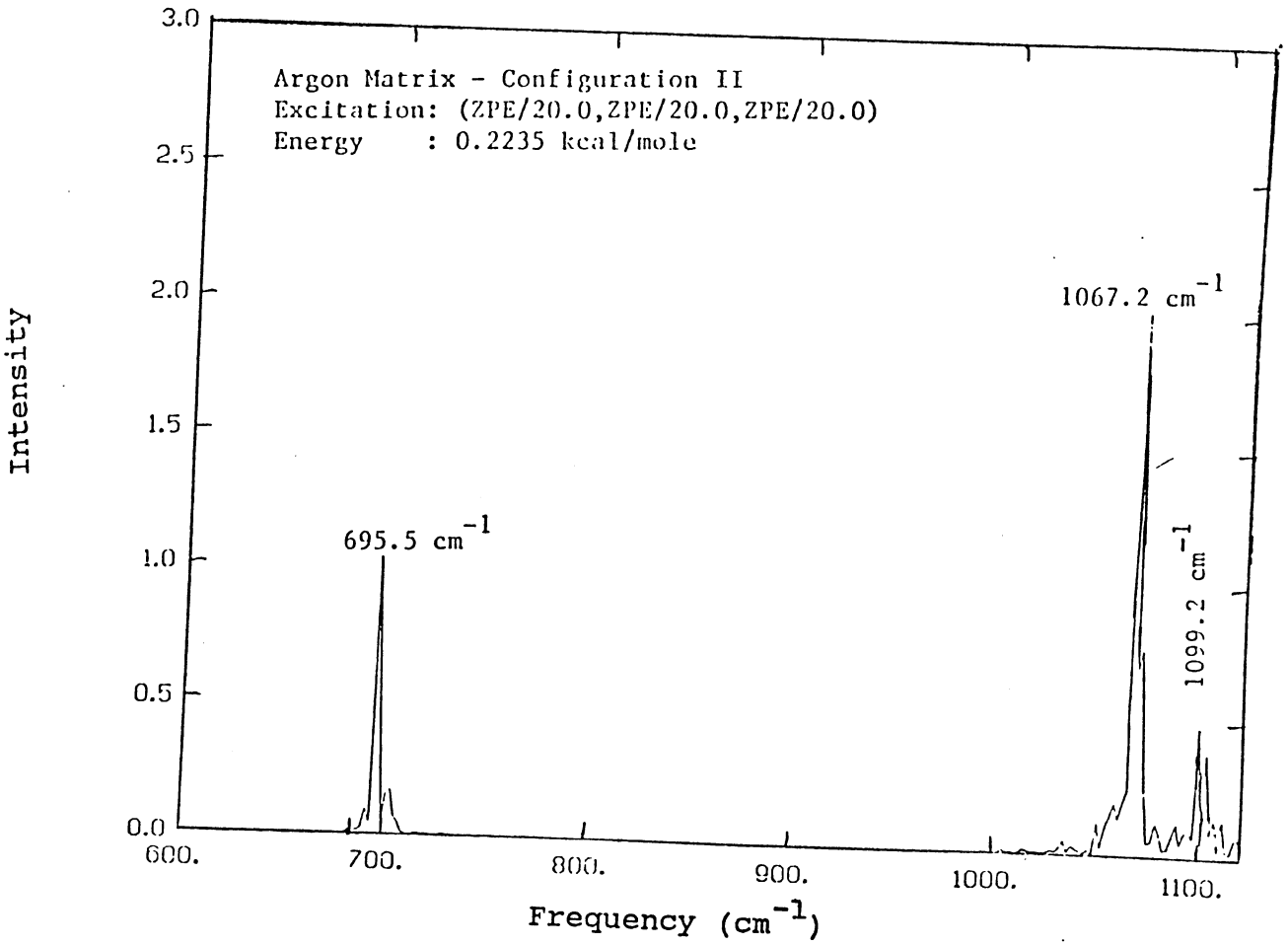

Figure 10. Power spectrum of ozone - E = 0.2235 kcal/mole

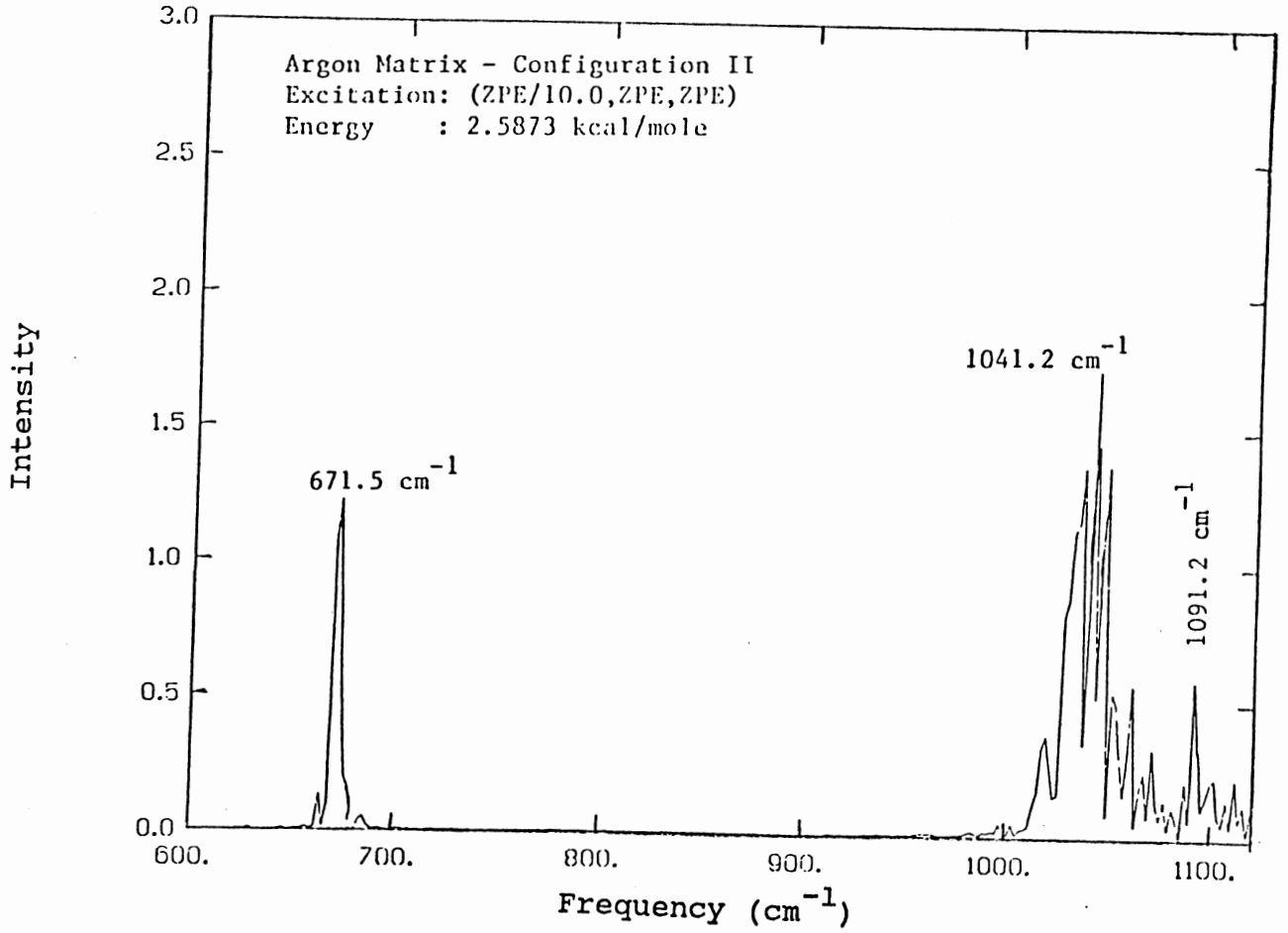

Figure 11. Power spectrum of ozone - E = 2.5873 kcal/mole

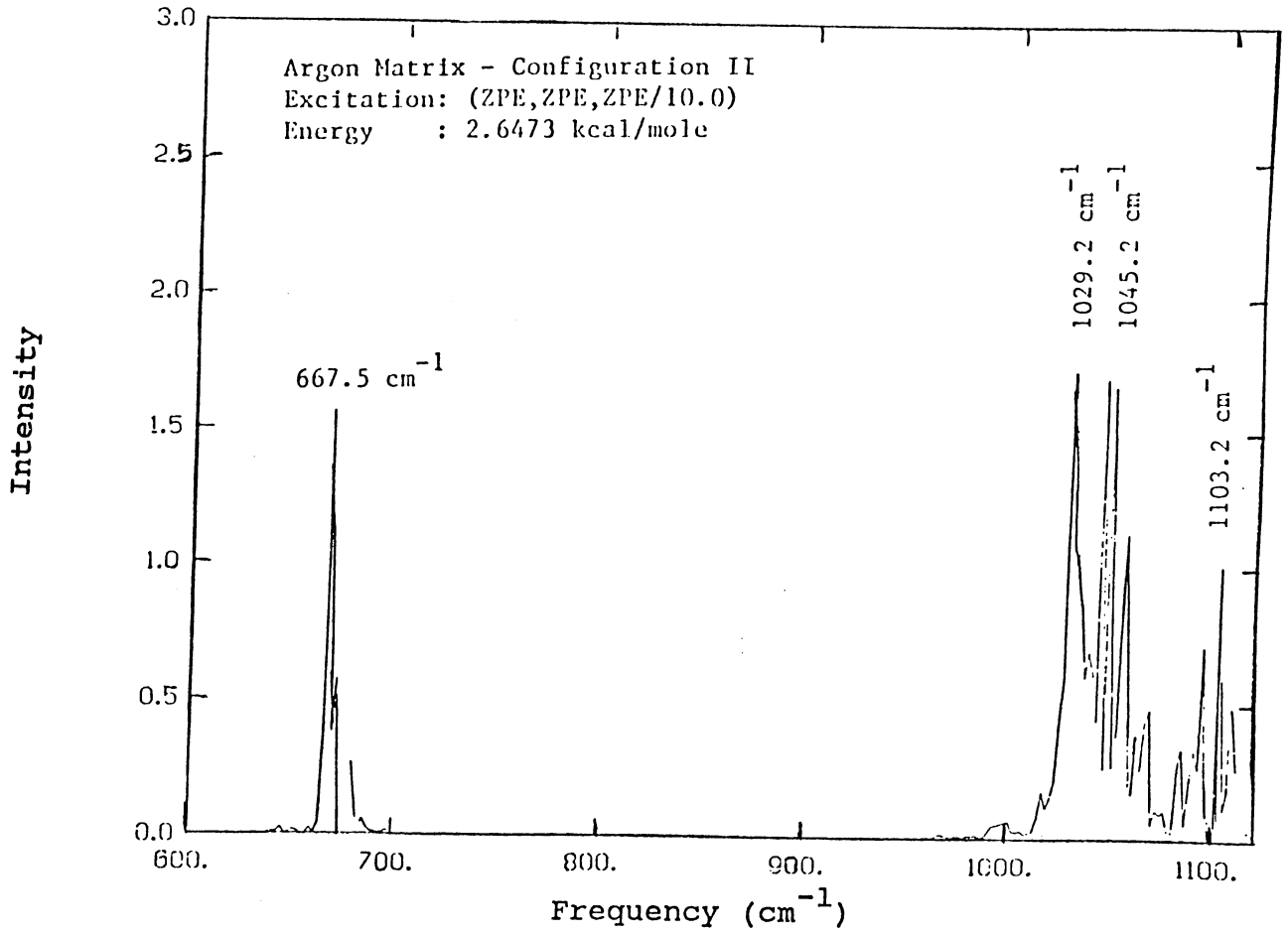

Figure 12. Power spectrum of ozone - E = 2.6473 kcal/mole

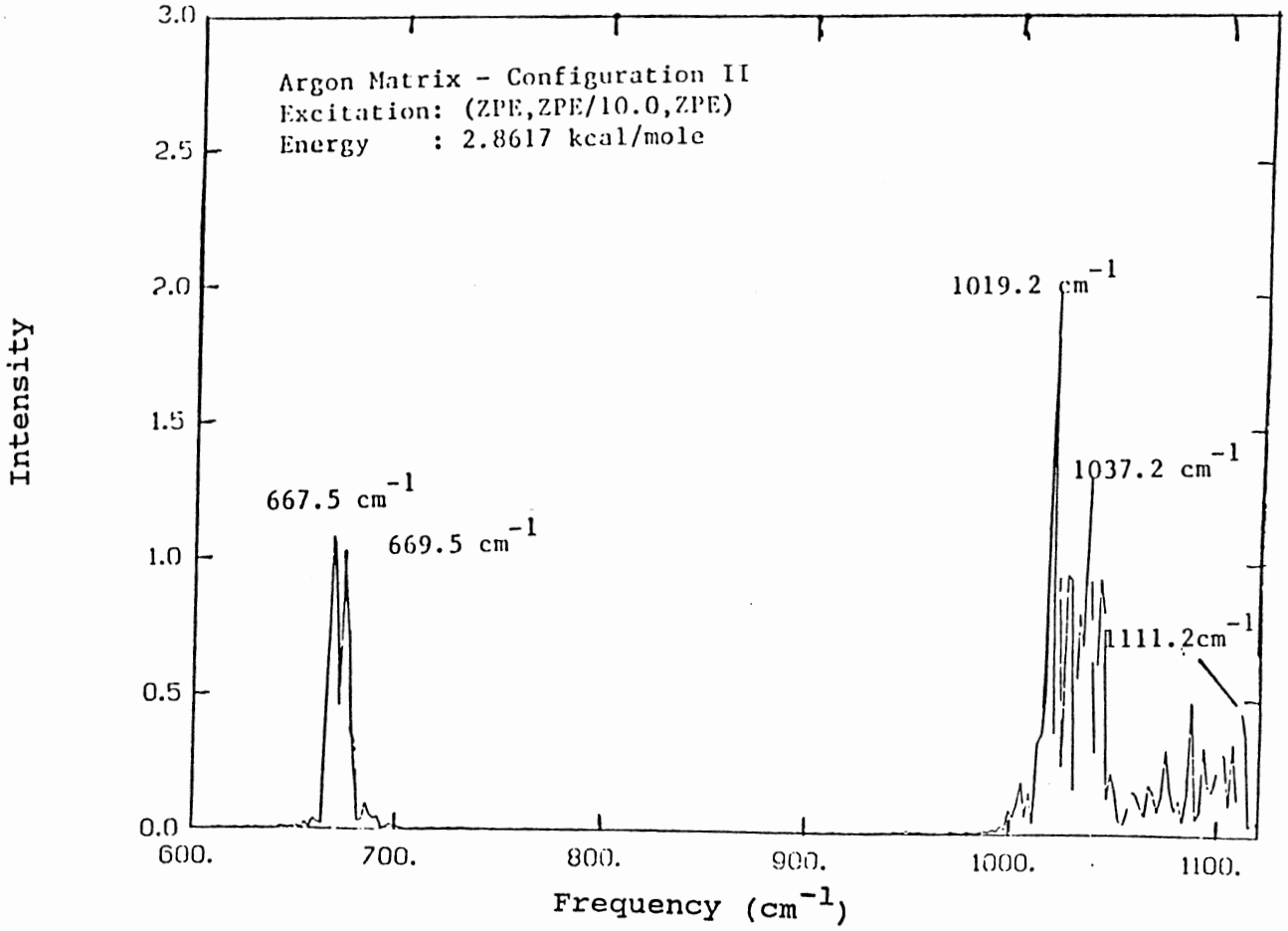

Figure 13. Power spectrum of ozone - E = 2.8617 kcal/mole

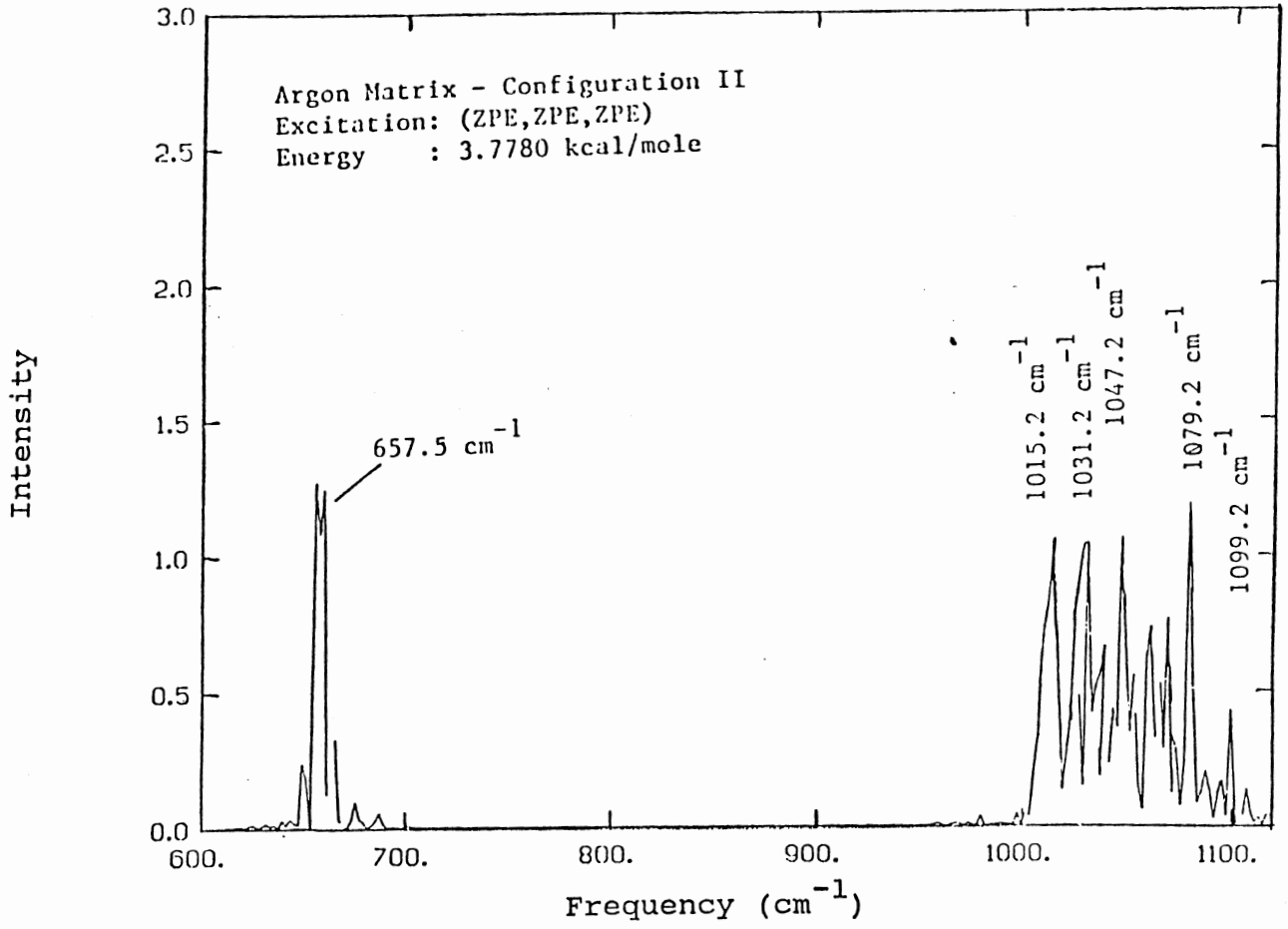

Figure 14. Power spectrum of ozone - E = 3.7780 kcal/mole

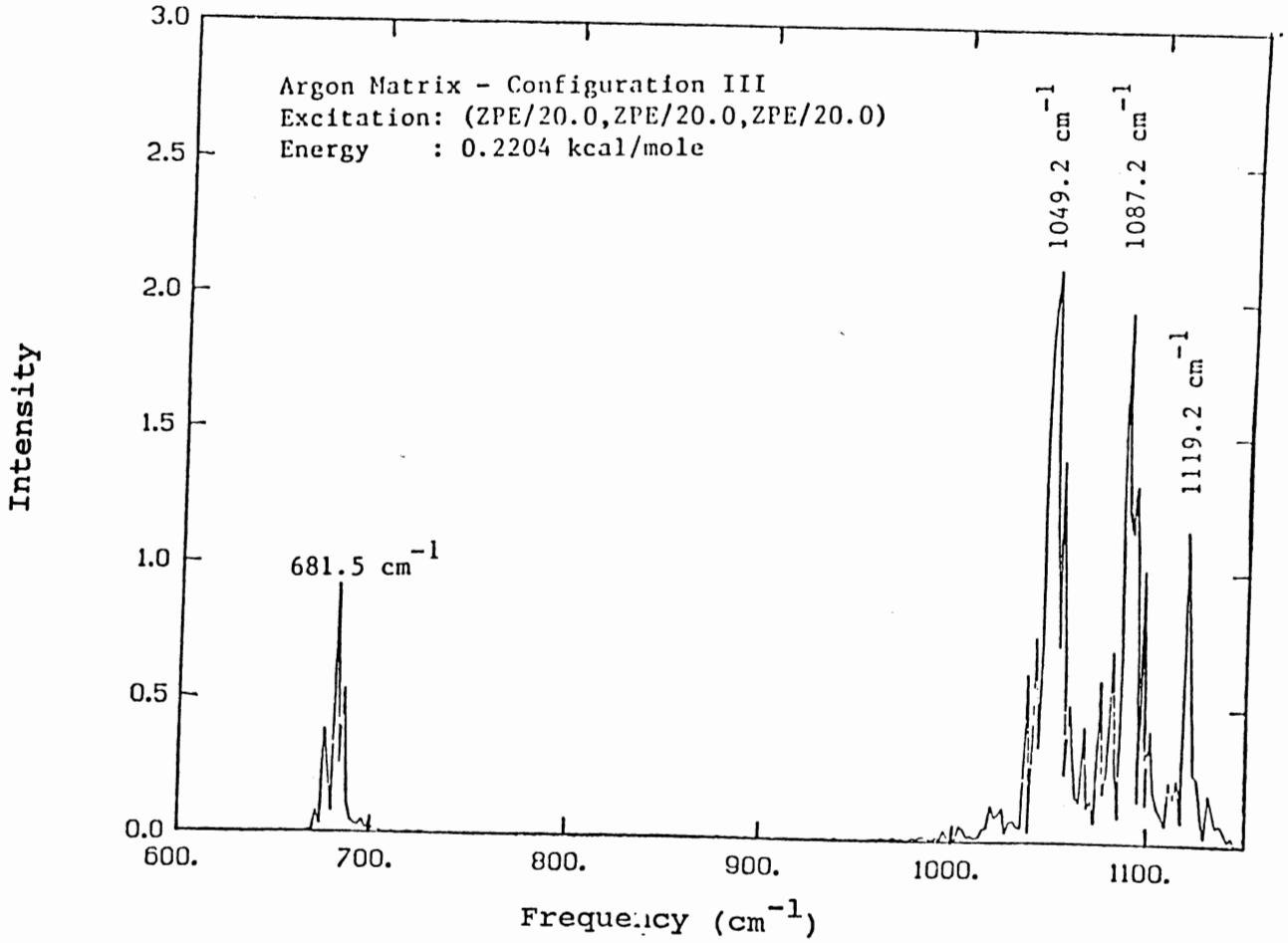

Figure 15. Power spectrum of ozone - E = 0.2204 kcal/mole

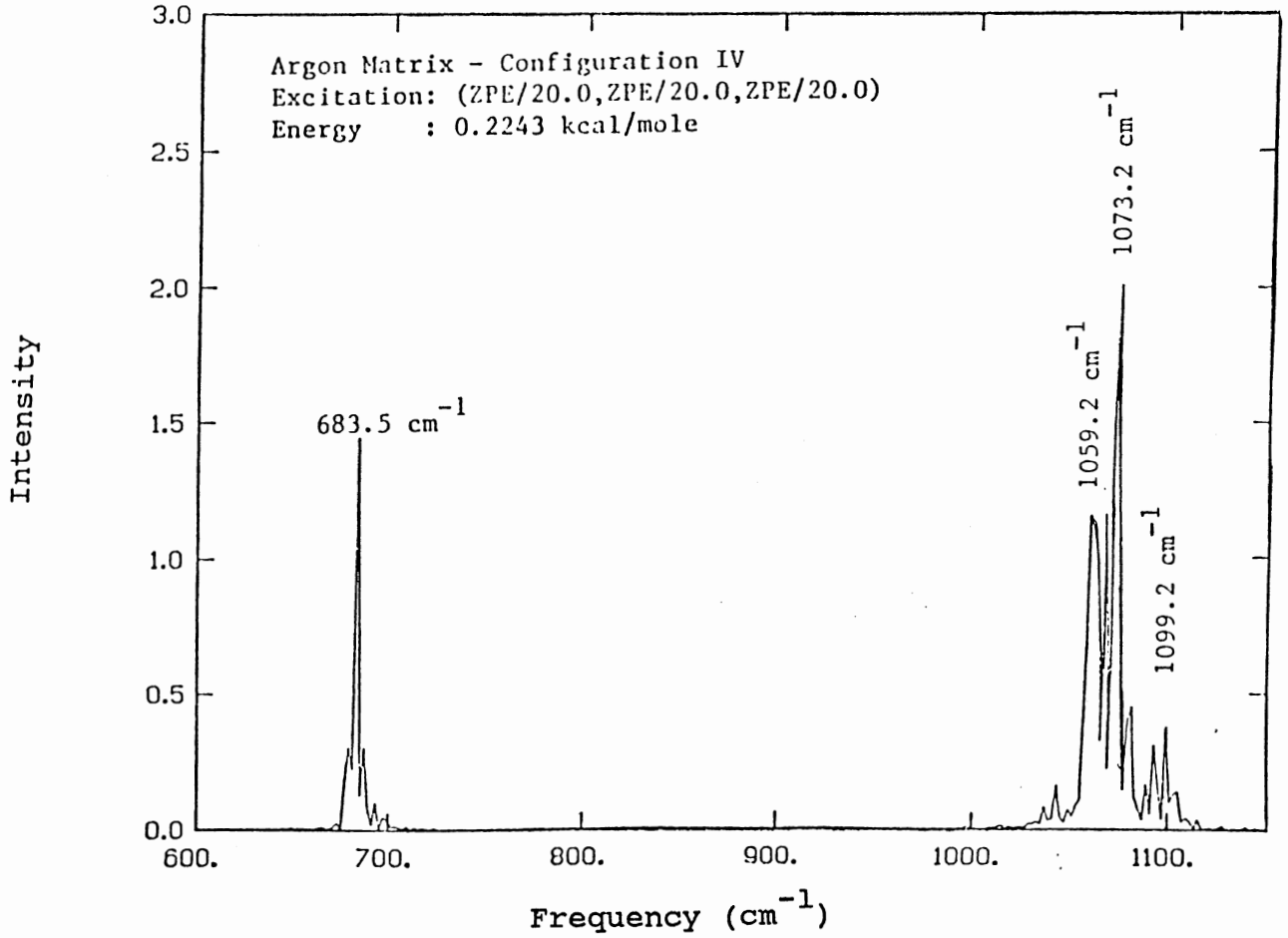

Figure 16. Power spectrum of ozone - E = 0.2243 kcal/mole

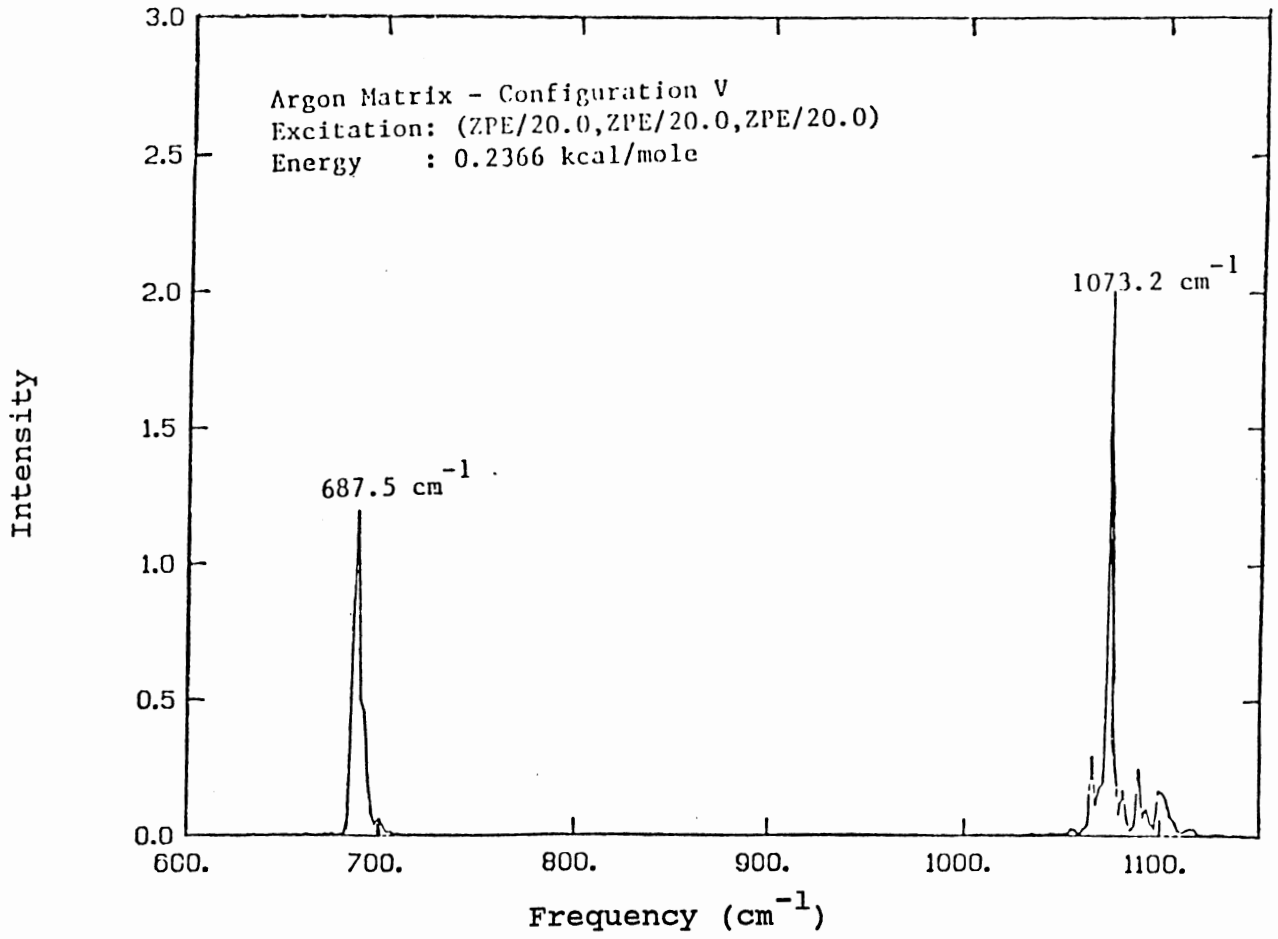

Figure 17. Power spectrum of ozone - E = 0.2366 kcal/mole

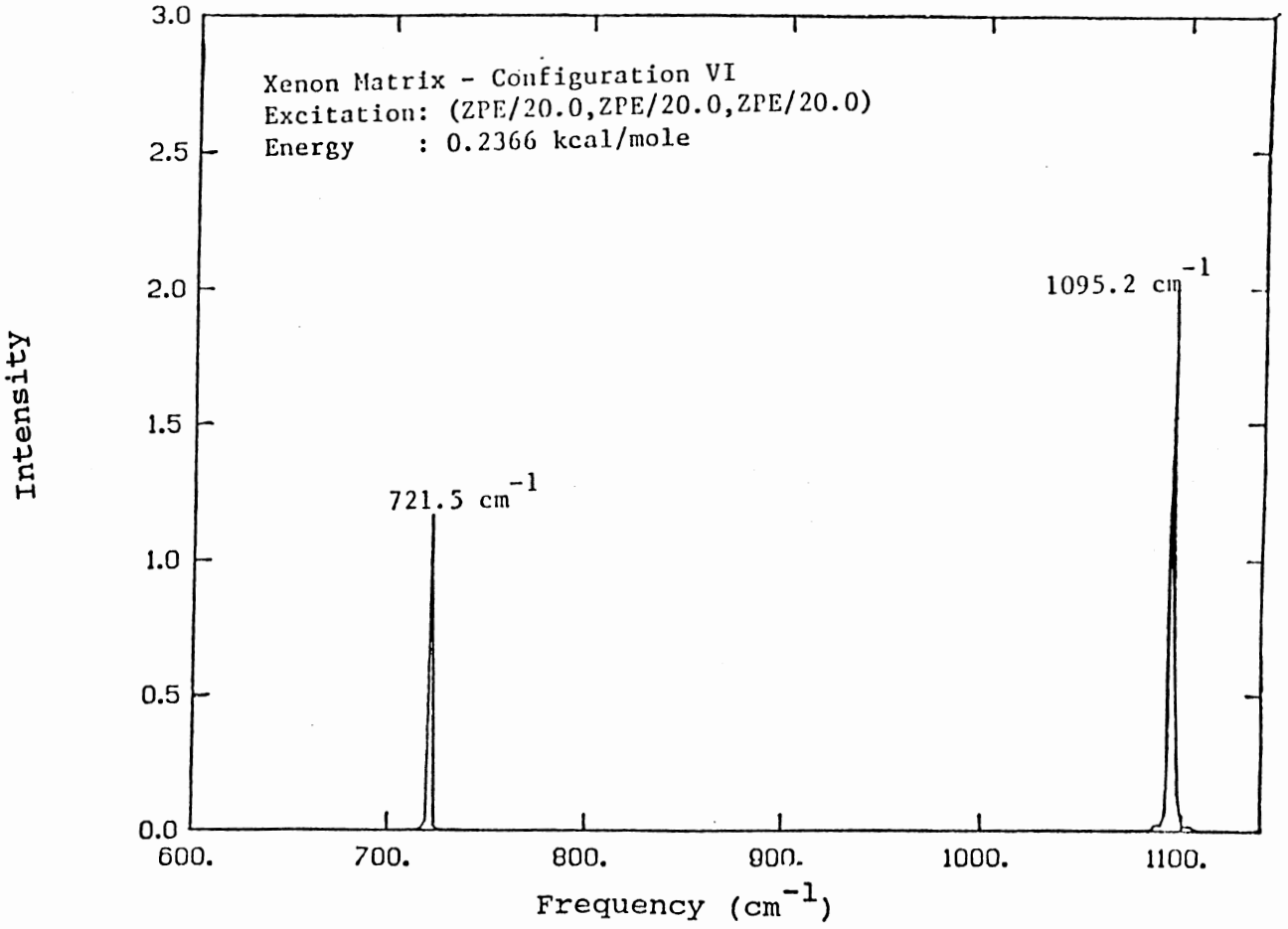

Figure 18. Power spectrum of ozone - E = 0.2366 kcal/mole

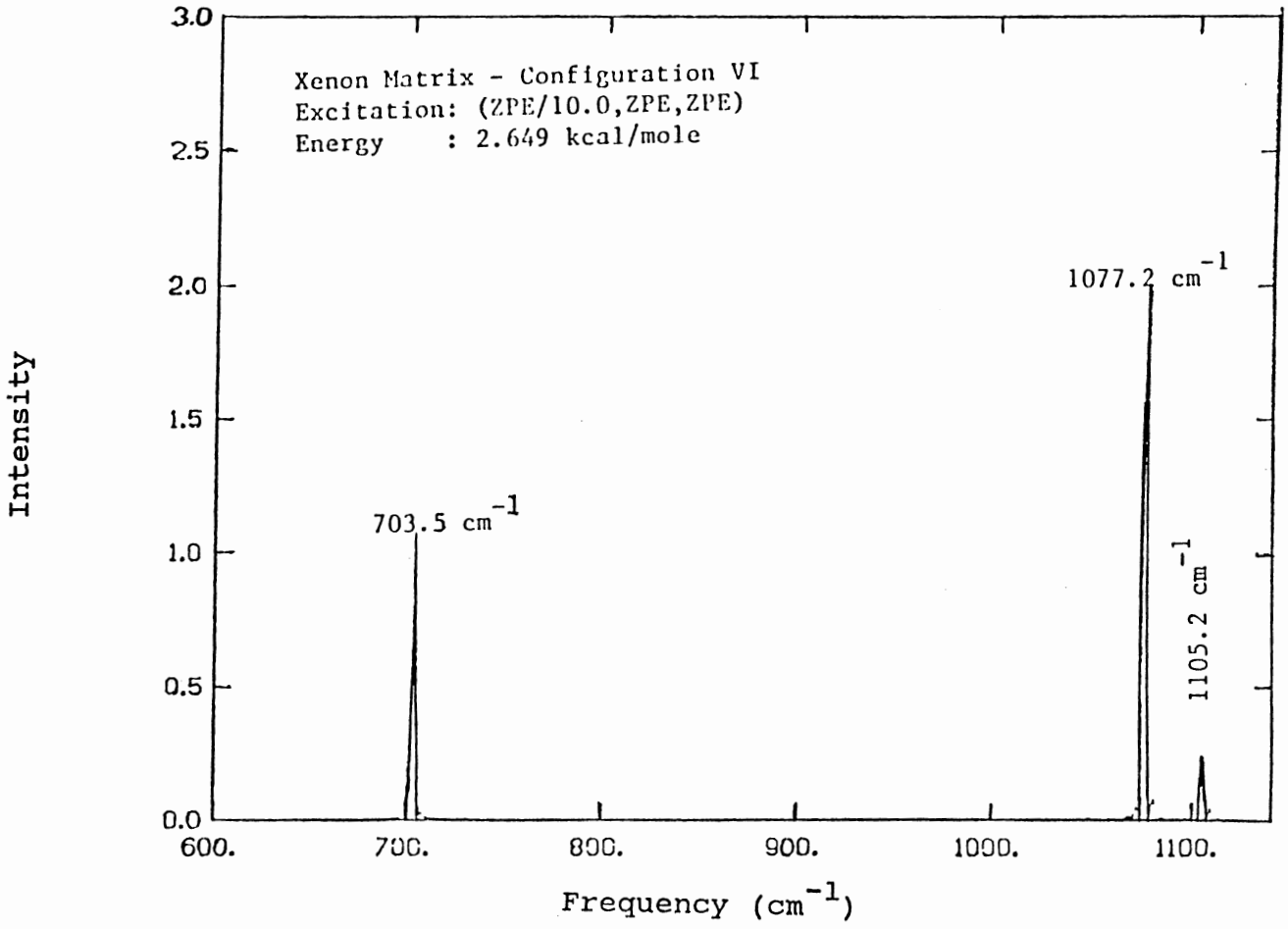

Figure 19. Power spectrum of ozone - E = 2.649 kcal/mole

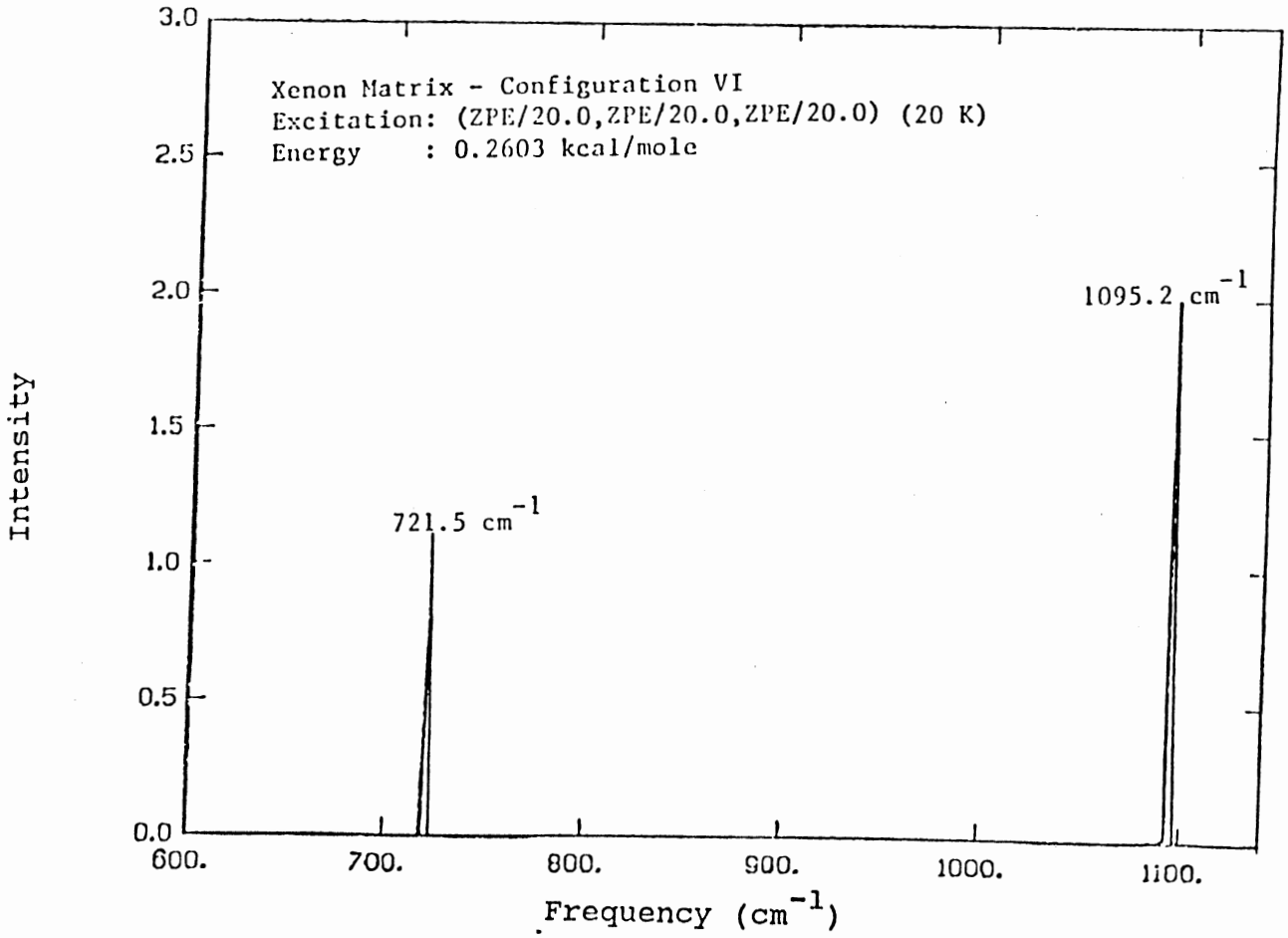

Figure 20. Power spectrum of ozone - E = 0.2603 kcal/mole

TABLE VI

CALCULATED FREQUENCIES OF OZONE IN ARGON, XENON MATRICES AT 12 K

Energy in ozone (kcal/mole)	Distribution	Peak position (cm^{-1})
	I. Gas Phase	
0.2008	ZPE/20,ZPE/20,ZPE/20	715.5, 1089.2
2.6138	ZPE/10,ZPE,ZPE	697.5, 1071.2, 1095.2
2.6980	ZPE,ZPE,ZPE/10	689.5, 1065.2, 1095.2
3.1223	ZPE,ZPE/10,ZPE	693.5, 1065.2, 1087.2
4.0170	ZPE,ZPE,ZPE	681.5, 1059.2, 1077.2
	II.1.Argon Matrix - Configuration II	
0.2235	ZPE/20,ZPE/20,ZPE/20	695.5, 1067.2, 1099.2
2.5873	ZPE/10,ZPE,ZPE	671.5, 1041.2, 1091.2
2.6473	ZPE,ZPE,ZPE/10	667.5, 1029.2, 1045.2, 1103.2
2.8617	ZPE,ZPE/10,ZPE	667.5, 669.5, 1019.2, 1037.2, 1111.2
3.7780	ZPE,ZPE,ZPE	657.5, 1015.2, 1031.2, 1047.2, 1079.2, 1099.2
	II.2.Argon Matrix - Configuration III	
0.2204	ZPE/20,ZPE/20,ZPE/20	681.5, 1040.2, 1087.2, 1119.2
	II.3.Argon Matrix - Configuration IV	
0.2243	ZPE/20,ZPE/20,ZPE/20	683.5, 1059.2, 1073.2, 1099.2
	II.4.Argon Matrix - Configuration V	
0.2366	ZPE/20,ZPE/20,ZPE/20	687.5, 1073.2
	III. Xenon Matrix - Configuration VI	
0.2366	ZPE/20,ZPE/20,ZPE/20	721.5, 1095.2
2.649	ZPE/10, ZPE, ZPE	703.5, 1077.2, 1105.2
0.2603	(ZPE/10,ZPE/20,ZPE/20)*	721.5, 1095.2

* Temperature is 20 K

complicated power spectra. In addition, power spectrum obtained for configuration V, which corresponds to a stable configuration has sharp peaks as seen in the gas-phase.

C. Vibrational energy transfer of ozone

The observed vibrational energy transfer rates of ozone on configurations I through VI are given in Tables VII-X. Similar results for the xenon matrix is given in Table XIV. Figures 21-58 show the corresponding first-order decay plots for vibrational energy transfer (V.E.T.) in argon and xenon matrices. In these plots, E_0 is the total energy in ozone at time t=0 and E_t is the same at time t. Each point on these decay plots is the average of 25 trajectories carried out for that configuration. The straight lines are least-square fits to the trajectory data. Error limits on the rate coefficients derived from the slope of these lines are given by equations (31-35). Furthermore, the notation (10,0,0);12;Ar;MS;1.4;XZ denotes the excitation, temperature, matrix material, stable/ metastable configuration, density and the initial starting plane of ozone, respectively. (Also, in all these plots, there exists a point at 0.0 on the y-axis)

In 1986, Arnold and coworkers (43) studied the dynamics of planar and transvers O_3.NO complex upon

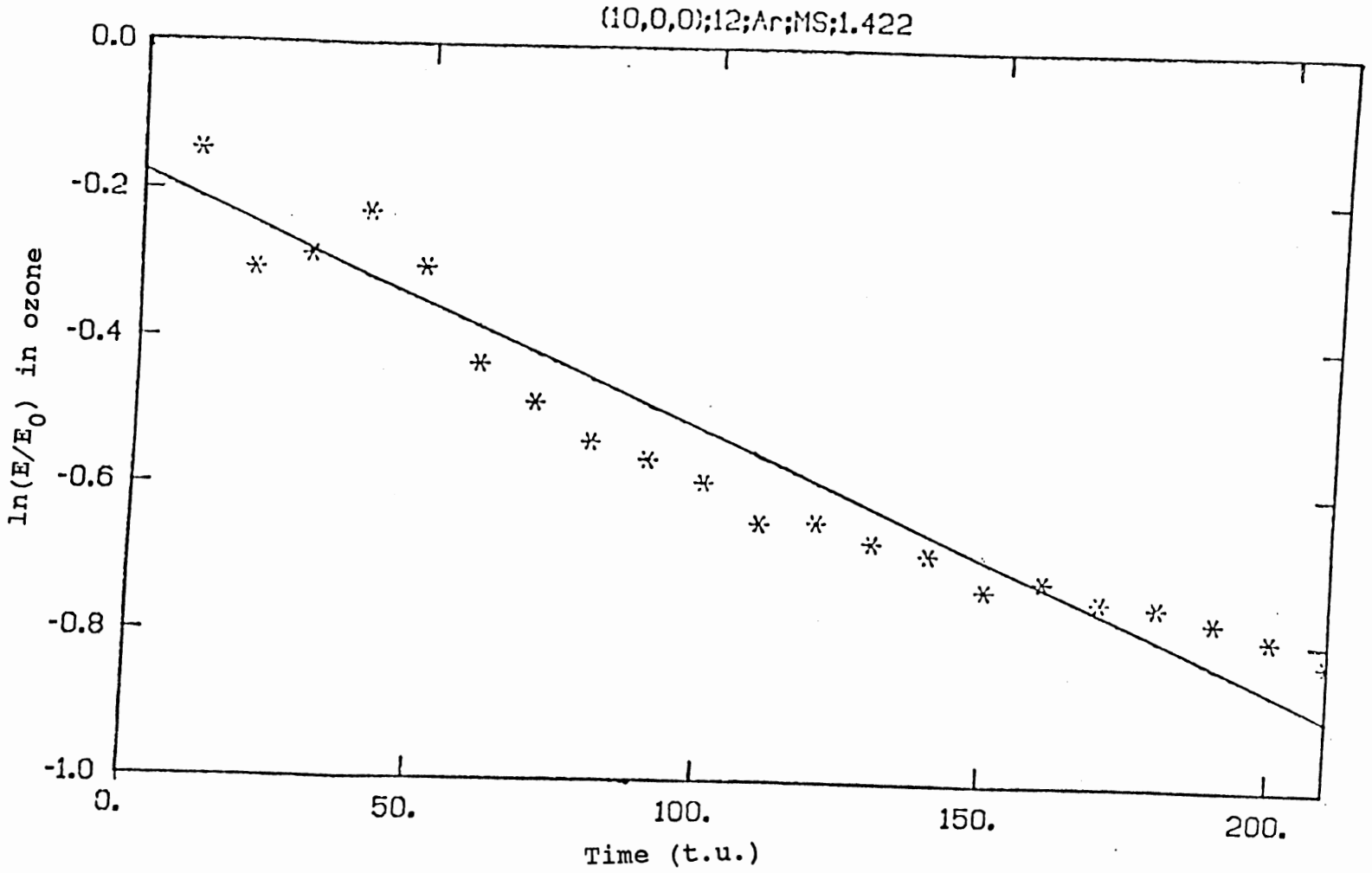

Figure 21. V.E.T. of ozone - (10,0,0);12;Ar;MS;1.422;XZ

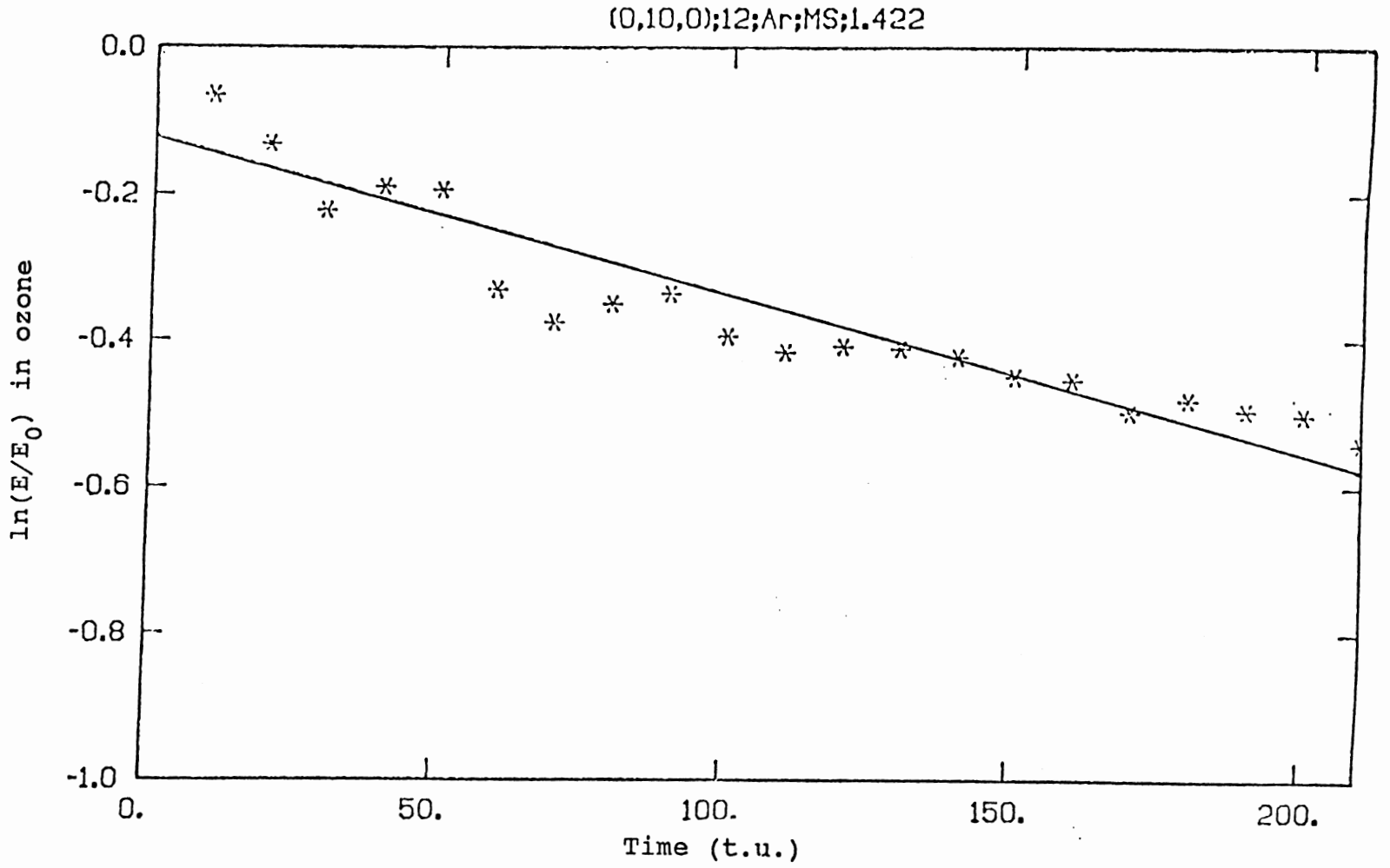

Figure 22. V.E.T. of ozone - (0,10,0);12;Ar;MS;1.422;XZ

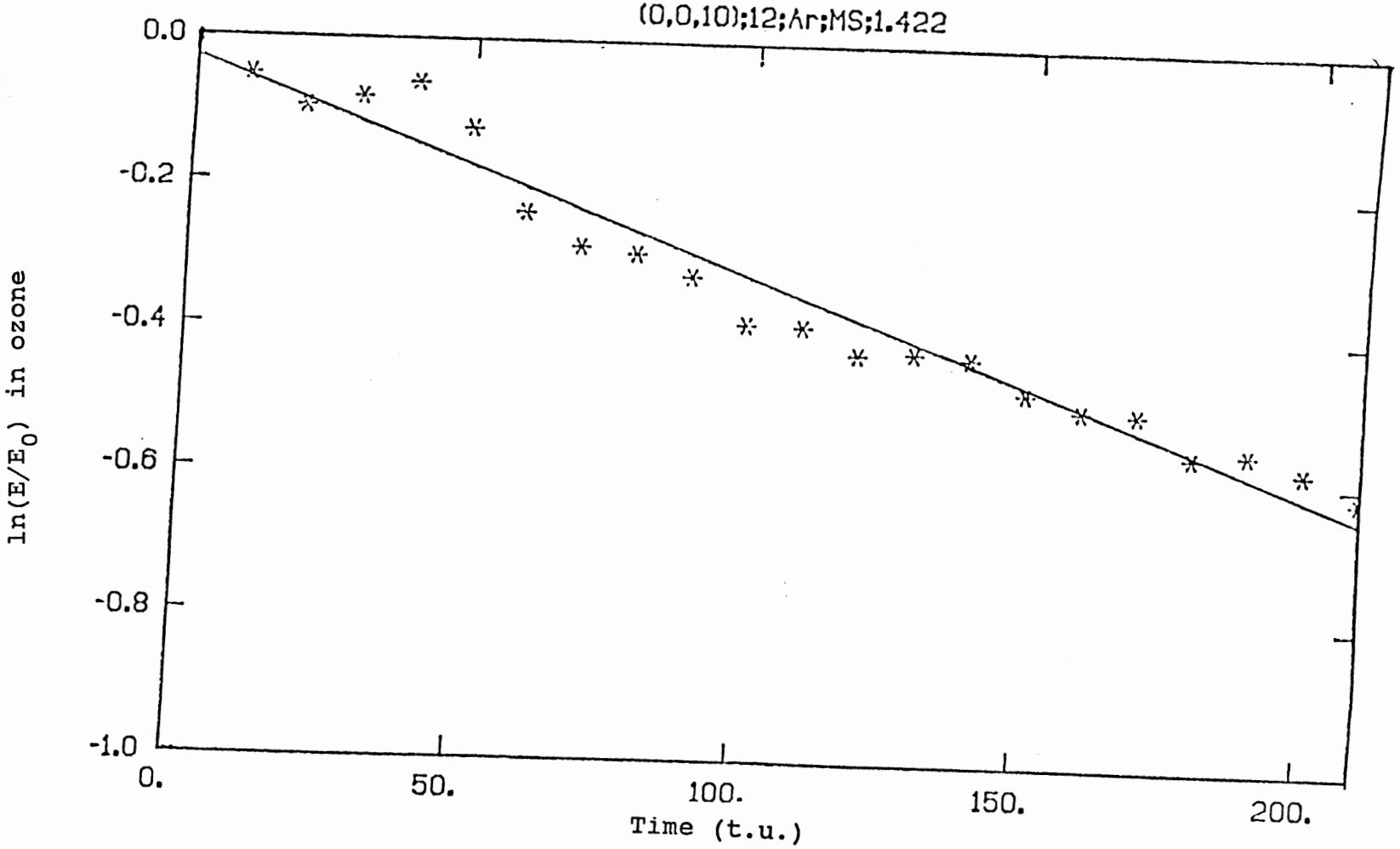

Figure 23. V.E.T. of ozone - (0,0,10);12;Ar;MS;1.422;XZ

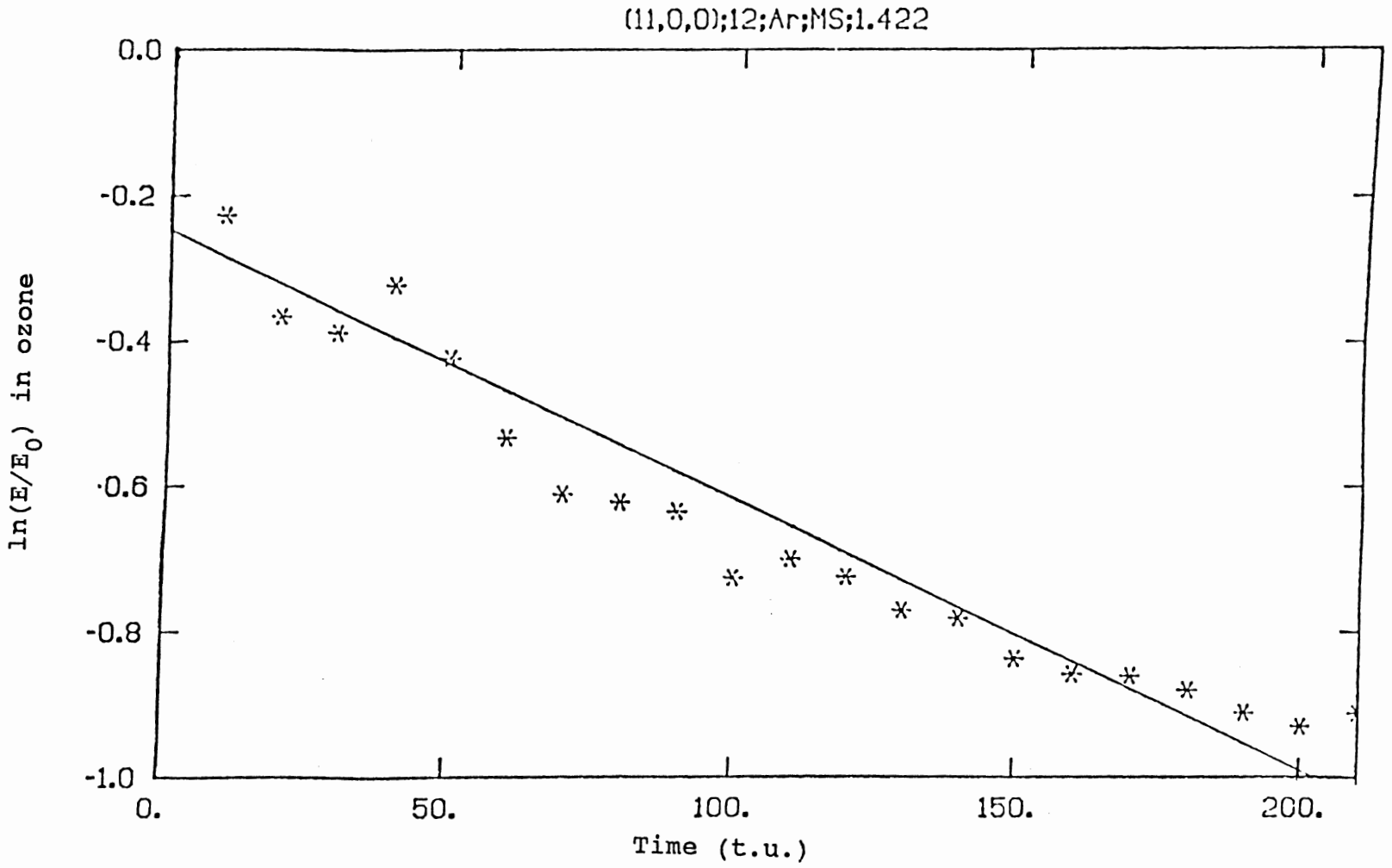

Figure 24. V.E.T. of ozone - (11,0,0);12;Ar;MS;1.422;XZ

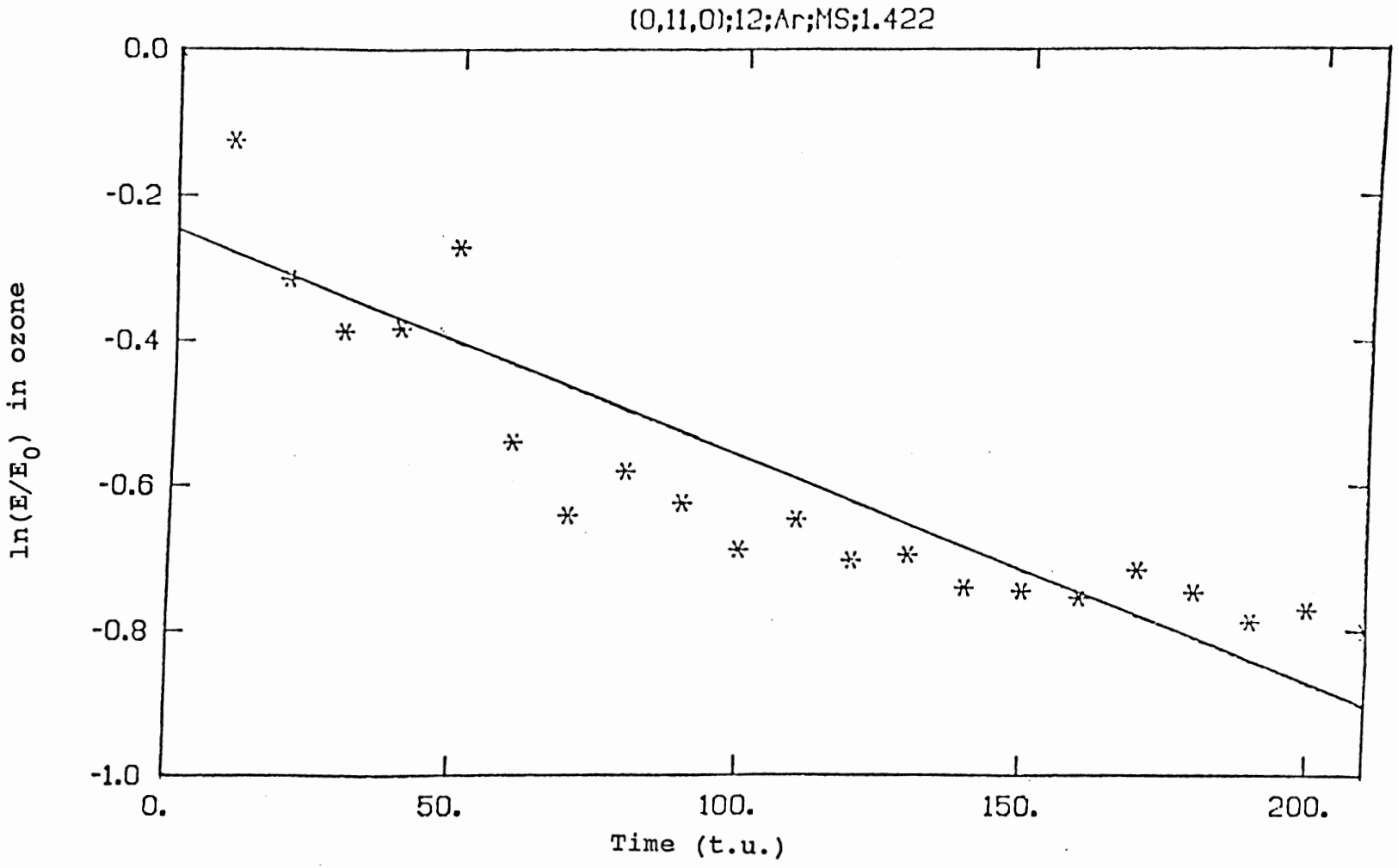

Figure 25. V.E.T. of ozone - (0,11,0);12;Ar;MS;1.422;XZ

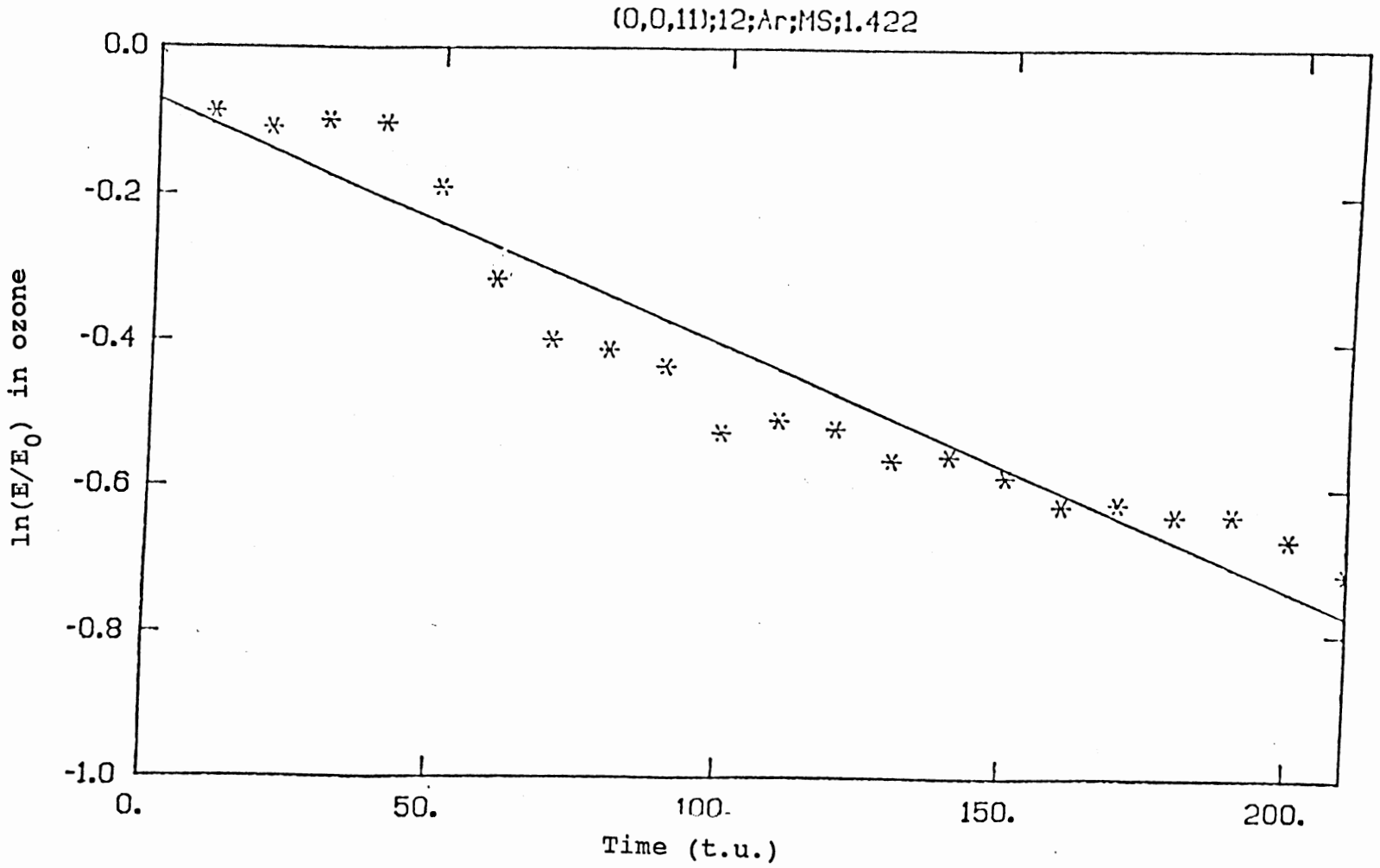

Figure 26. V.E.T. of ozone - (0,0,11);12;Ar;MS;1.422;XZ

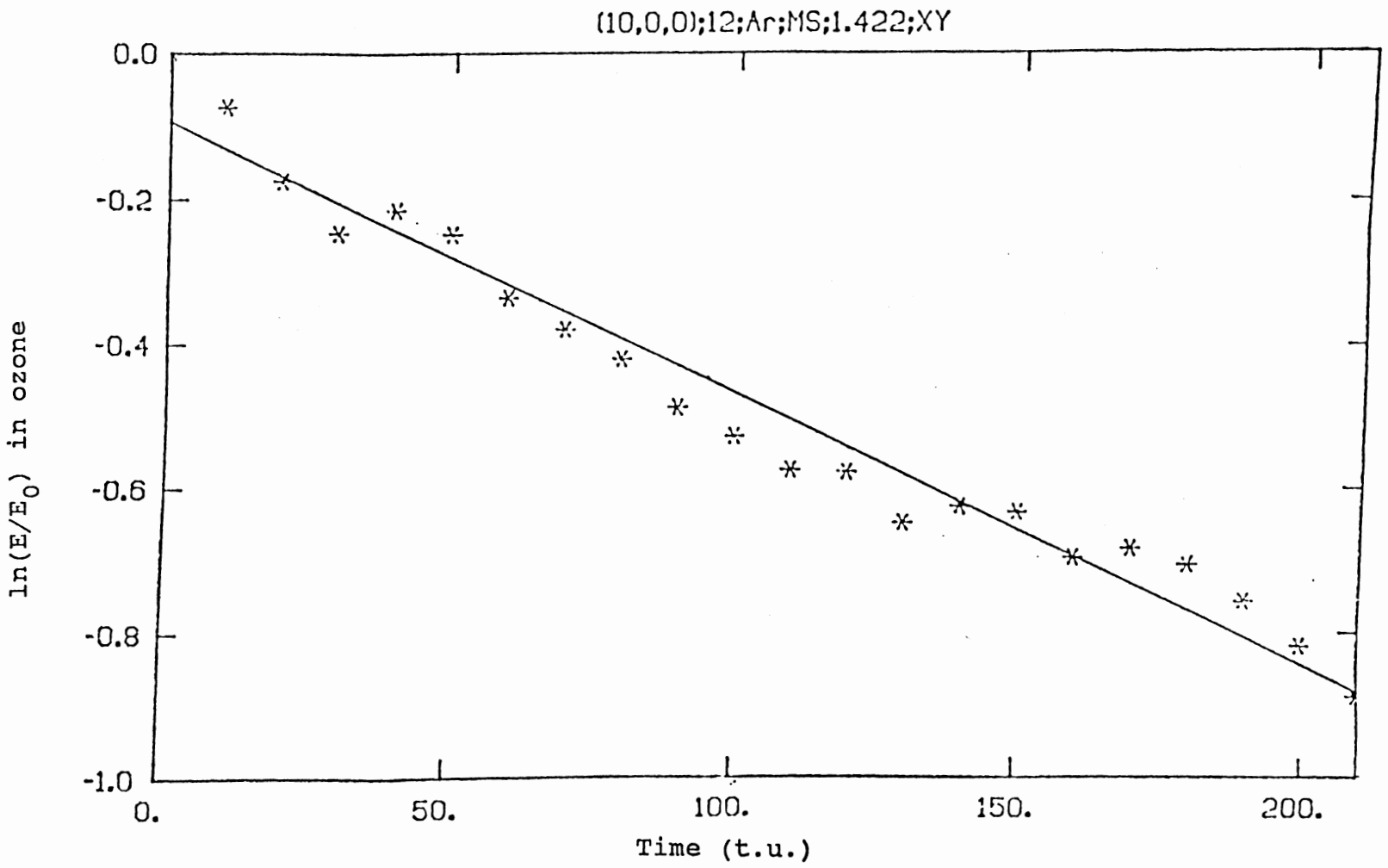

Figure 27. V.E.T. of ozone - (10,0,0);12;Ar;MS;1.422;XY

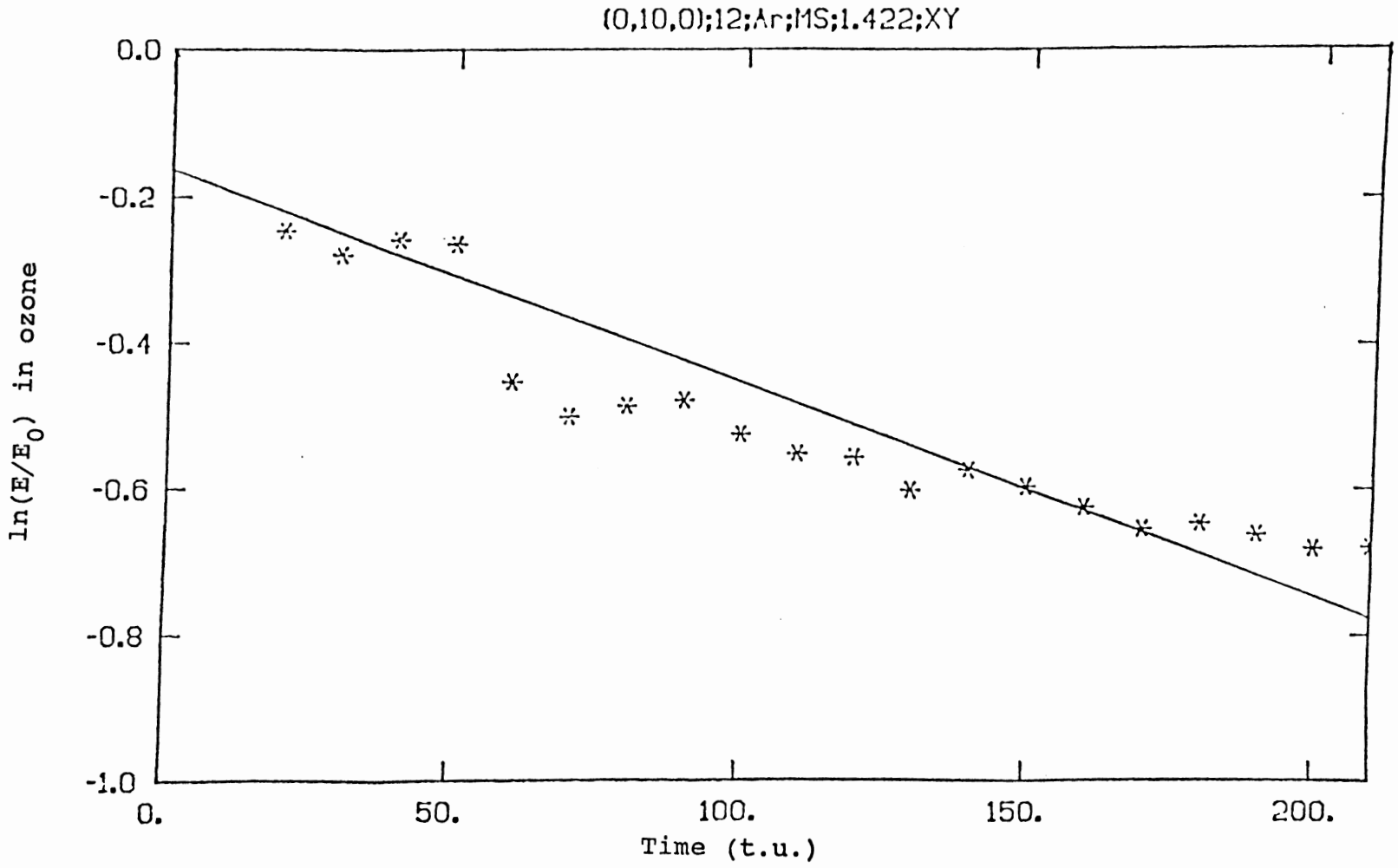

Figure 28. V.E.T. of ozone - (0,10,0);12;Ar;MS;1.422;XY

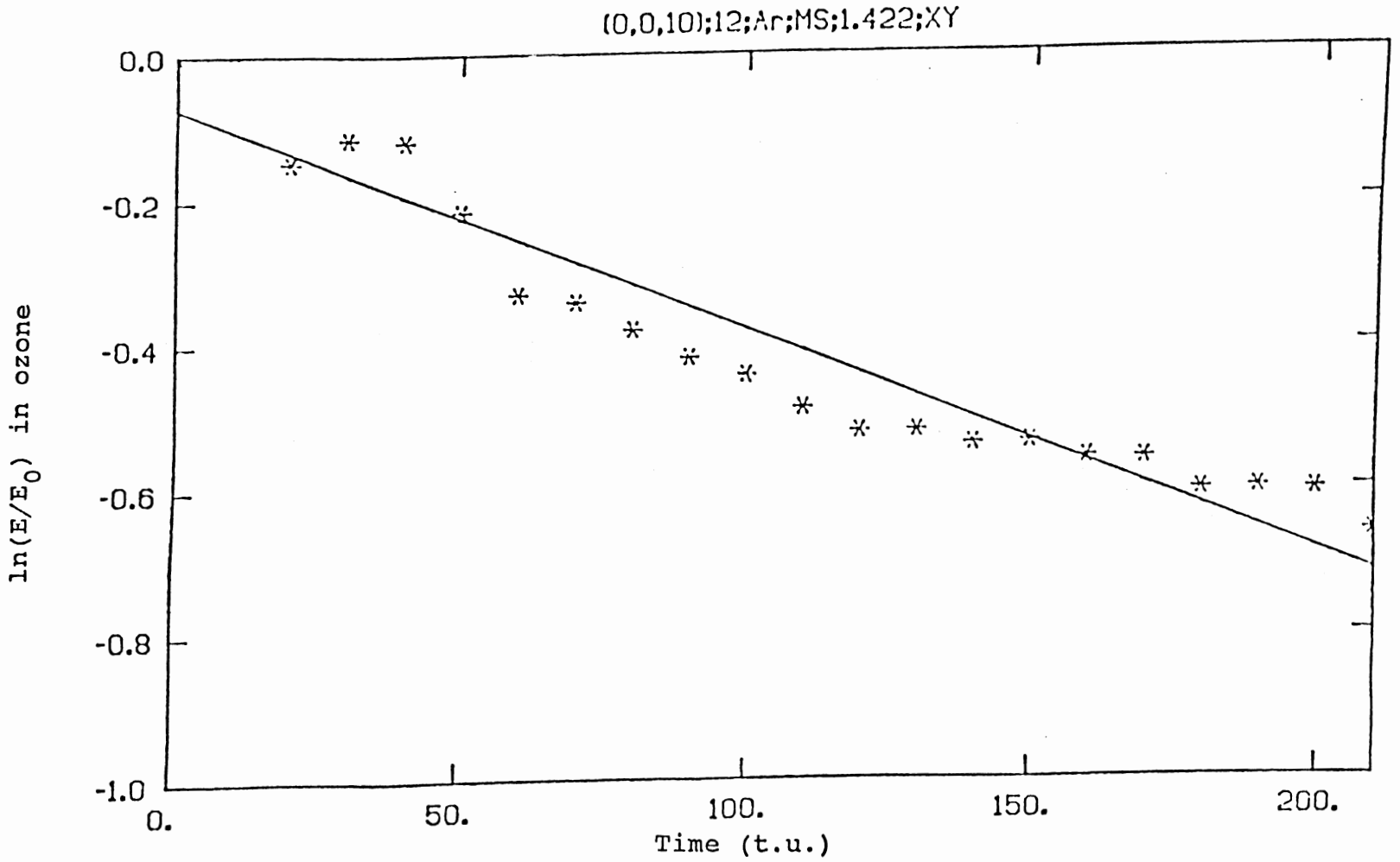

Figure 29. V.E.T. of ozone - (0,0,10);12;Ar;MS;1.422;XY

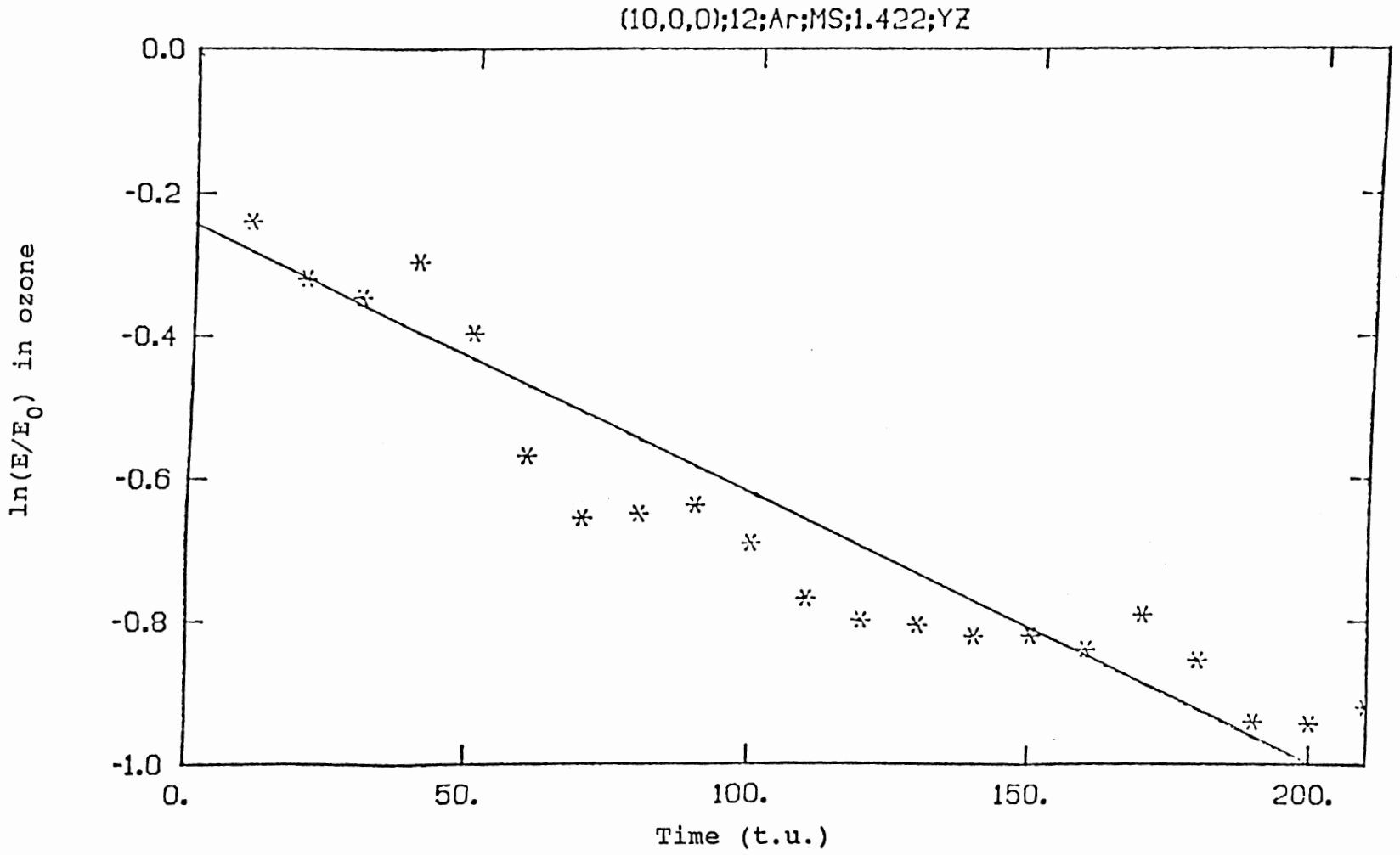

Figure 30. V.E.T. of ozone - (10,0,0);12;Ar;MS;1.422;YZ

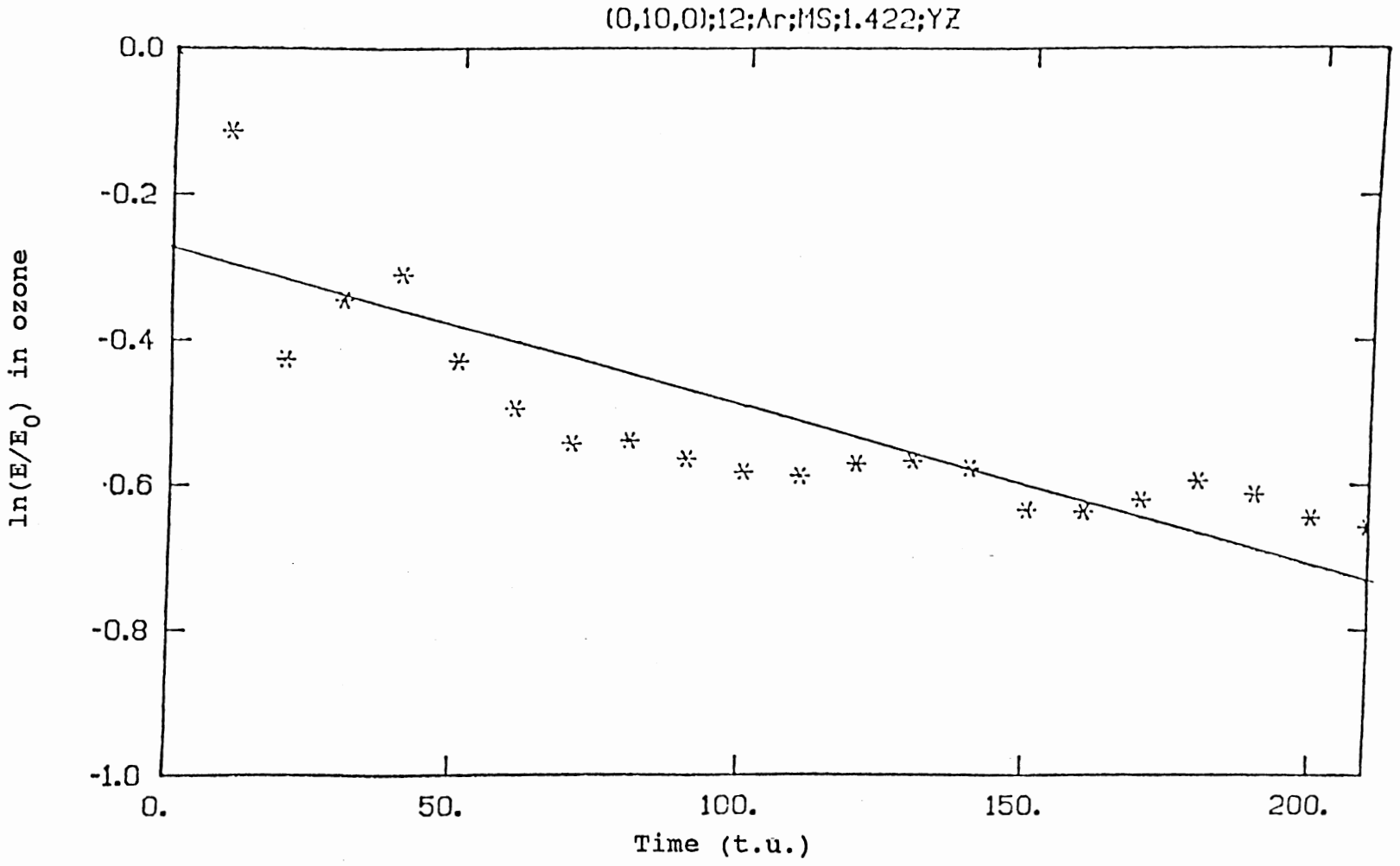

Figure 31. V.E.T. of ozone - (0,10,0);12;Ar;MS;1.422;YZ

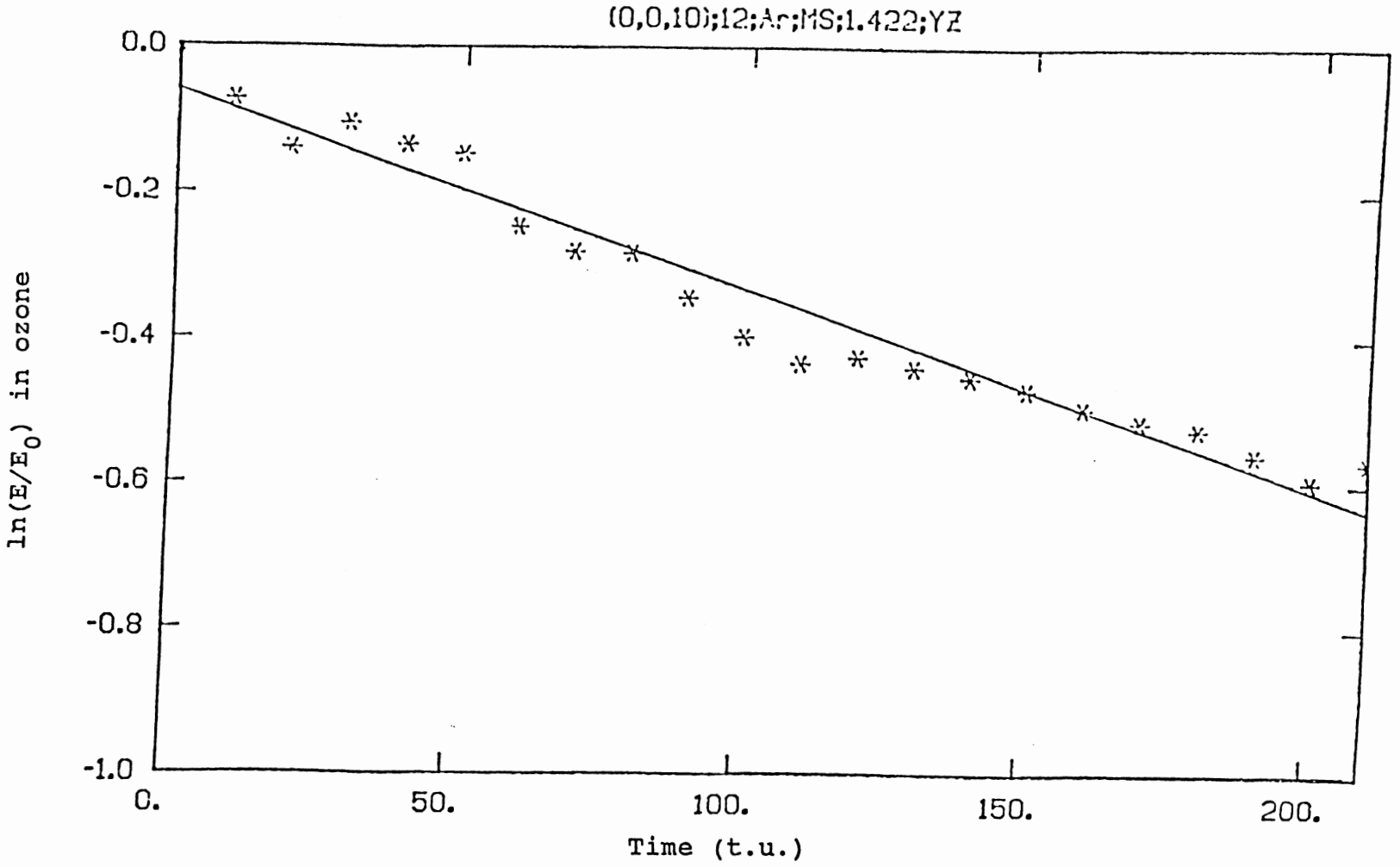

Figure 32. V.E.T. of ozone - (0,0,10);12;Ar;MS;1.422;YZ

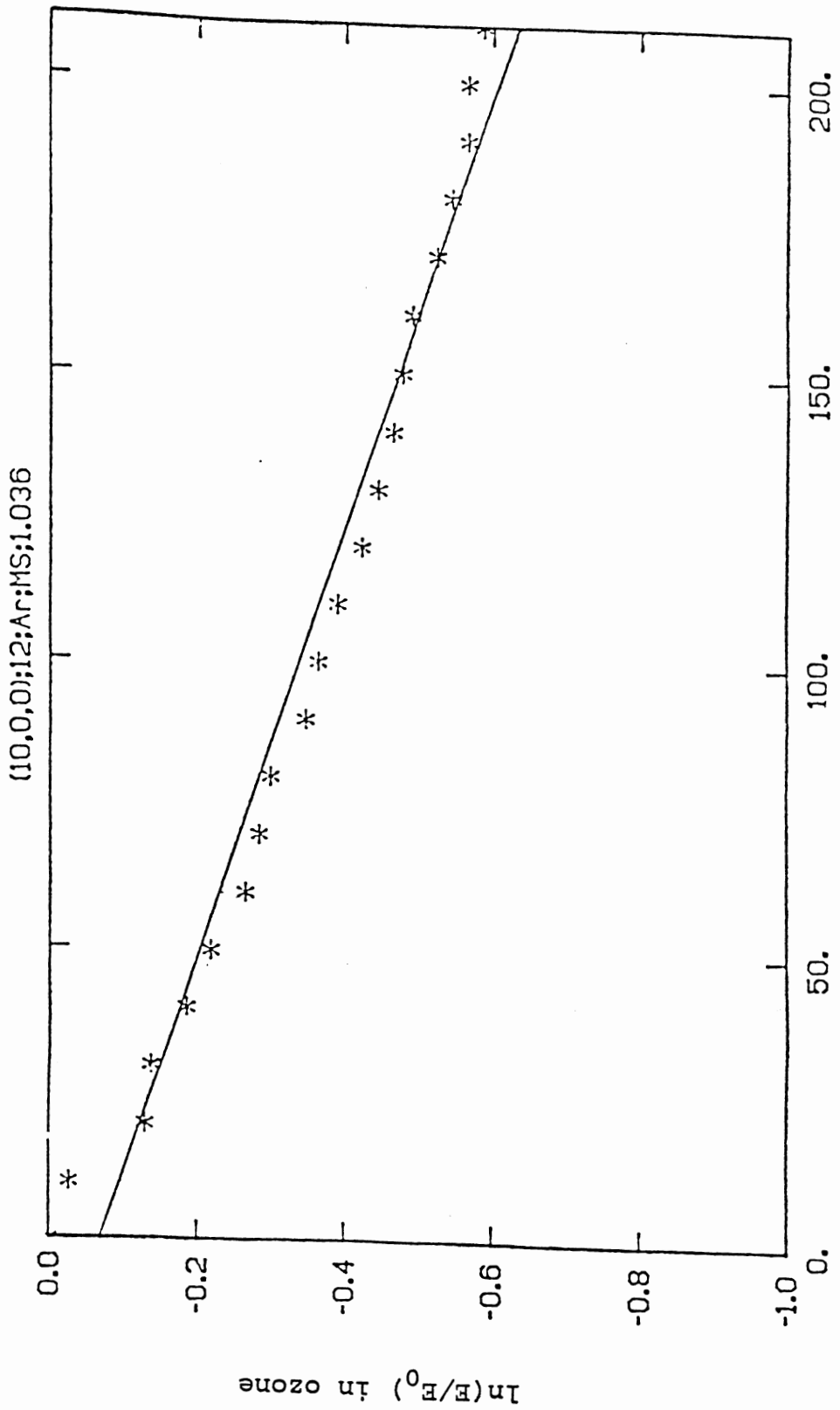

Figure 33. V.E.T. of ozone - (10,0,0);12;Ar;MS;1.036;XZ

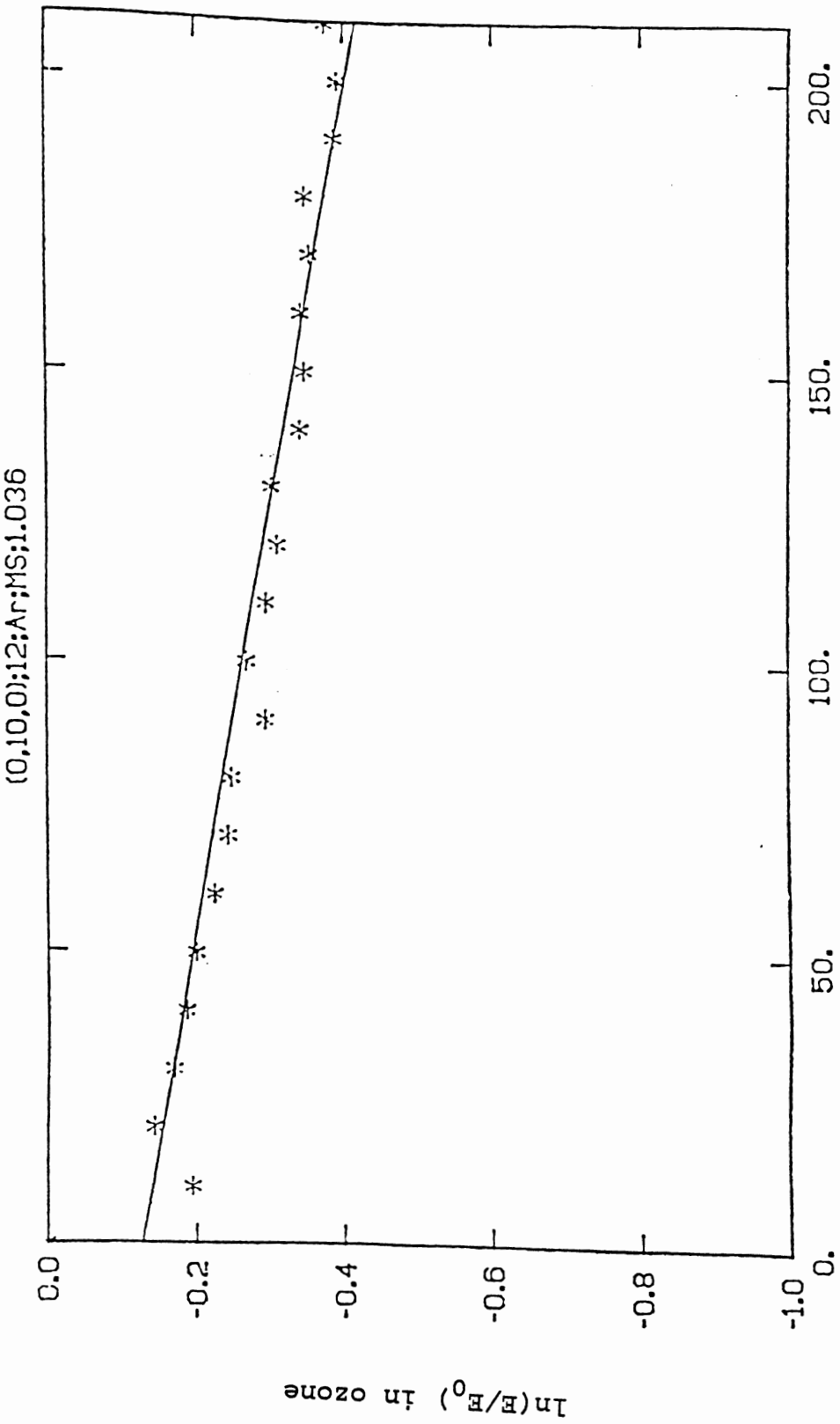

Figure 34. V.E.T. of ozone - (0,10,0);12;Ar;MS;1.036;XZ

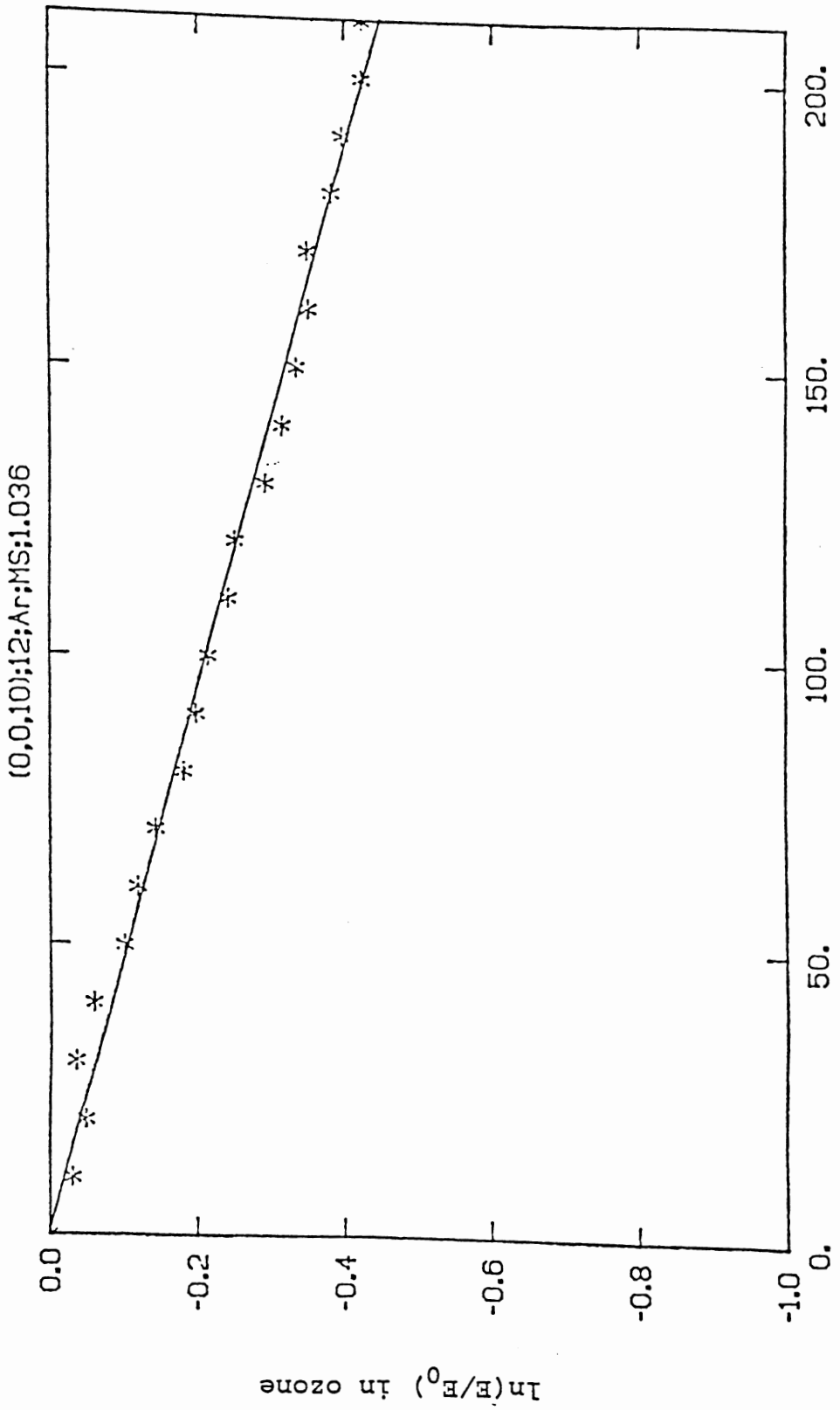

Figure 35. V.E.T. of ozone - (0,0,10);12;Ar;MS;1.036;XZ

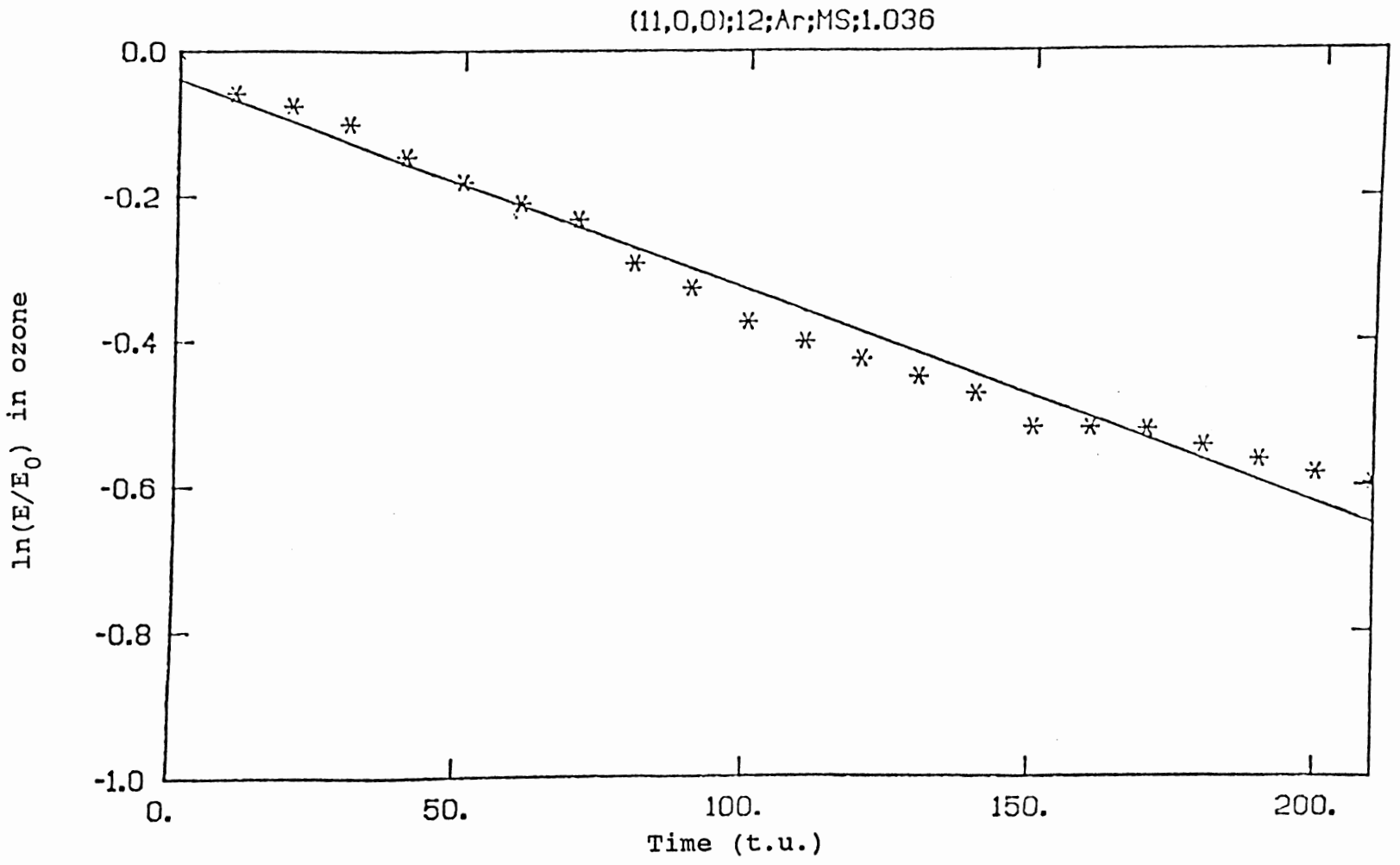

Figure 36. V.E.T. of ozone - (11,0,0);12;Ar;MS;1.036;XZ

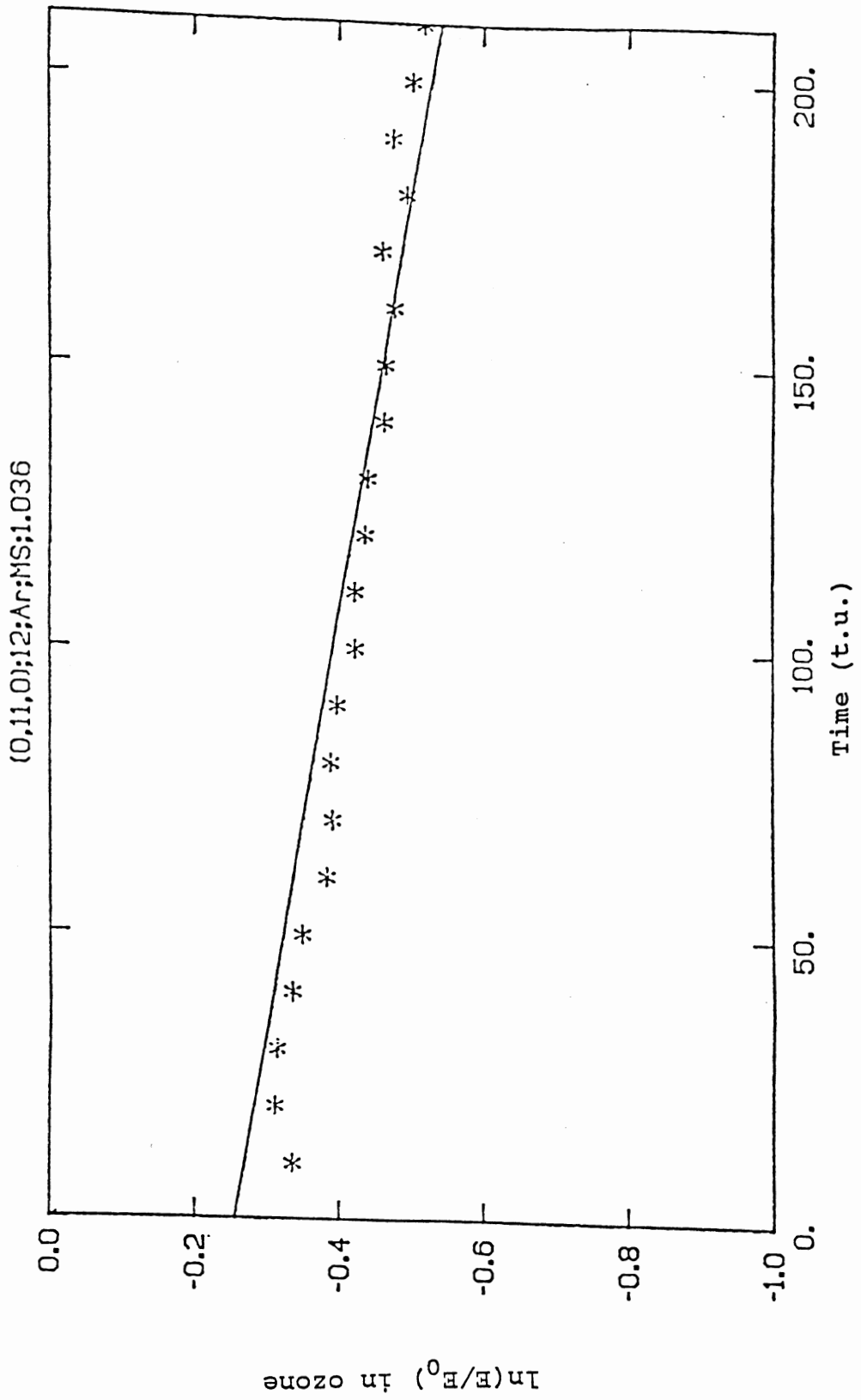

Figure 37. V.E.T. of ozone - (0,11,0);12;Ar;MS;1.036;XZ

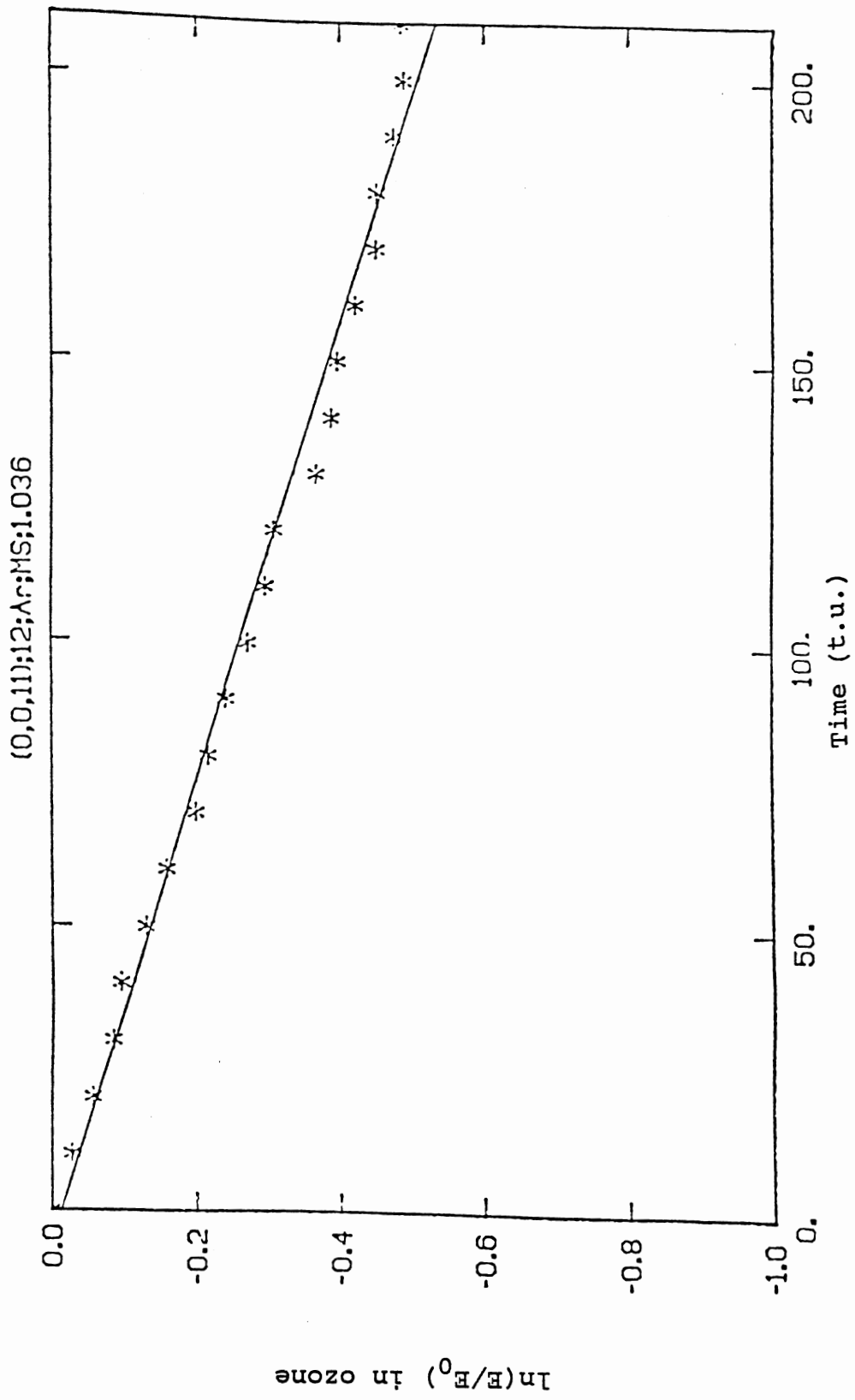

Figure 38. V.E.T. of ozone - (0,0,11);12;Ar;MS;1.036;XZ

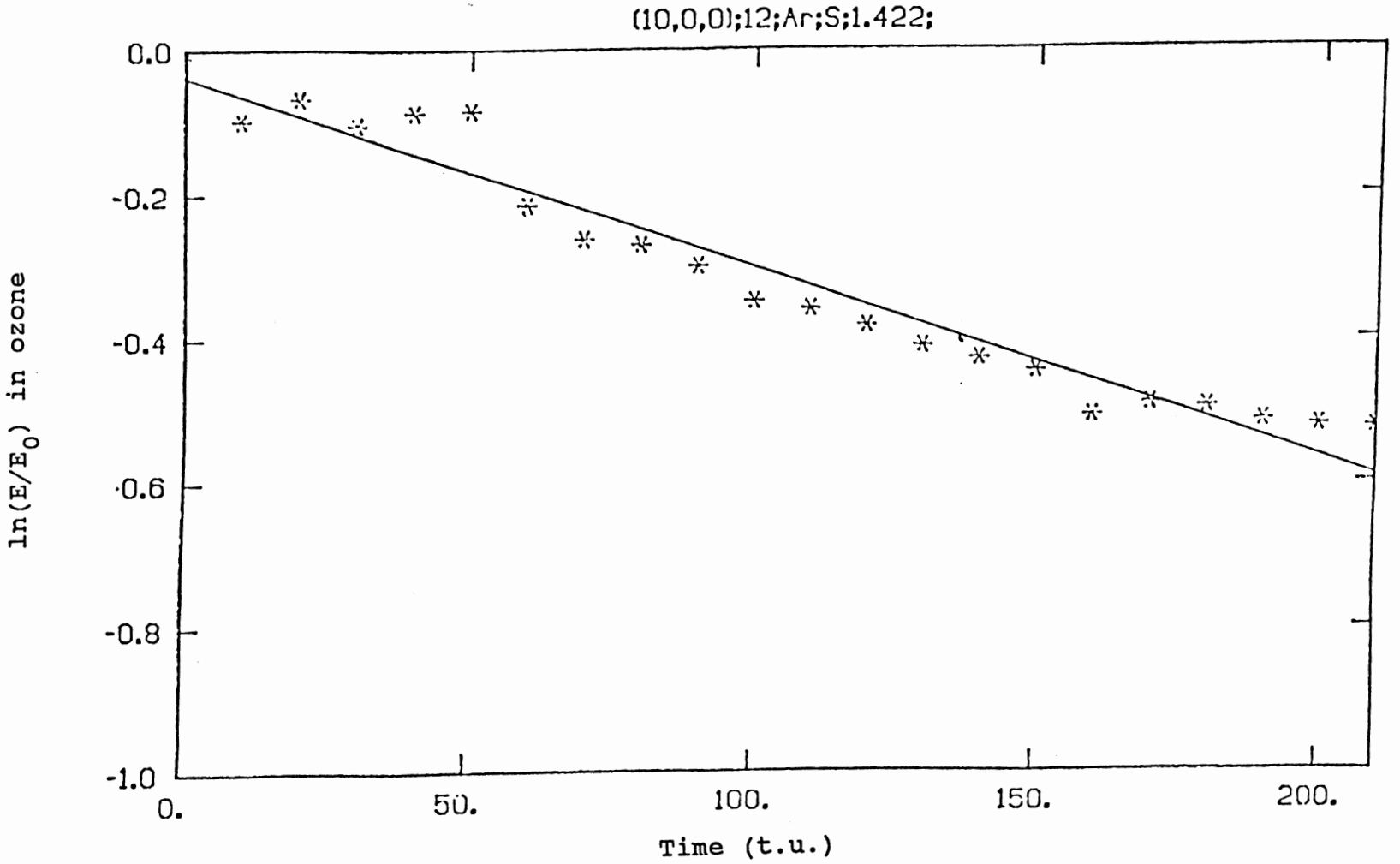

Figure 39. V.E.T. of ozone - (10,0,0);12;Ar;S;1.422;XZ

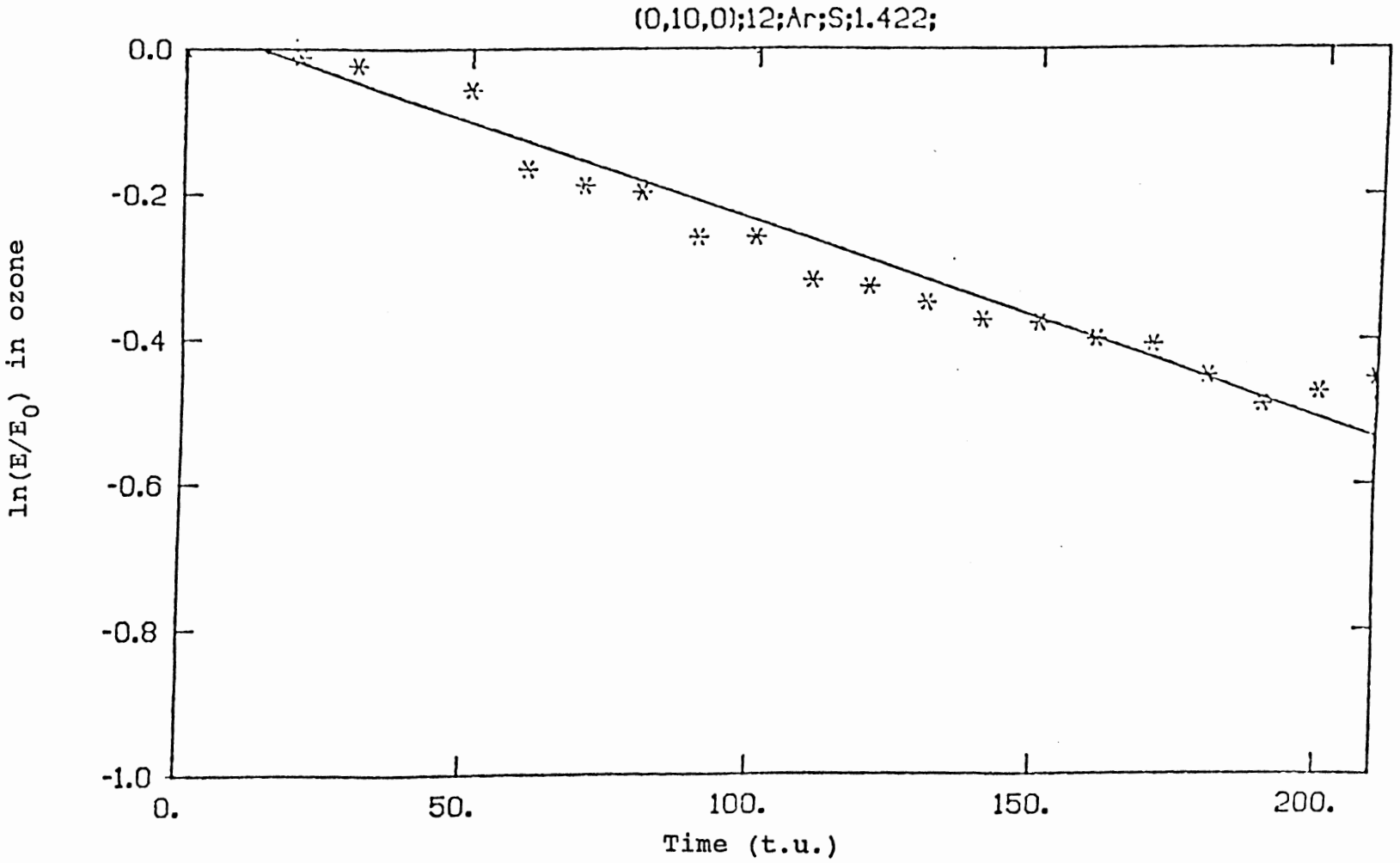

Figure 40. V.E.T. of ozone - (0,10,0);12;Ar;S;1.422;XZ

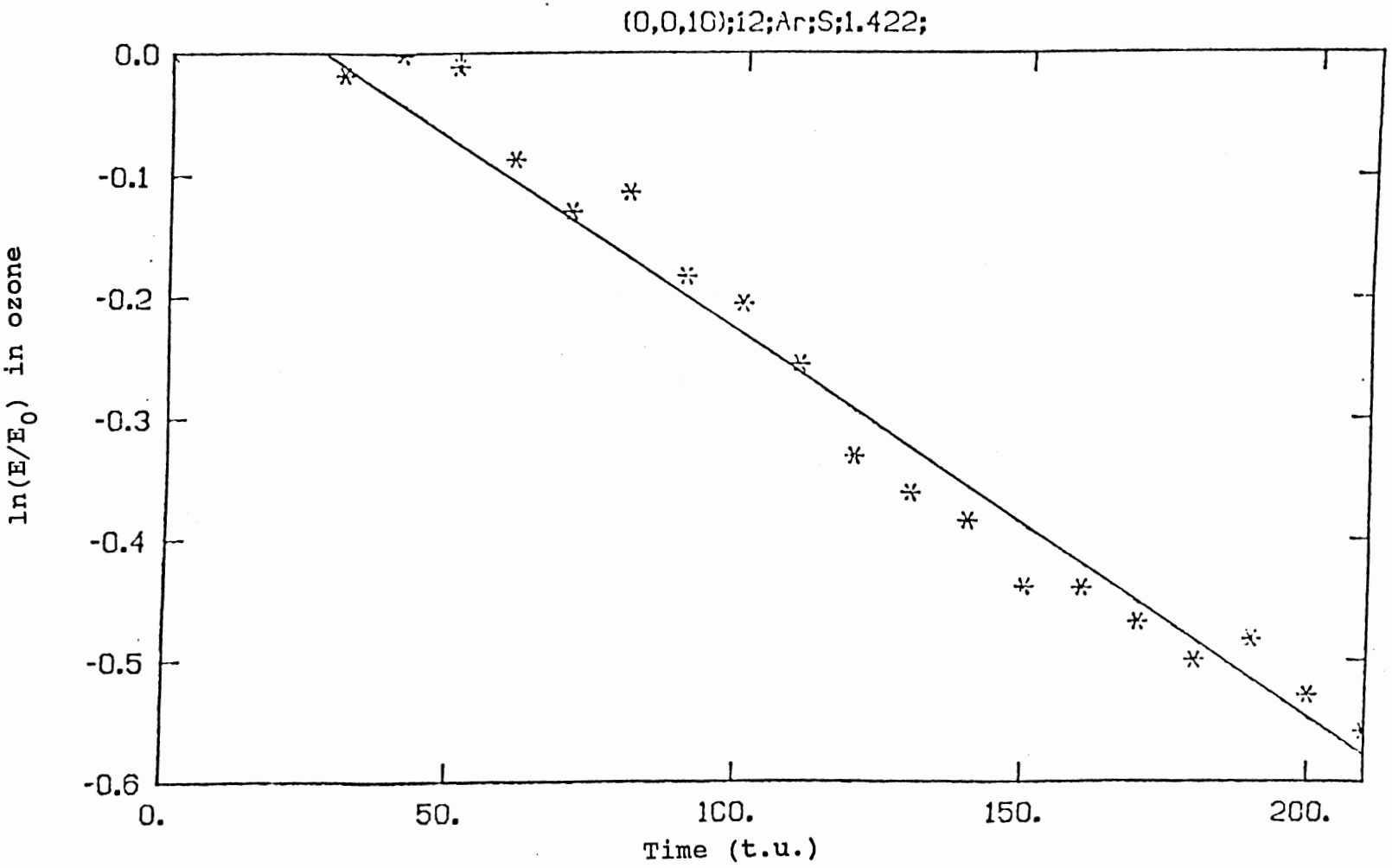

Figure 41. V.E.T. of ozone - (0,0,10);12;Ar;S;1.422;XZ

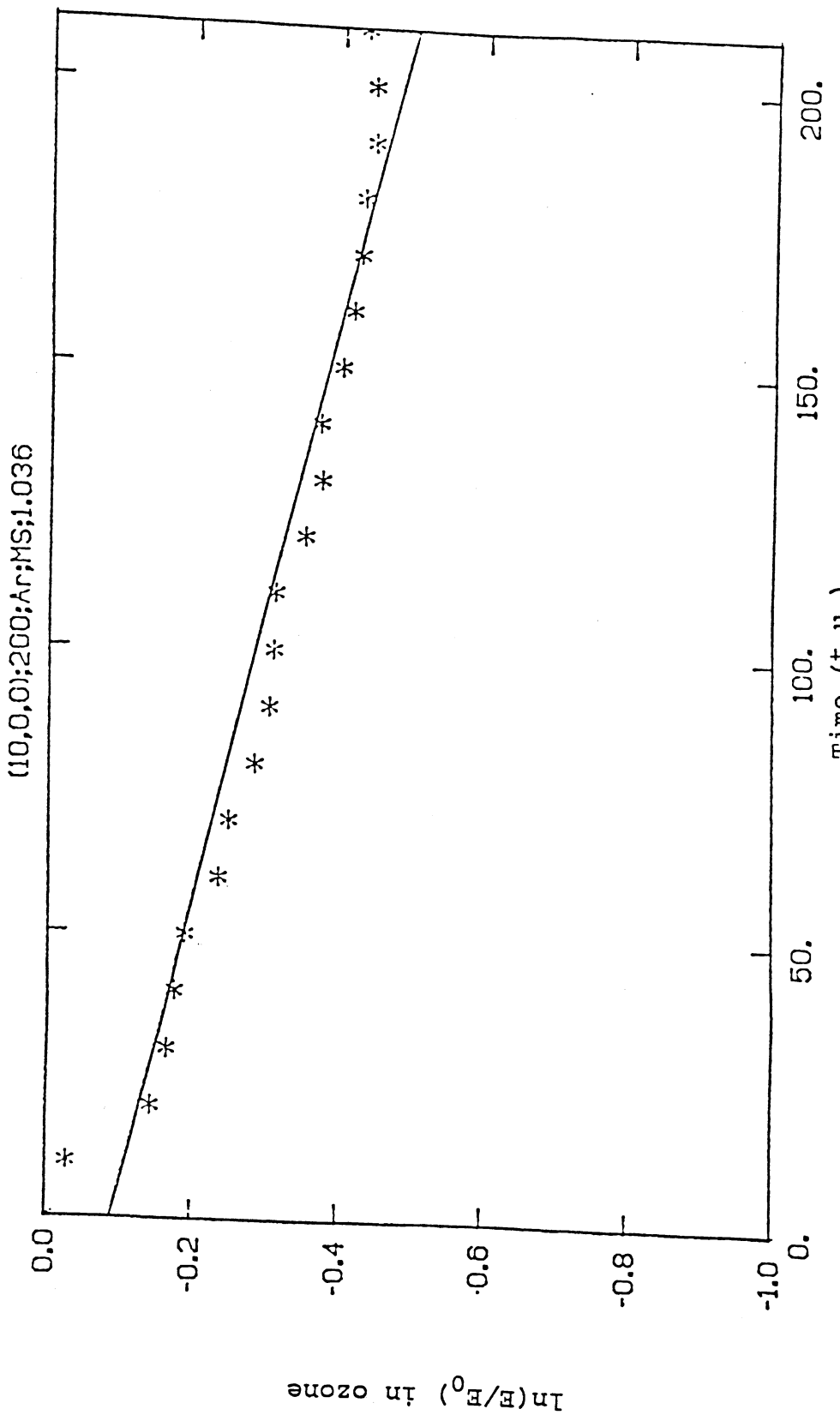

Figure 42. V.E.T. of ozone - (10,0,0);200;Ar;MS;1.036;XZ

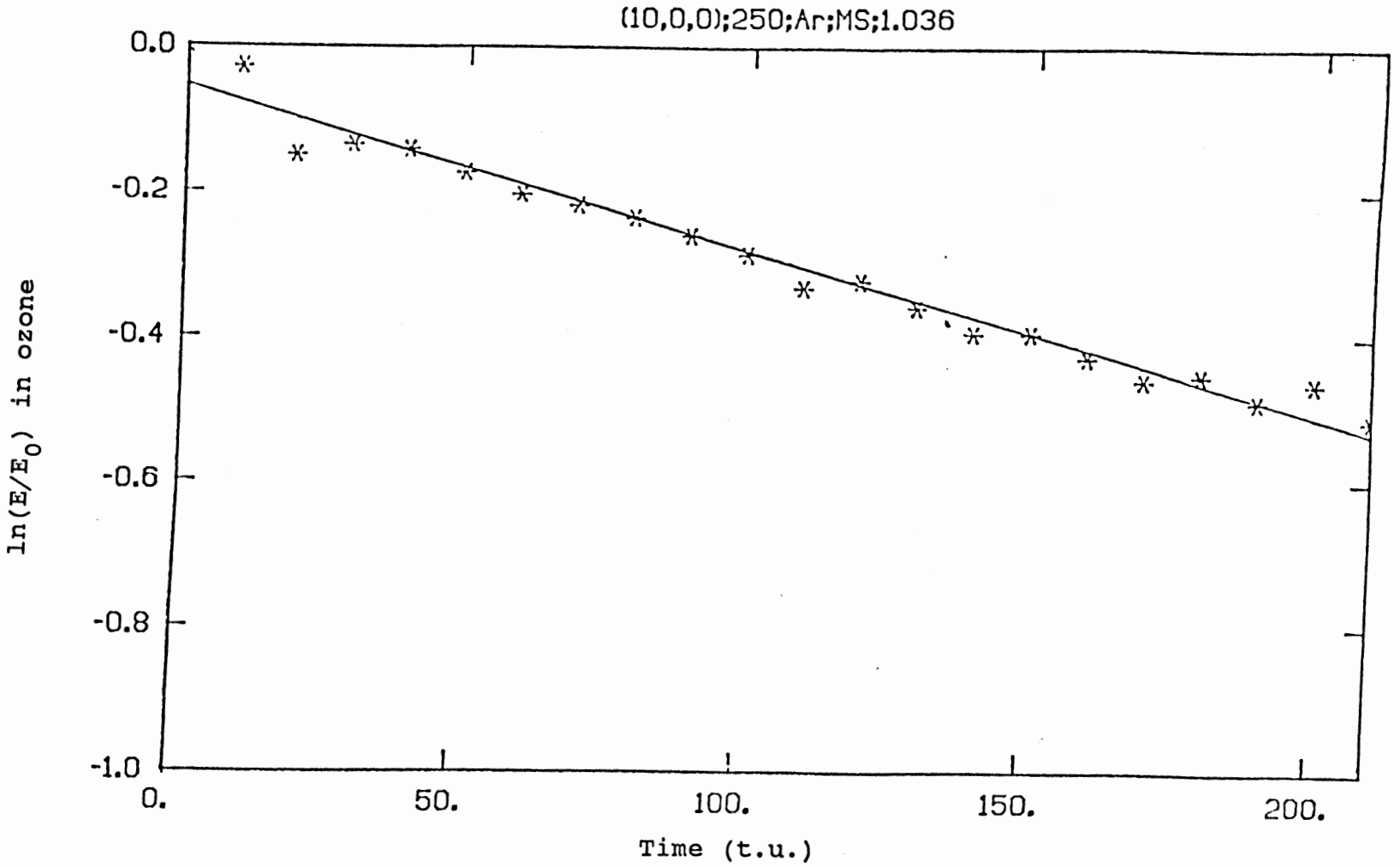

Figure 43. V.E.T. of ozone - (10,0,0);250;Ar;MS;1.036;XZ

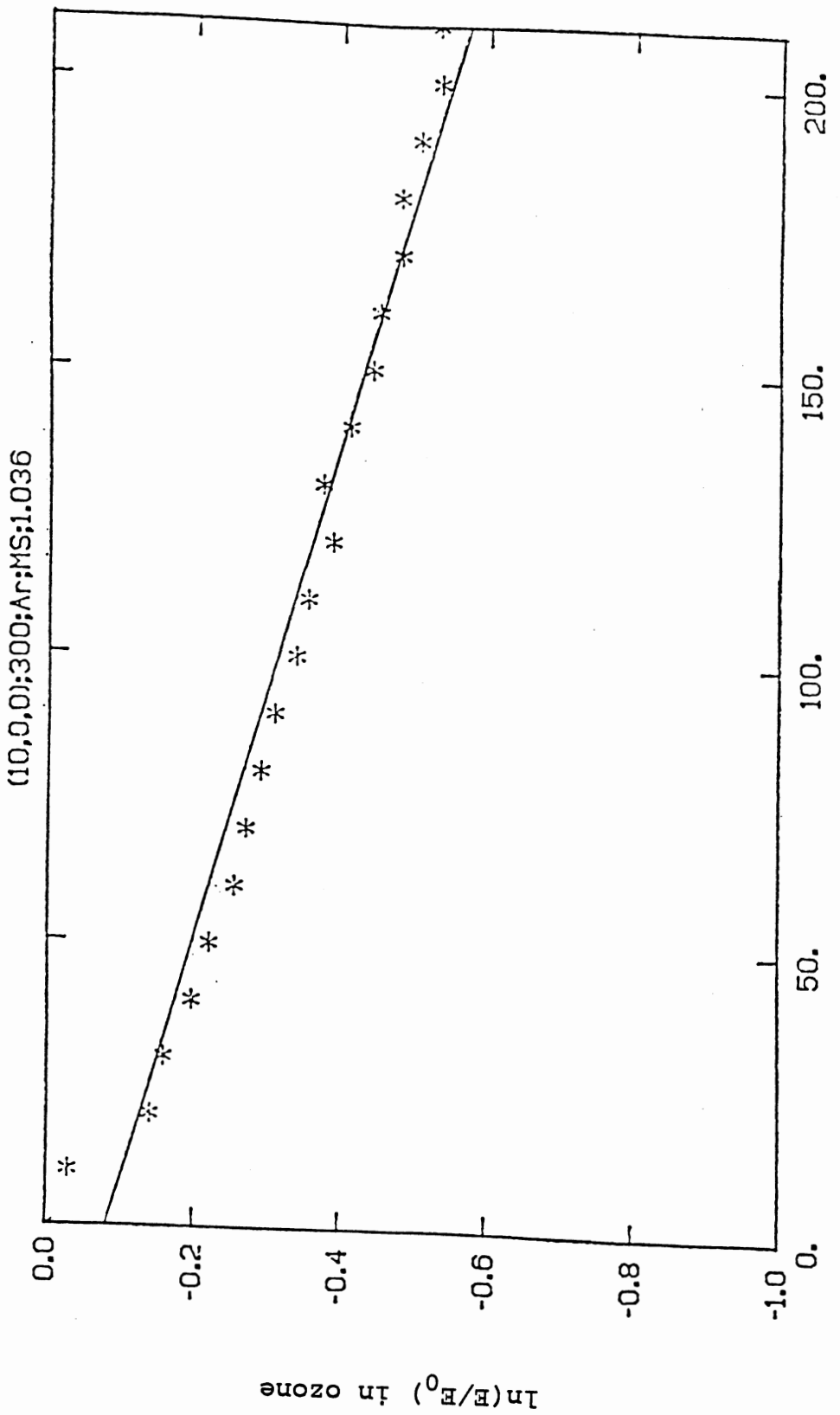

Figure 44. V.E.T. of ozone - (10,0,0);300;Ar;MS;1.036;XZ

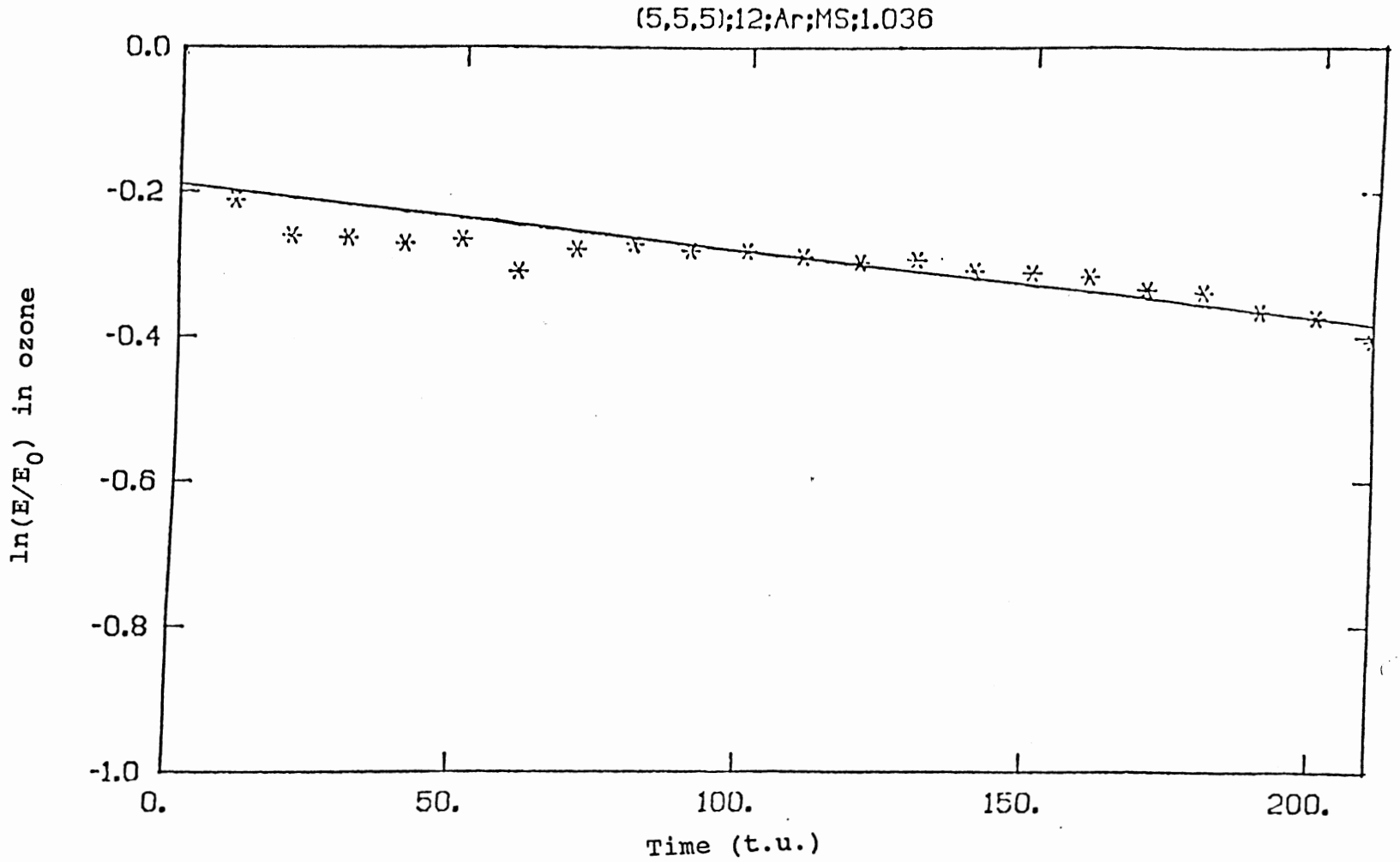

Figure 45. V.E.T. of ozone - (5,5,5);12;Ar;MS;1.036;XZ

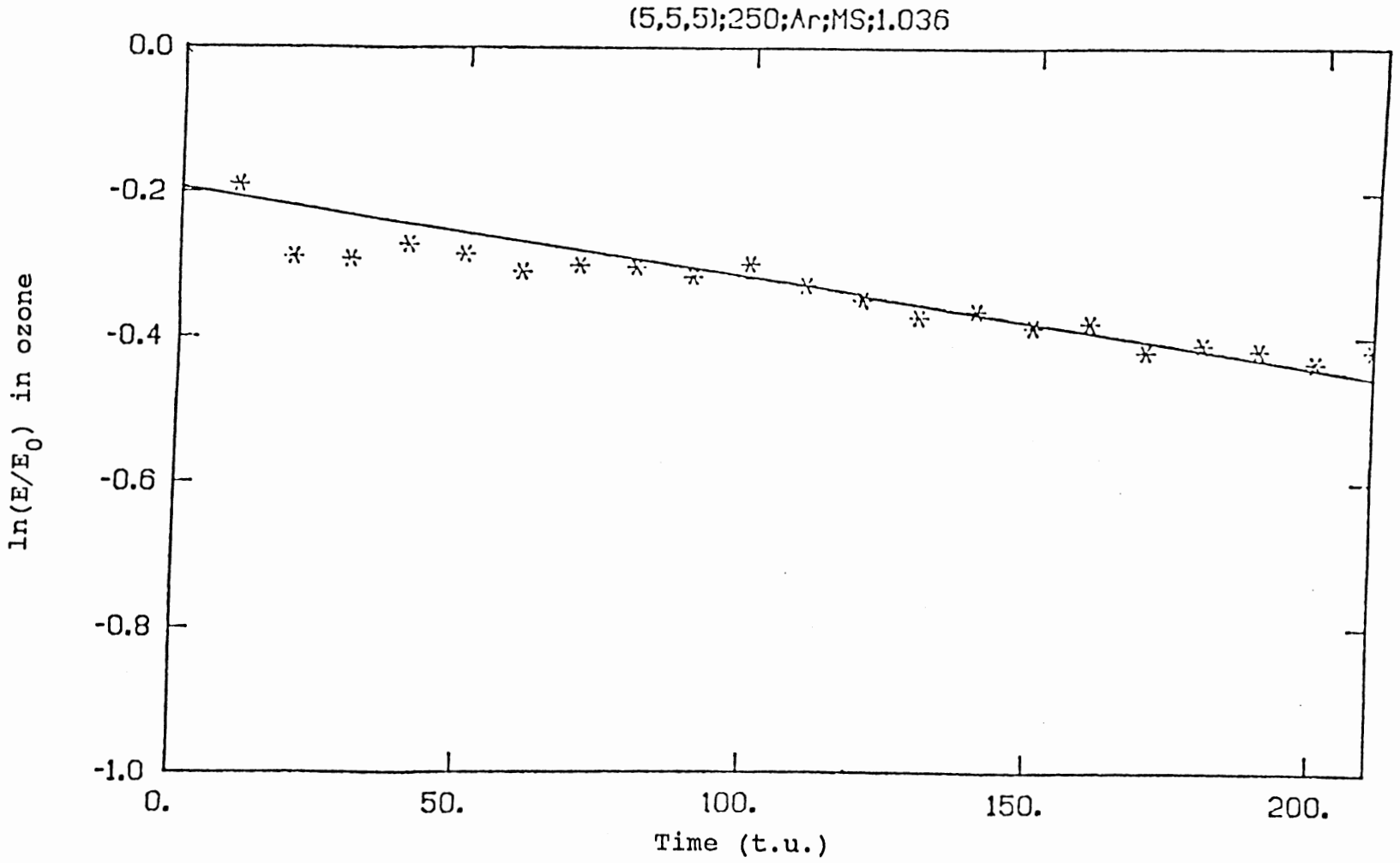

Figure 46. V.E.T. of ozone - (5,5,5);250;Ar;MS;1.036;XZ

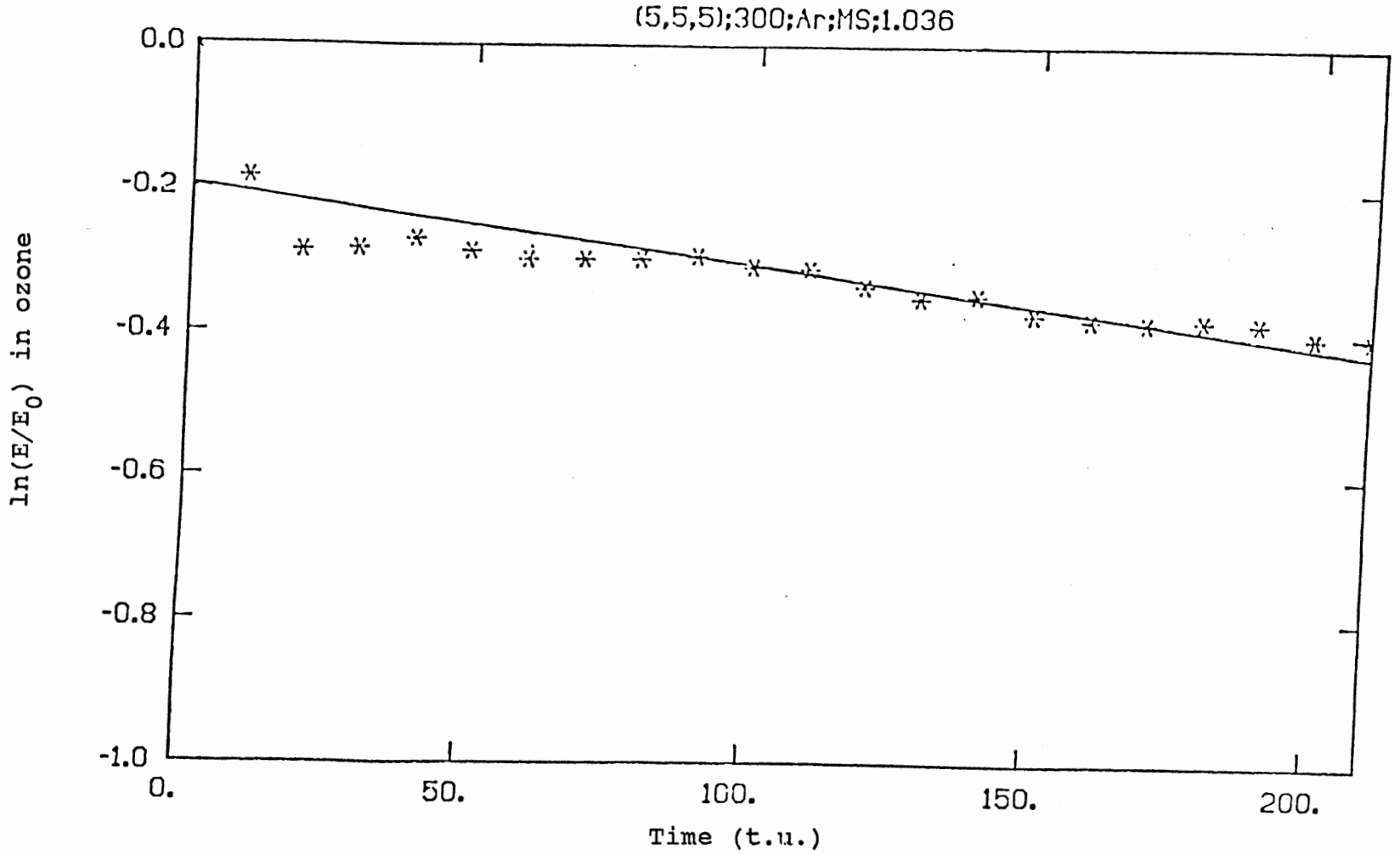

Figure 47. V.E.T. of ozone - (5,5,5);300;Ar;MS;1.036;XZ

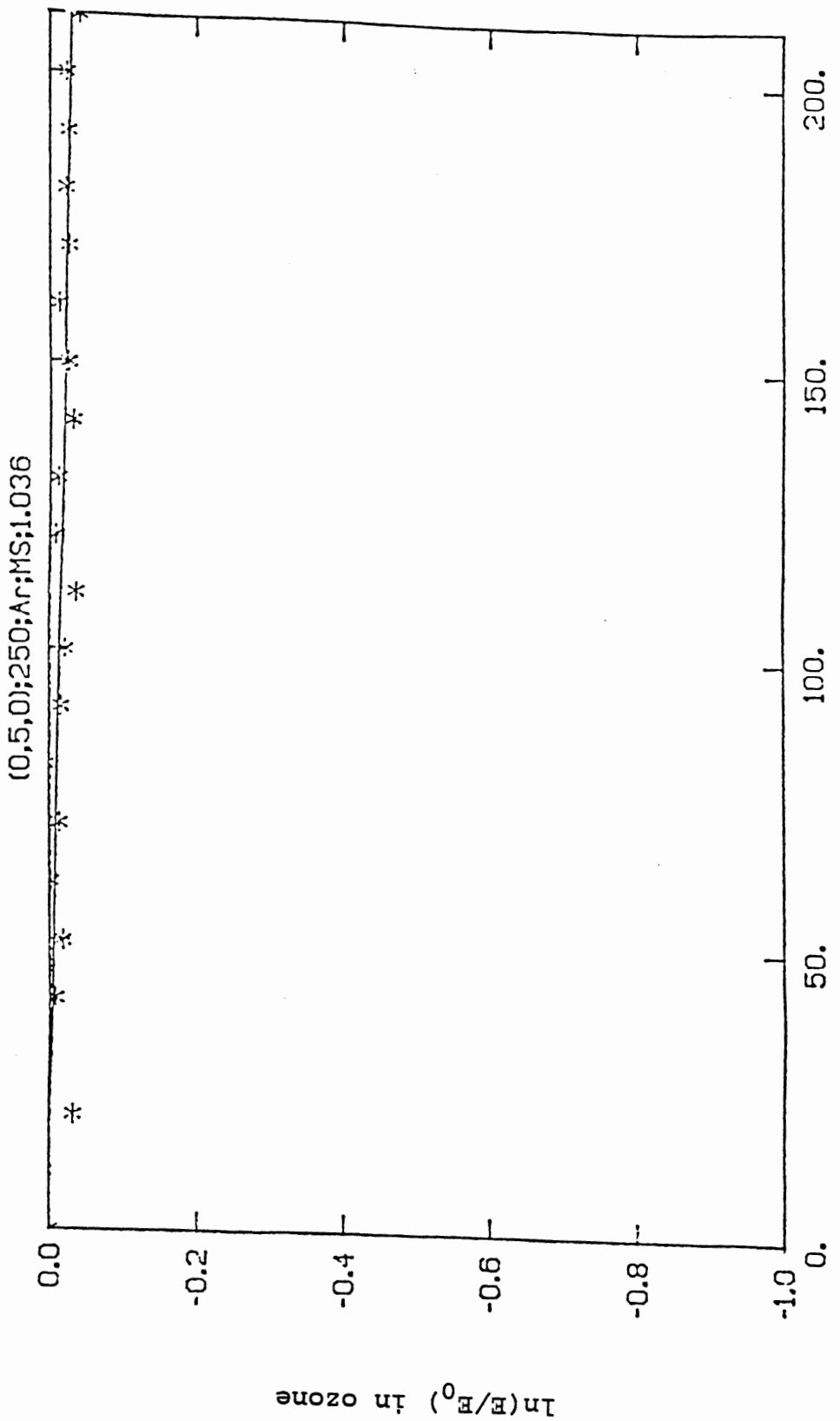

Figure 48. V.E.T. of ozone - (0,5,0);250;Ar;MS;1.036;XZ

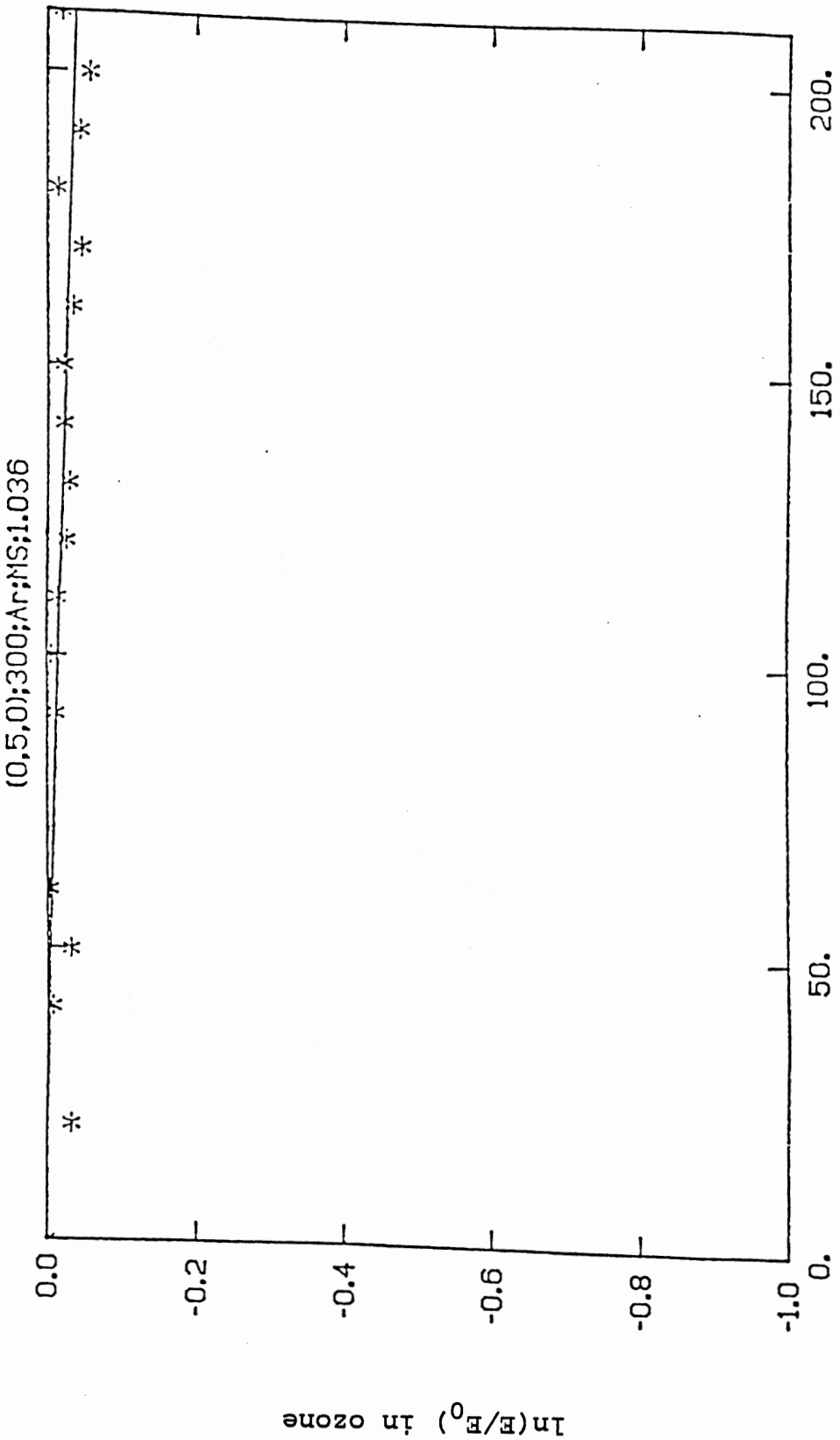

Figure 49. V.E.T. of ozone - (0,5,0);300;Ar;MS;1.036;XZ

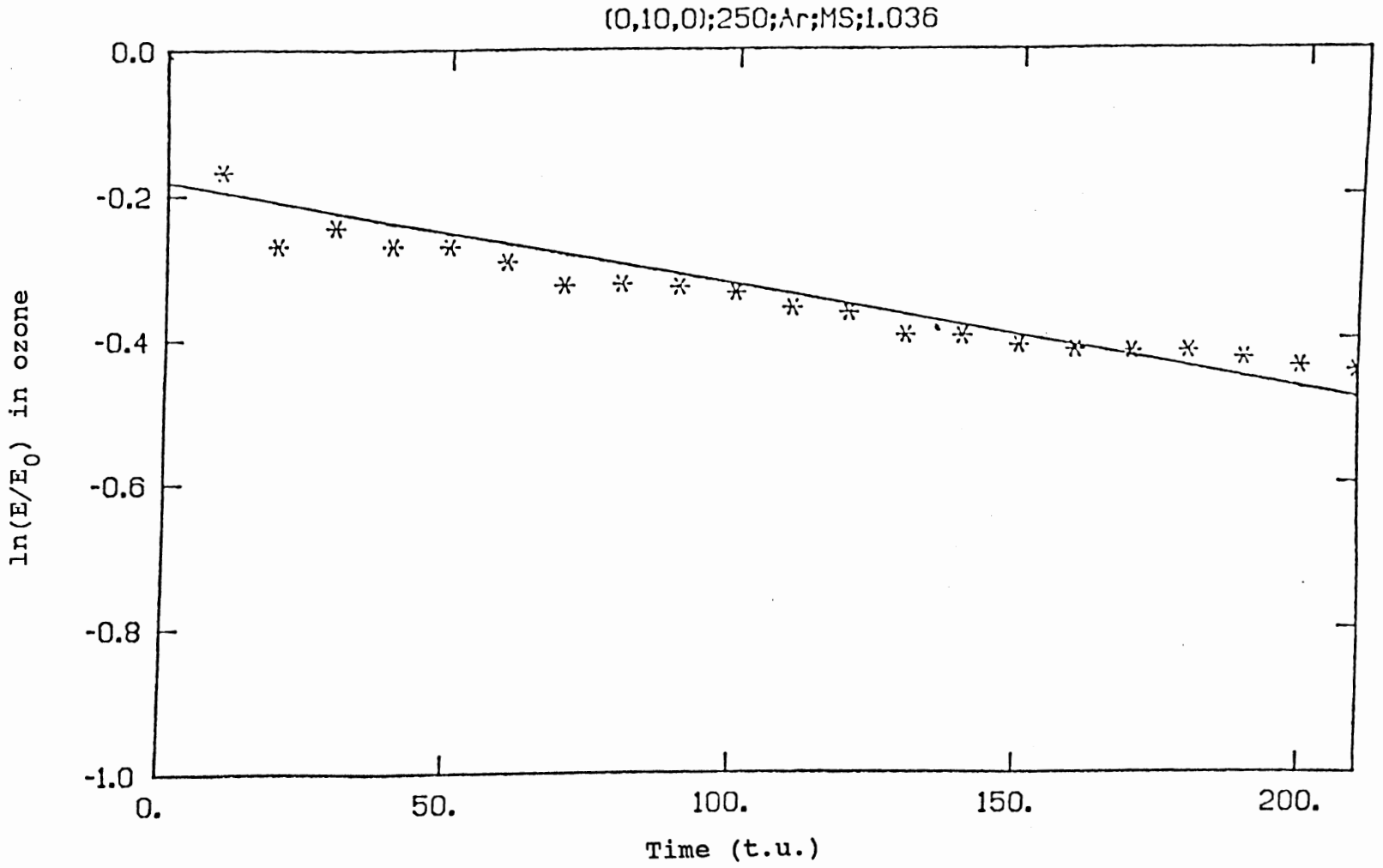

Figure 50. V.E.T. of ozone - (0,10,0);250;Ar;MS;1.036;XZ

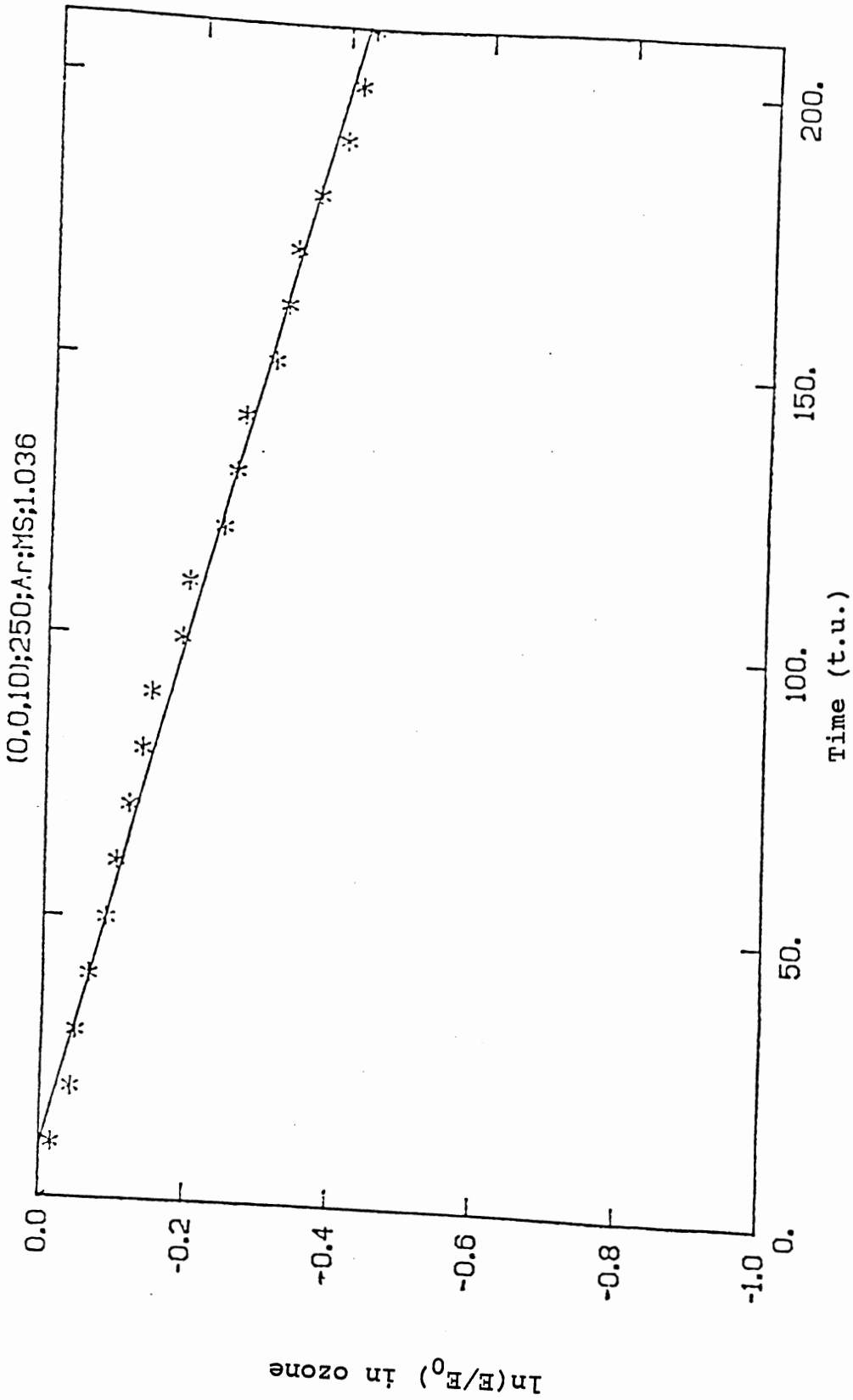

Figure 51. V.E.T. of ozone - (0,0,10);250;Ar;MS;1.036;XZ

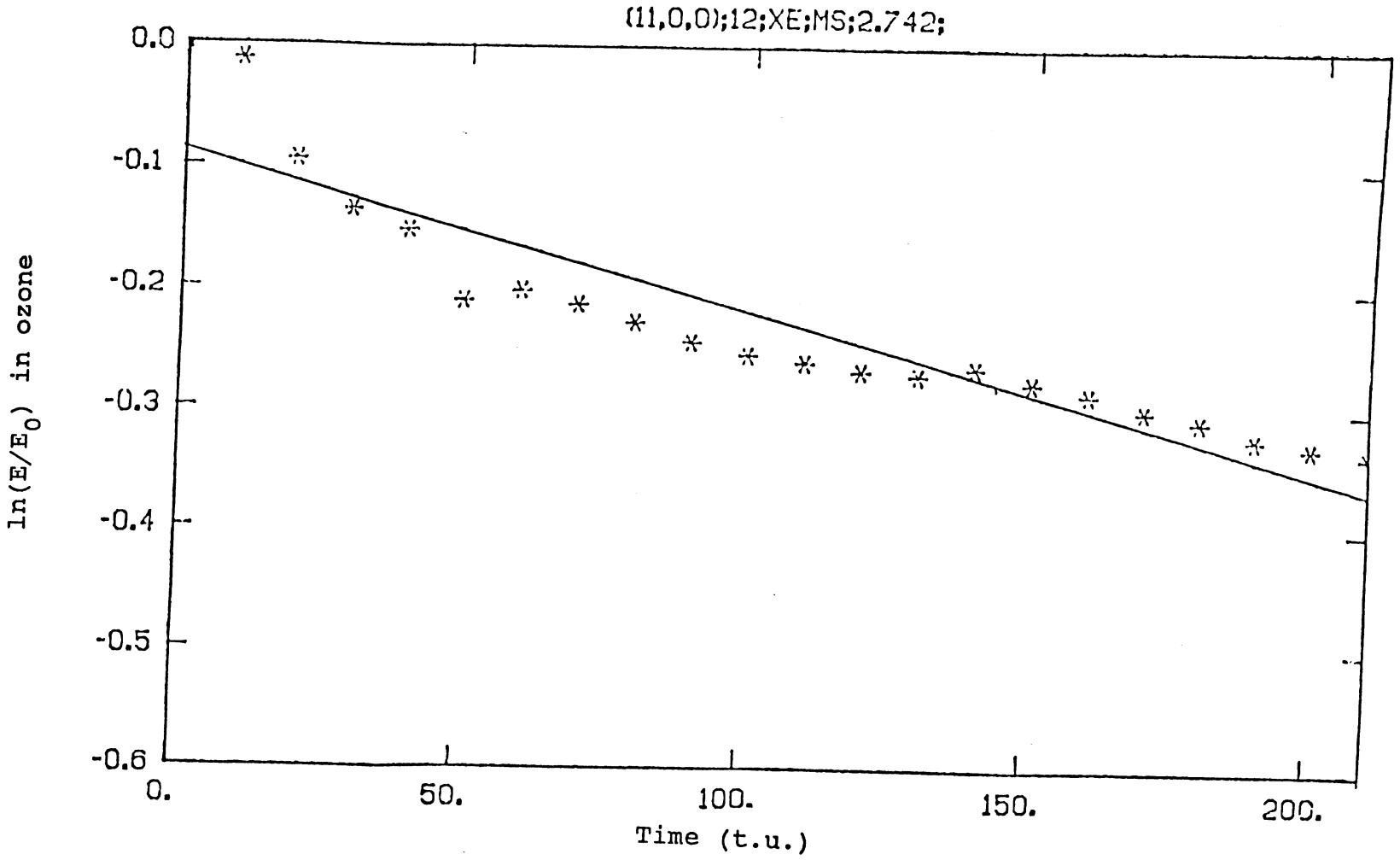

Figure 52. V.E.T. of ozone - (11,0,0);12;Xe;MS;2.742;XZ

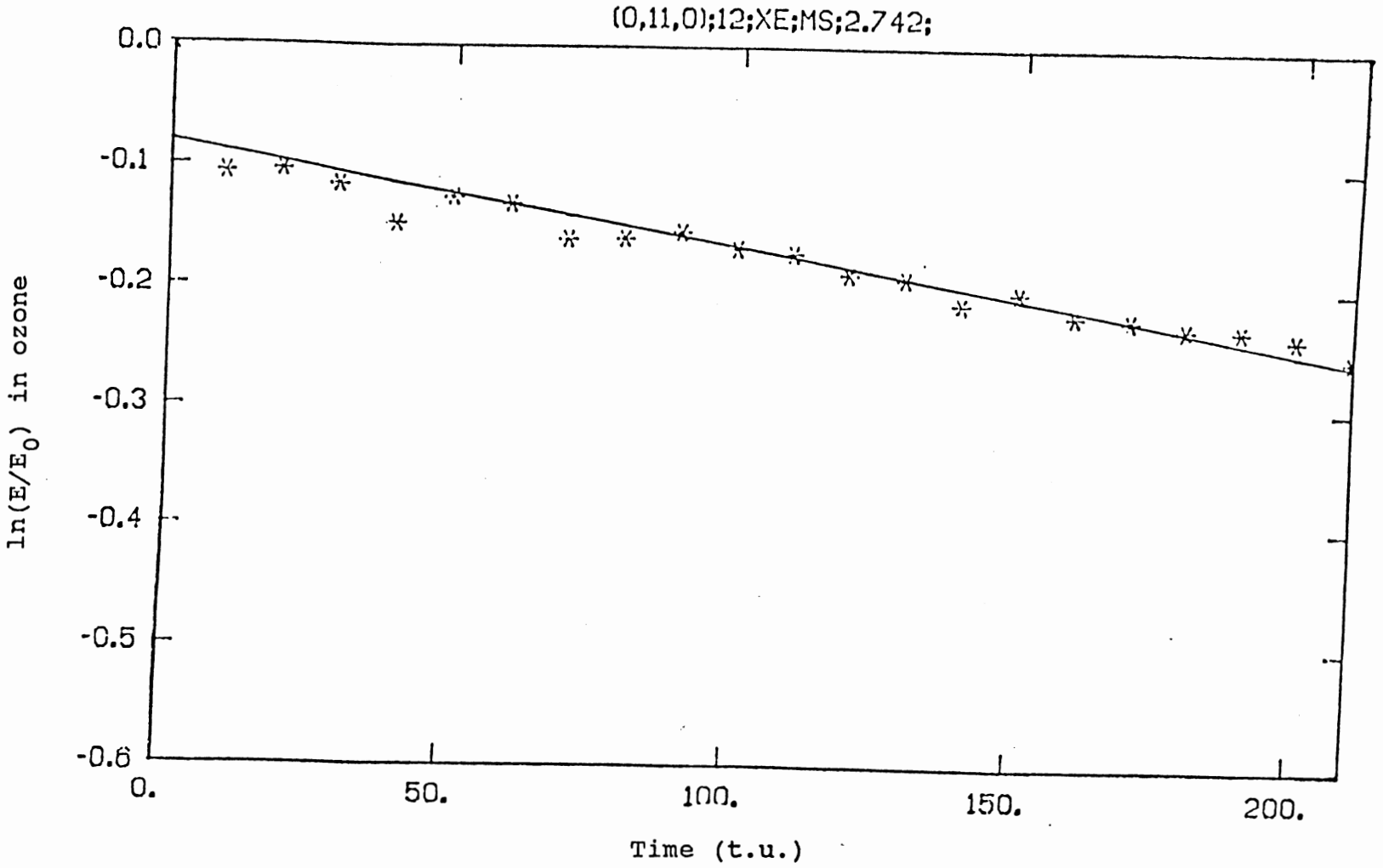

Figure 53. V.E.T. of oznoe - (0,11,0);12;Xe;MS;2.742;XZ

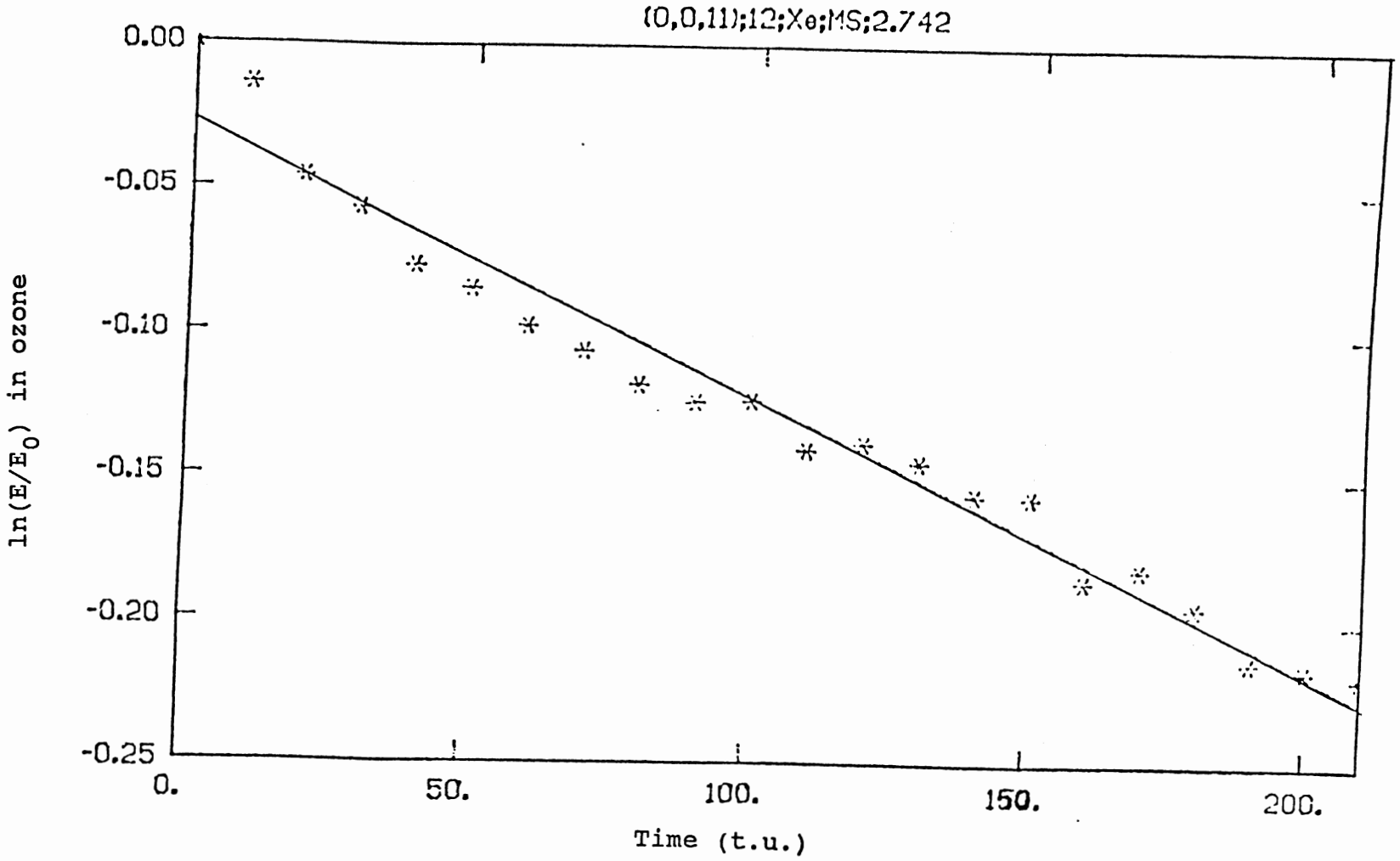

Figure 54. V.E.T. of ozone - (0,0,11);12;Xe;MS;2.742;XZ

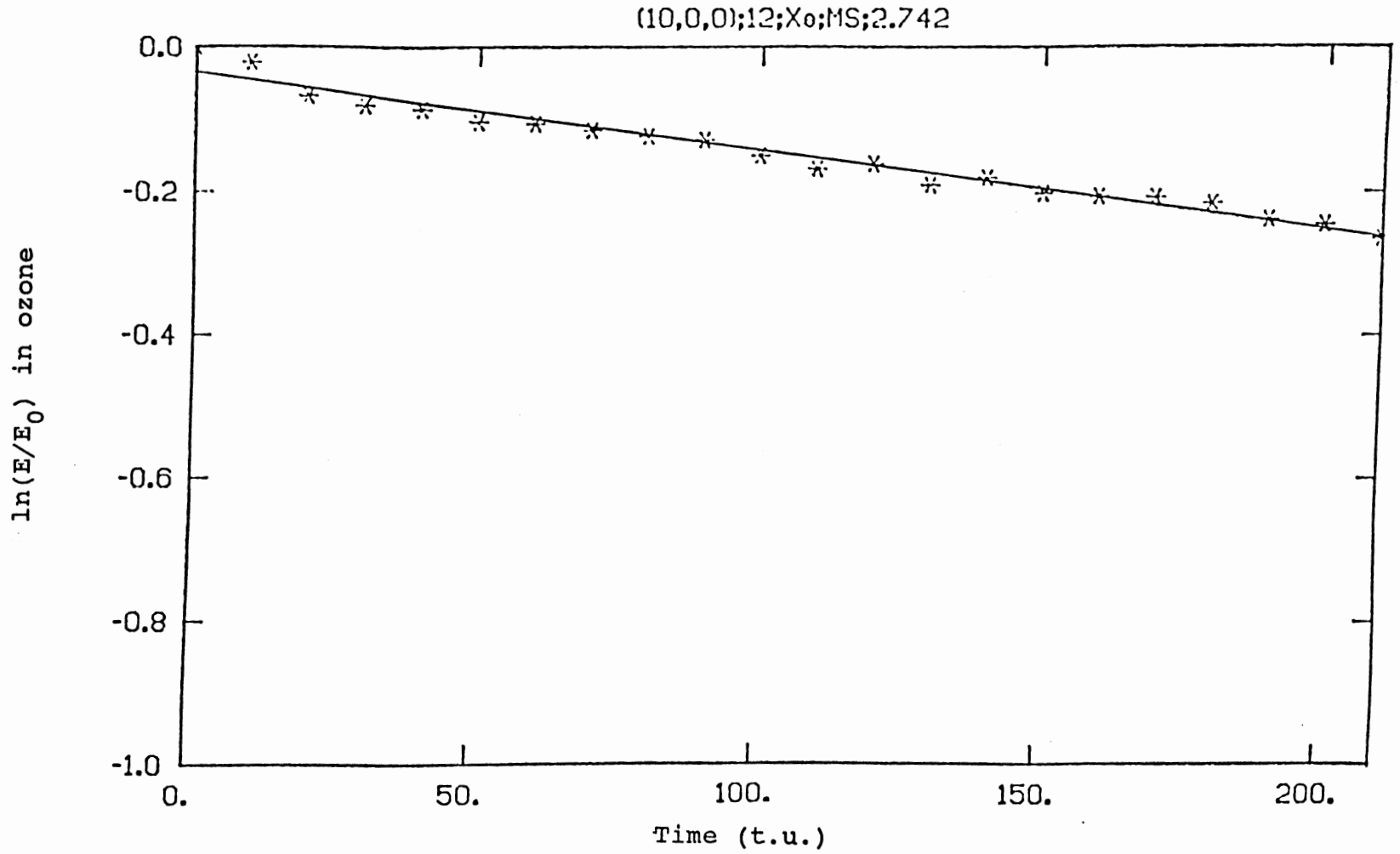

Figure 55. V.E.T. of ozone - (10,0,0);12;Xe;MS;2.742;XZ

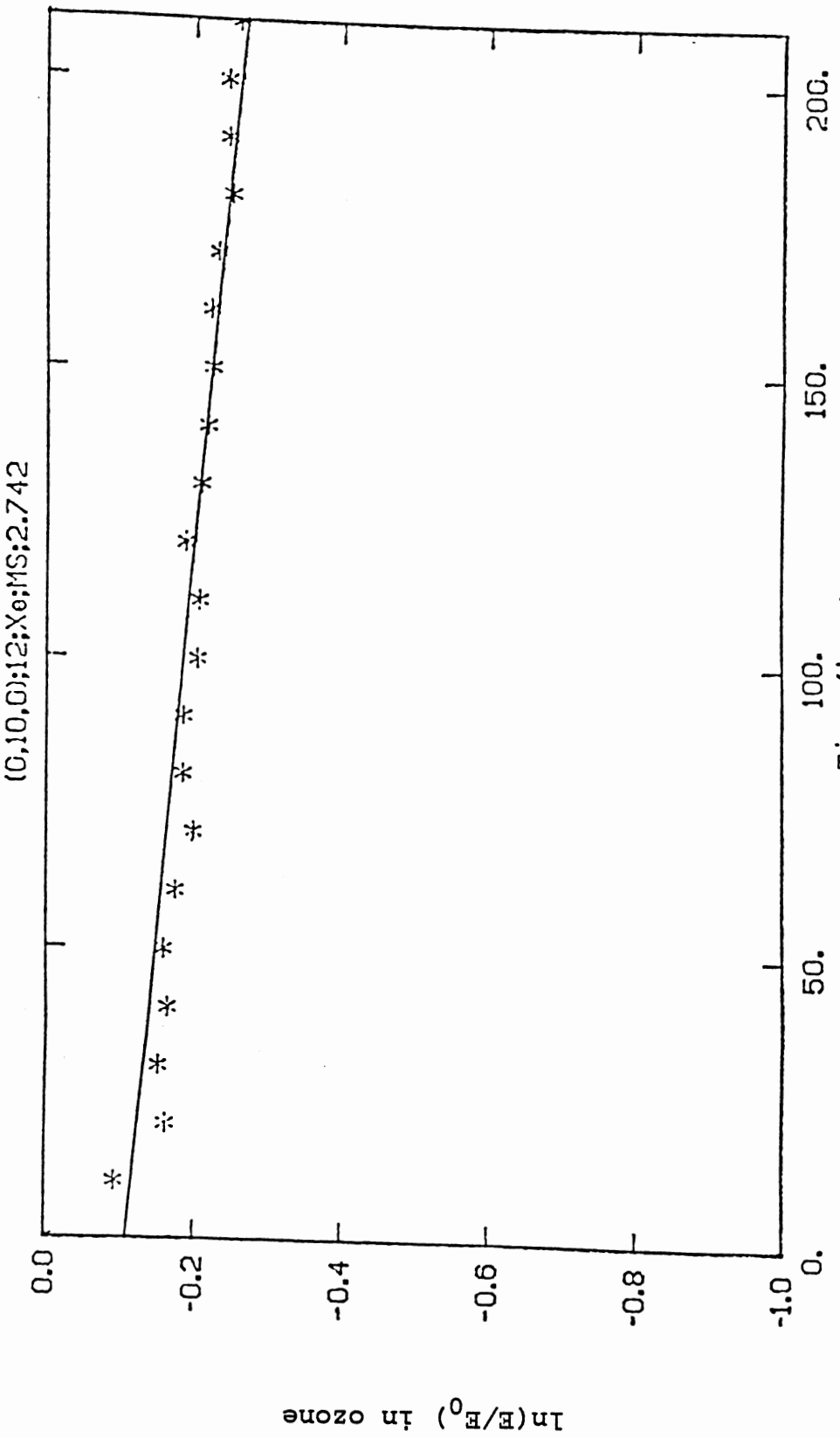

Figure 56. V.E.T. of ozone - (0,10,0);12;Xe;MS;2.742;XZ

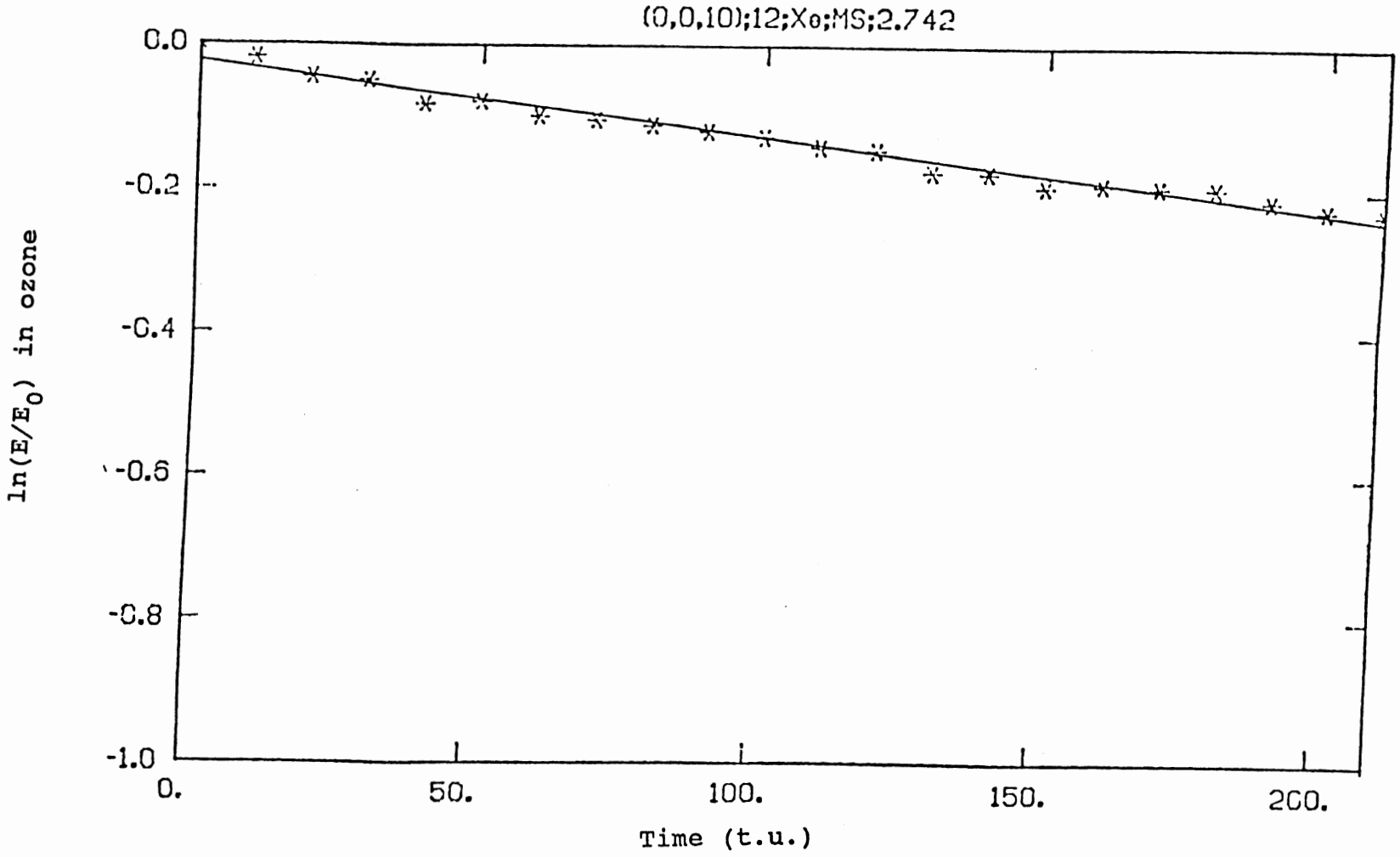

Figure 57. V.E.T. of ozone - (0,0,10);12;Xe;Ms;2.742;XZ

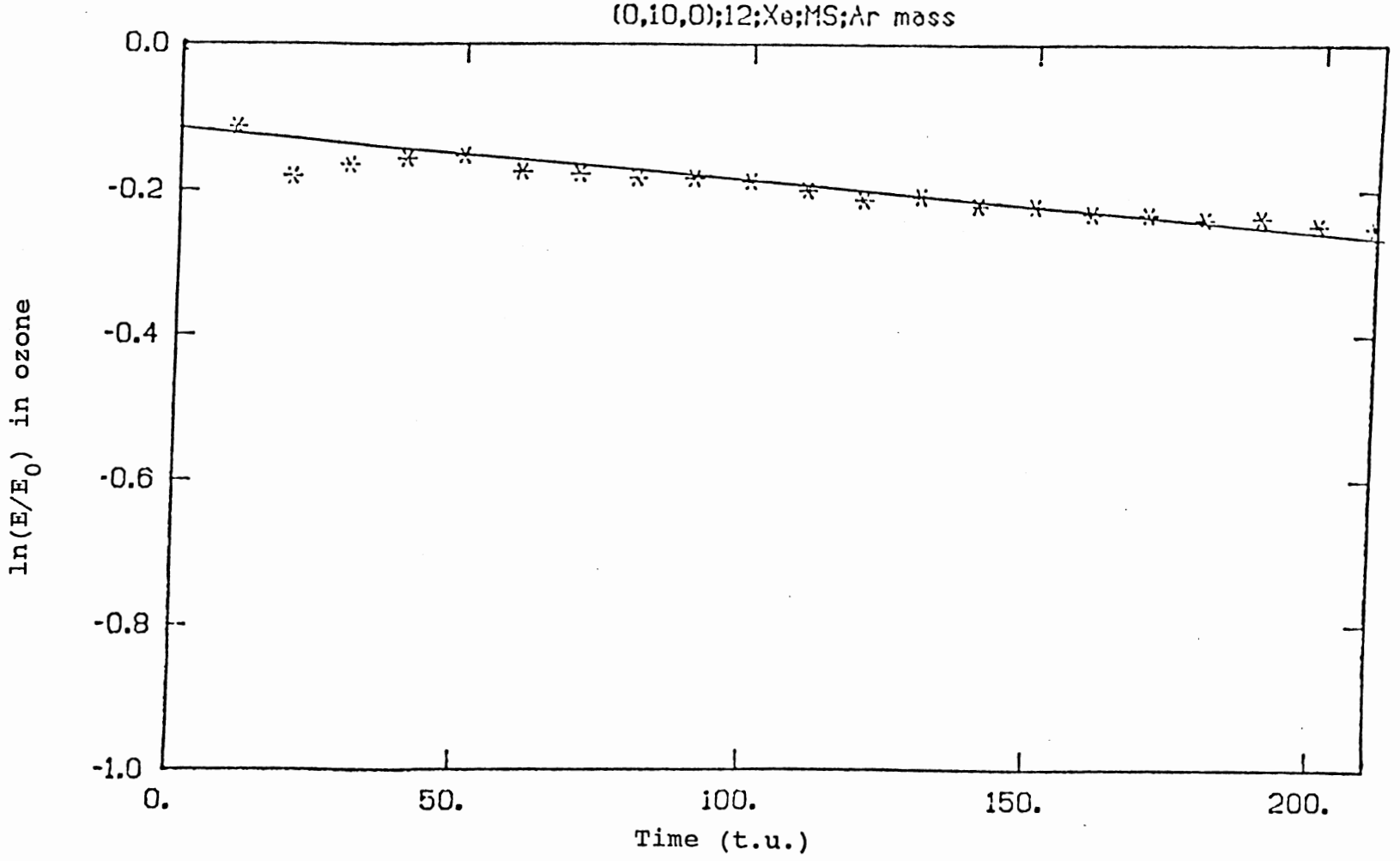

Figure 58. V.E.T. of ozone - (0,10,0);12;Xe;MS;2.742;XZ

TABLE VII

VIBRATIONAL ENERGY TRANSFER RATES OF O_3 IN ARGON MATRICES AT 12 K

Confgn. Number	Excitation	Energy in ozone		Density g/cm^3	Density $kx10^{11} sec^{-1}$
		eV	kcal/mole		
	(10,0,0)	1.3967	32.21		3.39 + 0.24
II	(0,10,0)	1.0097	23.28	1.422	2.13 + 0.18
	(0,0,10)	1.2448	28.70		2.88 + 0.13
	(10,0,0)	1.3849	31.94		3.68 + 0.16
III	(0,10,0)	1.0084	23.25	1.422	2.87 + 0.28
	(0,0,10)	1.2345	28.47		3.02 + 0.20
	(10,0,0)	1.4094	32.50		3.71 + 0.32
IV	(0,10,0)	1.0116	23.33	1.422	2.15 + 0.33
	(0,0,10)	1.2564	28.97		2.68 + 0.13
	(11,0,0)	1.5156	34.95		3.65 + 0.27
II	(0,11,0)	1.0927	25.20	1.422	3.08 + 0.35
	(0,0,11)	1.3406	30.91		3.28 + 0.21
	(11,0,0)	1.5718	36.24		2.86 + 0.10
I	(0,11,0)	1.0985	25.33	1.036	1.34 + 0.21
	(0,0,11)	1.3897	32.04		2.43 + 0.059
	(10,0,0)	1.4510	33.46		2.65 + 0.11
I	(0,10,0)	1.0159	23.42	1.036	1.35 + 0.12
	(0,0,10)	1.2925	29,80		2.10 + 0.044
	(10,0,0)	1.4504	33.45		2.59 + 0.13
V	(0,10,0)	1.0158	23.42	1.422	2.66 + 0.14
	(0,0,10)	1.2920	29.79		3.10 + 0.12

TABLE VIII

EFFECT OF VIBRATIONAL EXCITATION OF OZONE IN ARGON MATRICES AT 12 K

Excitation	Energy in ozone		$kx10^{11} sec^{-1}$
	eV	kcal/mole	
Configuration No. II_3 Density = 1.422 g/cm^3			
(10,0,0)	1.3967	32.21	3.39 + 0.24
(0,10,0)	1.0097	23.28	2.13 + 0.18
(0,0,10)	1.2448	28.70	2.88 + 0.13
(11,0,0)	1.5156	34.95	3.65 + 0.27
(0,11,0)	1.0927	25.20	3.08 + 0.35
(0,0,11)	1.3406	30.91	3.28 + 0.21
Configuration No. I_3 Density = 1.036 g/cm^3			
(10,0,0)	1.4510	33.46	2.65 + 0.11
(0,10,0)	1.0159	23.42	1.35 + 0.12
(0,0,10)	1.2925	29,80	2.10 + 0.044
(11,0,0)	1.5718	36.24	2.86 + 0.10
(0,11,0)	1.0985	25.33	1.34 + 0.21
(0,0,11)	1.3897	32.04	2.43 + 0.059

TABLE IX

EFFECT OF INITIAL ORIENTATION OF OZONE ON VIBRATIONAL ENERGY TRANSFER OF O_3 IN ARGON MATRICES AT 12 K

Mode	Excitation	Energy in ozone		$kx10^{11}sec^{-1}$
		eV	kcal/mole	
	Configuration No. II			
S.S	(10,0,0)	1.3967	32.21	3.39 + 0.24
B	(0,10,0)	1.0097	23.28	2.13 + 0.18
A.S	(0,0,10)	1.2448	28.70	2.88 + 0.13
	Configuration No. III			
S.S	(10,0,0)	1.3849	31.94	3.68 + 0.16
B	(0,10,0)	1.0084	23.25	2.87 + 0.28
A.S	(0,0,10)	1.2345	28.47	3.02 + 0.20
	Configuration No. IV			
S.S	(10,0,0)	1.4094	32.50	3.71 + 0.32
B	(0,10,0)	1.0116	23.33	2.15 + 0.33
A.S	(0,0,10)	1.2564	28.97	2.68 + 0.13

S.S = symmetric stretch B = bending

A.S = asymmetric stretch Density = 1.422 g/cm^3

TABLE X

EFFECT OF DENSITY ON THE VIBRATIONAL ENERGY TRANSFER OF OZONE IN ARGON MATRICES AT 12 K

Excitation	Energy in ozone		$kx10^{11}sec^{-1}$
	eV	kcal/mole	
Configuration No. I			Density = 1.036 g/cm^3
(10,0,0)	1.4510	33.46	2.65 + 0.11
(0,10,0)	1.0159	23.42	1.35 + 0.12
(0,0,10)	1.2925	29.80	2.10 + 0.044
Configuration No. II			Density = 1.036 g/cm^3
(10,0,0)	1.3967	32.21	3.39 + 0.24
(0,10,0)	1.0097	23.28	2.13 + 0.18
(0,0,10)	1.2448	28.70	2.88 + 0.13
Configuration No. I			Density = 1.036 g/cm^3
(11,0,0)	1.5718	36.24	2.86 + 0.10
(0,11,0)	1.0985	25.33	1.34 + 0.21
(0,0,11)	1.3897	32.04	2.43 + 0.059
Configuration No. II			Density = 1.422 g/cm^3
(11,0,0)	1.5156	34.95	3.65 + 0.27
(0,11,0)	1.0927	25.20	3.08 + 0.35
(0,0,11)	1.3406	30.91	3.28 + 0.21

TABLE XI

PREDICTED[a] AND OBSERVED RATE COEFFICIENTS
IN ARGON MATRIX AT 12 K

Configuration No. II				
Excitation	Energy in ozone		$k_o x10^{11} sec^{-1}$	$k_p x10^{11} sec^{-1}$
	eV	kcal/mole		
(10,0,0)	1.3967	32.21	3.39 + 0.24	3.64 + 0.16
(0,10,0)	1.0097	23.28	2.13 + 0.18	1.86 + 0.17
(0,0,10)	1.2448	28.70	2.88 + 0.13	2.89 + 0.06
(11,0,0)	1.5156	34.95	3.65 + 0.27	3.93 + 0.14
(0,11,0)	1.0927	25.20	3.08 + 0.35	1.84 + 0.29
(0,0,11)	1.3406	30.91	3.28 + 0.21	3.34 + 0.09

k_p = predicted

k_o = observed

a = density-scaled

TABLE XII

EFFECT OF TEMPERATURE ON ENERGY TRANSFER RATE IN ARGON MATRIX AT 12 K

Configuration No. I	Density = 1.036 g/cm^3		
	Energy in ozone		
Temp.(K)	eV	kcal/mole	$kx10^{11}sec^{-1}$
	I. (10,0,0) Excitation		
12	1.4510	33.46	2.65 + 0.11
200	1.4753	34.02	1.92 + 0.12
250	1.4818	34.17	2.24 + 0.083
300	1.4882	34.32	2.29 + 0.11
	II. (5,5,5) Excitation		
12	1.6548	38.16	0.90 + 0.016
250	1.6855	38.87	1.22 + 0.17
300	1.6920	39.02	1.08 + 0.17
	III. (0,5,0) Excitation		
250	0.6297	14.52	0.16 + 0.045
300	0.6362	14.67	0.21 + 0.054
	IV. (0,10,0) Excitation		
12	1.0159	23.42	1.35 + 0.12
250	1.0467	24.14	1.40 + 0.16
	V. (0,0,10) Excitation		
12	1.2925	29.80	2.10 + 0.044
250	1.3233	30.52	2.07 + 0.042

TABLE XIII

THRESHOLD ENERGY REQUIREMENT OF ENERGY TRANSFER RATE IN ARGON MATRIX AT 12 K

Configuration No. I

Density = 1.036 g/cm^3 Temperature 12 K

Excitation	Energy in ozone		$kx10^{11}sec^{-1}$
	eV	kcal/mole	
5,0,0	0.8287	19.10	0.069 + 0.034
10,0,0	1.4510	33.46	2.65 + 0.11
5,5,5	1.6548	38.16	0.90 + 0.016

TABLE XIV

VIBRATIONAL ENERGY TRANSFER RATES OF OZONE IN XENON MATRIX

Configuration No. VI			
	Energy in ozone		
Excitation	eV	kcal/mole	$kx10^{11}sec^{-1}$
10,0,0	1.4503	33.44	1.08 + 0.043
0,10,0	1.0158	23.42	0.75 + 0.10
0,0,10	1.2919	29.79	1.01 + 0.036
0,10,0*	1.0158	23.42	0.70 + 0.10
11,0,0	1.5711	36.23	1.31 + 0.13
0,11,0	1.0985	25.33	0.84 + 0.071
0,0,11	1.3891	32.03	0.94 + 0.038

* mass of lattice atom is 39.948 (= argon mass)

vibrational excitation of ozone. They have observed significant vibrational rate enhancement for reaction as the internal energy content of the molecule is increased. Also, greater propensity for reaction has been observed when the initial internal energy is partitioned into the asymmetric stretching mode of ozone. For vibrational predissociation, the O_3 bending mode has been found to be very effective. In our calculations, it can be seen from Table VIII that the rate coefficicent values for (11,0,0), (0,11,0) and (0,0,11) excitations are greater when compared with (10,0,0), (0,10,0) and (0,0,10) values. In general, we find that the rate coefficients increase as the initial excitation energy in ozone increases. Furthermore, at high density, increasing the energy in O_3 bending mode results in a considerable increase in the energy transfer rate coefficient whereas a similar trend is absent for the other modes. Clearly, this indicates that mode specificity is present for O_3-matrix energy transfer.

When similar comparisions are made for ozone-Ar(M) systems at a reduced density, we note the same trends as mentioned aboe, except that when the bending mode energy is increased, there is no significant change in the rate coefficient. This is due to the increased volume available in the innermost cube containing the O_3 molecule. Such structure specificity has previously been obtained by Arnold and coworkers who found that O_3.NO vibrational

predissociation rates to be dependent upon the structure of the complex.

Consideration of the values given in Table IX again shows the rate coefficient to increase with increasing energy. Furthermore, for the bending mode $k_{III} > k_{IV} \gtrsim k_{II}$ where the subscripts denote the configuration number. However, for symmetric and asymmetric stretching modes rate coefficient values remain more or less the same within the error limits. Thus, at high density, the bending mode exhibits orientational and structural effect in argon matrices. In general, the metastable structures transfer energy to the matrix at a greater rate than the equilibrium configuration.

The effect of density on the rate coefficient is summarized in Table X for argon matrices. We note that the rate coefficients increase with increasing density. This can be expected because at high density, the probability of ozone coming in contact with neighboring rare gas atoms is more and hence the flow of energy occurs at a faster rate. In addition, there seems to be a near direct proportionality between the ozone-matrix density and the energy transfer coefficients. At 12 K, the ratio between densities of the argon matrices is (1.422/1.036) = 1.372 and the maximum and minimum rate coefficient values at the low density for the (10,0,0) state of configuration I are 2.76×10^{11} sec^{-1} and 2.54×10^{11} sec^{-1} respectively. When these values are

multiplied with the above mentioned ratio (1.372), we obtain 3.79×10^{11} sec^{-1} and 3.48×10^{11} sec^{-1}, respectively. That is, we obtain a density-scaled value of $(3.64 \pm 0.16) \times 10^{11}$ sec^{-1} for the (10,0,0) rate coefficient. At 12 K and at a density of 1.422 g/cm^3 the rate coefficient obtained for the (10,0,0) state in an argon matrix is $(3.39 \pm 0.24) \times 10^{11}$ sec^{-1}. That is, the density-scaled value of $((3.64 \pm 0.16) \times 10^{11})$ sec^{-1} is within the error range of the observed value. Similar calculations have been performed for other cases and these results are presented in Table XI.

The effect of temperature on the vibrational energy transfer rate of ozone in an argon matrix is shown in Table XII. At low density, it can be seen that increasing the temperature does not alter te rate coefficient significantly. Furthermore, considering values shown in Table XIII, it appears that there exists a 'threshold energy' for each mode such that the energy transfer is rapid only beyond this value. Also, it is interesting to note that for the argon matrix with density 1.036 g/cm^3 at 12 K, the rate coefficient for (10,0,0) excitation (= 33.46 kcal/mole) is about three times greater than the corresponding (5,5,5) excitation (= 38.16 kcal/mole) although the former has less excitation energy. Furthermore, the (5,0,0) excitation has a lower rate value.

With reference to values in Table XIV, it can be seen that the rate coefficients observed in xenon matrices are considerably less than those observed in argon matrices. The rate coefficient value does not change even when the mass is changed (from 131.3 to 39.948 amu) keeping the potential energy parameters the same (namely, that of the Xe matrix). This may perhaps be due to the ratio of well depths between (Ar-O, Ar-Ar) and (Xe-O, Xe-Xe). That is , the ratio of well depths between Ar-O and Ar-Ar is 7 (0.07/0.01). Similarly for Xe-O and Xe-Xe is 0.5 (0.01/0.02). Thus, in an argon matrix where we have a high well depth ratio, the energy transfer takes place more rapidly than it does so in a Xe matrix.

Thus, in general our energy transfer calculations for several configurations show mode selectivity and orientational effects as has been reported by other workers. Furthermore, our power spectra calculations are in fairly good agreement with the previously reported values thereby showing the validity of the proposed model.

CHAPTER IV

CONCLUSIONS

A. Summary of results

In this work, we have studied the vibrational energy transfer of ozone in argon and xenon matrices. We considered 64 movable rare gas atoms along with ozone. There are 80 rare gas-rare gas interactions and 24 rare gas-oxygen interactions and the motion of the atoms are assumed to obey classical equations of motion. The total interaction potential of the system is given as the sum of rare gas-rare gas, oxygen-rare-gas interaction potentials and the ozone potential. By solving the 402 diffefrential equations using a fourth-order Runge-Kutta-Gill procedure, we have calculated the power spectra of ozone in argon, and xenon matrices as a function of density, temperature and initial excitation energy and the observed results are summarized below:

in general, our power spectra results are in fairly good agreement with the experimentally determined values. For our argon matrix calculation, we find the rate coefficient values to increase with increase in ozone excitation energy. Also, at high density, the bending

mode shows orientational and structure specificity. In addition, the metastable structures transfer energy to the matrix at a greater rate than the equilibrium configuration. Furthermore, at high density, increasing the energy in O_3 bending mode results in a considerable increase in the energy transfer rate coefficient whereas a similar trend is absent for the other modes. Clearly, this indicates that mode specificity is present O_3-matrix energy transfer.

When we consider the rate coefficient values for the xenon matrix, we observe the values to be less than the corresponding argon matrix values. This may be a direct consequence of the potential energy parameters used in this calculation.

B. Suggestions for future work

In this study, we have only considered argon and xenon matrix and hence an investigation using a krypton matrix will be very useful to compare the results. In the present model, each oxygen atom interacts with only the rare gas atoms of the innermost cube. Instead, we can consider all oxygen-rare gas interactions. This will, ofcourse, increase the computational time. For the present calculations, we have used gas-phase well-depths values for the rare-gas-oxygen interactions. On the other hand, by using arbitrary well depth values for the

rare-gas-oxygen interactions and adjusting the same to obtain the measured frequency shifts, we can get the best well depth value that will truly describe the nature of the rare-gas-oxygen interaction in a matrix. However, this will be a tedious procedure.

BIBLIOGRAPHY

1. I.Norman and G.Porter, Nature,174, 508 (1954).

2. I.Norman and G.Porter, Proc.Roy.soc.,A230, 399 (1955).

3. E.Whittle, D.A.Dows and G.C.Pimentel, J.Chem.Phys., 22, 1943 (1954).

4. G.C.Pimentel, Spectrochim.Acta,12, 94 (1958).

5. E.D.Becker, G.C.Pimentel and van Thiel, J.Chem.Phys.,26, 195 (1957).

6. Vibrational spectroscopy of trapped species, edited by H.E.Hallam, John Wiley and Sons, 1973.

7. H.Frei and G.C.Pimentel, Ann.Rev.Phys.Chem.36,491 (1985).

8. D.J.Diestler in Advances in Chemical Physics: 'Potential Energy Surfaces' (Ed. K.P.Lawley), Wiley, London, 1979.

9. V.E.Bondybey and L.E.Brus, Advances in Chemical Physics, Vol. XLI, John Wiley and Sons, 1980.

10. B.Davies, A.McNeish, M.Poliakoff and J.J.Turner, J.Amer.Chem.Soc.,99, 7573 (1977).

11. M.Poliakoff, N.Breedon, B.Davies, A.McNeish and J.J.Turner, Chem.Phys.Lett.,56, 474 (1978).

12. B.Davies, A.McNeish, M.Poliakoff, M.Tranquille and J.J.Turner, Chem.Phys.Lett.,52,477 (1977).

13. C.B.Murchison and J.Overend, Spectrochim.Acta.,27A, 1509 (1971).

14. D.F.Smith Jr., J.Overend, R.C.Spiker and L.Andrews, Spectrochim.Acta.,28A, 87 (1972).

15. L.Andrews and R.C.Spiker Jr., J.Phys.Chem.,76, 3208 (1972).

16. a) L.Brewer and L.F.Wang, J.Chem.Phys.,56, 759 (1972).

b) G.C.Pimentel and S.W.Charles, Pure Appl.Chem.,7, 111 (1963).

17. J.D.Baldeschwieler and G.C.Pimentel, J.Chem.Phys.,33, 1008 (1960).

18. R.T.Hall and G.C.Pimentel, J.Chem.Phys.,38, 1889 (1963).

19. R.H.Hauge, S.Gransden, J.L.F.Wang and J.L.Margrave, J.Amer.Chem.Soc.,101, 6950 (1979).

20. E.Catalano and R.E.Barletta, J.Chem.Phys.,66, 4706 (1977).

21. E.Catalano, R.E.Barletta and R.K.Pearson, J.Chem.Phys., 70, 3291 (1979).

22. H.Frei and G.C.Pimentel, J.Chem.Phys.,78, 3698 (1983).

23. A.K.Knudsen and G.C.Pimentel, J.Chem.Phys.,78, 6780 (1983).

24. H.Frei and L.Fredin and G.C.Pimentel, J.Chem.Phys.,74, 397 (1981).

25. M.A.A.Clyne, B.A.Thrush and R.P.Wayne, Trans.Faraday Soc., 60, 359 (1964).

26. a) P.N.Clough and B.A.Thrush, Trans.Faraday Soc.,63, 915 (1967).

b) P.N.Clough and B.A.Thrush, Trans.Faraday Soc.,65, 23 (1969).

27. W.Braun, M.J.Kurylo, A.Kaldor and R.P.Wayne, J.Chem.Phys., 61, 461 (1974).

28. M.J.Kurylo, W.Braun, A.Kaldor, S.M.Freund and R.P.Wayne, J.Photochem.,3, 71 (1974).

29. M.J.Kurylo, W.Braun, C.N.Xuan and A.Kaldor, J.Chem.Phys., 62, 2065 (1975).

30. K.K.Hui and T.A.Cool, J.Chem.Phys.,68, 1022 (1978).

31. K.K.Hui, D.T.Rosen and T.A.Cool, Chem.Phys.Lett., 32, 141 (1975).

32. R.J.Gordon and M.C.Lin, J.Chem.Phys.,64, 1058 (1976).

33. R.J.Gordon and M.Lin, Chem.Phys.Lett.,22, 262 (1973).

34. S.M.Freund and J.C.Stephenson, Chem.Phys.Lett.,41, 157 (1976).

35. J.C.Stephenson and S.M.Freund, J.Chem.Phys.,65, 4303 (1976).

36. a) D.Lucas and G.C.Pimentel, J.Phys.Chem.83, 2311 (1979).

b) H.Frei and G.C.Pimentel, J.Phys.Chem.85,3355 (1981).

37. D.L.Bunker,'Classical Trajectory Methods' in Computational Physics, Vol.10, Academic Press, 1971.

38. R.N.Porter and L.M.Raff, Classical Trajectory Methods in Molecular Collisions, in Modern Theoretical Chemistry, Ed. W.H.Miller, Plenum Press, New York, 1976.

39. L.M.Raff and D.L.Thompson, The Classical Trajectory Approach to Reactive Scattering in The Theory of Chemical Reaction Dynamics, Ed. M.Baer, CRC Press, Boca Raton, Fl. 1985.

40. G.C.Schatz, Quasiclassical Trajectory Studies of State to State Collisional Energy Transfer in Polyatomic Molecules in Molecular Collision Dynamics, Ed. J.M.Bowman, Springer-Verlag, 1983.

41. S.Chapman, J.Chem.Phys.,74, 1001 (1981).

42. R.Viswanathan and L.M.Raff, J.Phys.Chem.,87, 325 (1983).

43. C.Arnold, N.S.Gettys, D.L.Thompson and L.M.Raff, J.Chem.Phys.,84, 3803 (1986).

44. Submitted to J.Phys.Chem.

45. L.M.Raff, J.Phys.Chem.,91, 3266 (1987).

46. J.N.Murrell and S.Farantos, Mol.Phys.,34, 1185 (1977).

47. D.L.Bunker and B.S.Jacobson, J.Amer.Chem.Soc.,94, 1843 (1972).

48. a) R.Viswanathan, L.M.Raff and D.L.Thompson, J.Chem.Phys.,79, 2857 (1983).

b) R.S.Berry, S.A.Rice and J.Ross, Physical Chemistry, John Wiley and Sons, part one, p.419 (1980).

c) D.L.Thompson, J.Phys.Chem.,86, 2538 (1982).

d) A.J.Stace and J.N.Murrell, J.Chem.Phys.,68, 3028 (1978).

49. R.J.Whitehead and N.C.Handy, J.Mol.Spectrosc.,55, 356 (1975).

50. C.E.Froberg, Introduction to Numerical Analysis, 2nd Edition, Addision-Wesley Pub. Co., 1969.

51. A.Barbe, C.Secroun and P.Jouve, J.Mol.Spectrosc.,49, 171 (1974).

52. G.C.Schatz and T.Mulloney, J.Chem.Phys.,71, 5257 (1979).

53. W.Mendenhall, James E.Reinmuth, Robert Beaver and Dale Duhan, Statistics for Management and Economics, 5th Edition, 1986, PWS Publications, Boston, MA.

54. E.O.Brigham, The Fast Fourier Transform, Prentice-Hall Inc., New Jersey, 1974.

55. Harris, IEEE Trans.Audio (June) 1967.

56. CRC handbook of Chemistry and Physics, 61st Edition, 1980-81, CRC Press, Boca Raton, Fl.

57. Ihor O.Bohachevsky, Mark E.Johnson and Myron L.Stein, Technometrics,28, 209 (1986).

58. M.Lundy, A.Mees, Mathematical Programming,34, 111, 1986.

59. S.Kirkpartick, C.D.Gelatt.Jr.,and M.P.Vechhi, Science, 220, 671 (1983).

60. N.Metroposis, A.W.Rosenbluth, M.N.Rosenbluth and A.H.Teller, J.Chem.Phys.,21, 1087 (1953).

VITA

Meenakshisundaram Padmasani Sudhakaran

Candidate for the Degree of

Doctor of Philosophy

Thesis: THEORETICAL INVESTIGATION OF ENERGY TRANSFER OF OZONE IN ARGON AND XENON MATRICES

Major Field: Chemistry

Biographical:

Personal Data: Born in India, on July 27, 1959.

Education: Graduated from M.C.N. High School in 1975; received the Bachelor of Science degree in Chemistry from the University of Madras, India, in 1979; received the Master of Science degree in Chemistry from the University of Madras, India in 1981; completed requirements for the Doctor of Philosophy at Oklahoma State University in May 1988.

Professional Experience: From June 8,81 to Sep.11,81 worked as a Research Assistant in Chemistry at Loyola College, Madras, India. From Jan.82, working as a Graduate Teaching Assistant at OSU.

Professional Organizations: Phi Kappa Phi, Sigma Xi, ACS and Member of Phi Lambda Upsilon.